EG&G Idaho, Inc.

P.O. BOX 1625, IDAHO FALLS, IDAHO 83415

October 31, 1984

Mrs. S. M. Prestwich
Advanced Technology Branch
Idaho Operations Office - DOE
Idaho Falls, Idaho 83401

INJECTION PROGRAM ANNUAL PROGRESS REPORT FY-1984 - RAM-66-84

Dear Mrs. Prestwich:

Enclosed is a draft of the Annual Progress Report for the Hydrothermal Injection Program. ESL/UURI has not reviewed the enclosed draft and when their comments are received the report will be published in final form.

Very truly yours,

J. H. Ramsthaler
Geothermal/ Hydropower Programs

ms

Enclosure:
As Stated

bcc: R. C. Diehl
B. F. Russell
Central File

HYDROTHERMAL INJECTION PROGRAM

FY-1984 ANNUAL PROGRESS REPORT

EG&G IDAHO, INCORPORATED

EARTH SCIENCES LABORATORY

UNIVERSITY OF UTAH RESEARCH INSTITUTE

CONTENTS

CONTENTS (Continued)

TABLES

FIGURES

FIGURES (Continued)

FIGURES (Continued)

1.0 ABSTRACT

This report summarizes work accomplished by EG&G Idaho, The Earth Sciences Laboratory of the University of Utah Research Institute and Republic Geothermal Inc. during FY-1984 on Geothermal Injection Research.

Studies are described to develop tracers which do not interact with a reservoir and to calculate the mixing of injected fluids and native reservoir fluids. Techniques to calculate the reactions of injected fluids with reservoir rocks are presented.

Test results at East Mesa and Raft River Geothermal fields are described and interpretations of field mixing in terms of reservoir characteristics are developed. Supporting laboratory experiments on fracture flow are used to assure that interpretations of field data are based on sound theoretical concepts.

A computer code, FRACSL, is described which is used to analyze the fluid mixing data obtained in laboraory and field experiments.

2.0 INTRODUCTION

Injection of spent geothermal fluids has been established as a major research need by the industrial geothermal community and by the Department of Energy Division of Geothermal and Hydropower Technology (DOE/DGHT). A series of meetings have been held by industry and DOE/DGHT and the following have been established as the priority injection research areas.

1) Means to predict and measure subsurface fluid movement.
2) Means to predict and measure subsurface fluid chemical reactions.
3) Surface treatment technology.
4) Improved injection well completion technology.

EG&G Idaho, Inc. and the Earth Sciences Laboratory of the University of Utah Research Institute (ESL/UURI) working for the Idaho Operations Office of the Department of Energy have been planning and conducting a significant injection research program since its identification as a priority research area by DOE/DGHT. Republic Geothermal Inc. joined the program as an industrial participant for the second test series conducted at East Mesa.

The program has concentrated on the priority one and two research areas; subsurface fluid movement and subsurface chemical reactions. The research has been guided by the fundamental concept that carefully controlled field experiments are required to develop data which can be used to develop techniques for predicting and measuring injected fluid movement and chemical reactions. Field experiments are inherently expensive and an extensive laboratory program is being conducted to assure that techniques developed to analyze the field data are based on sound fundamental principals.

Initial work in this program has concentrated on an evaluation of the injection/backflow technique as a means to measure and predict injected

fluid movement and reactions. With this technique, fluid is injected into a test well with tracers which are not reactive with the reservoir fluids or rocks surrounding the test well. The test well is then backflowed and analyzed for tracer content. With this information the mixing of the injected and native reservoir fluid can be calculated. Heat transfer and chemical reactions can then be calculated and analyses conducted to assess the hydraulic characteristics of the portion of the reservoir into which fluid was injected.

In the first annual report summarizing work on this research[1] results were described for experimental test series at Raft River and at East Mesa. In FY-1984 two additional tests were conducted at East Mesa but the primary emphasis has been on the analysis of data and the development of techniques to interpret the data. This report summarizes work accomplished in FY-1984.

3.0 SUMMARY

The computer code FRACSL was made operational during the year. This code is required to analyze the mixing which occurs between injected fluids and natural reservoir fluids. The code tracks mixing using a continuous series of marker particles which are added to the injected fluid. The marker particle routine has been verified by comparing predictions with laboratory data. Models have been programmed with FRACSL to simulate laboratory single and multiple fracture models, the Raft River fractured reservoir and the East Mesa homogeneous reservoir.

The two test wells at East Mesa (56-19 and 56-30) were backflowed after a six month quiescent period. No tracer was recovered from Well 56-19 whereas 96% of the continuous tracer was recovered from 56-30. Recovery of tracers from Well 56-30 was delayed considerably compared to a baseline test with a short quiescent period conducted in FY-1983. A FRACSL model of Wells 56-19 and 56-30 was constructed to assist in interpreting the test data. An injection plume which was eliptical in shape and drifted 32 feet in the direction of the minor axis of the elipse gave the best fit to the tracer return data. Consideration was given to other potential causes of the tracer delay such as local thermal or hydraulic gradients tracer adsorption etc., but none of these potential causes could explain the shape of the tracer return curve. It is tentatively concluded the delay in tracer return at well 56-30 is due to fluid movement within the reservoir. A regional hydraulic gradient due to vertical faulting is theorized as a most likely cause of the fluid movement.

Analysis of the three baseline tests with the short quiescent period in Well 56-19 with FRACSL indicates there is a problem which might be due to interzonal flow. A dispersion coefficient of 0.54 was calculated for two of the tests. No dispersion coefficient was calculated for the test with a low flow rate. FRACSL couldnot duplicate the results of the low flow rate test. In theory, the dispersion coefficient should not change with flow rate but an interzonal flow would result in the calculation of a superficially high dispersion coefficient. There is, however, no good explanation for why the interzonal flow should effect the low flow rate test and not the high flow rate tests. Analysis is continuing on this anomoly.

Tracer analysis for the East Mesa test series has been completed. The continuously added tracers, bromine and iodine, behaved conservatively as well as the two natural tracers present in the injected fluid, clorine and the sulfate ion. The slug tracers, boron and the thioscanate ion, did not perform conservatively. The data indicate thiocyanate may have been lost by adsorption during one test and recovered during a later test. Conservative tracer recovery ranged between 96 and 104%.

Best estimate mixing curves were prepared based on the performance of the conservative tracers. Silica and calcium were found to have precipitated in the reservoir. Negligible reaction of other chemicals in the injected fluid has been detected to date. The value of the injection backflow technique as a means to assess formation reaction was demonstrated by the RGI work on calcium precipitation. An inhibitor was added to the injected fluid to delay the precipitation of calcium carbonate. By monitoring the calcium content of the injected and backflowed fluids, RGI was able to determine the decay in the effectiveness of the inhibitor. They concluded precipitation near the wellbore was not a problem for long term injection.

Laboratory runs have been made in the single fracture and fracture junction models. Good agreement has been obtained between the lab results and the PNLFRAC and SALE codes which were used to simulate the results from the two models. The good agreement verifies that the multidimensional effects which can be a problem when using laboratory data have been properly simulated and that the particle tracking algorithm being used in the simulation codes properly predicts fluid mixing. An important conclusion from the junction model is that under most conditions fluids do not mix at junctions. Extensive theoretical work has been done to support the analysis of the laboratory and field data. This work has developed an explanation for the results obtained at Raft River based on parallel plate theory. The work shows promise as a means to increase sensitivity in discriminating between fractured and homogeneous flow during an injection backflow test.

To analyze the Raft River mixing data obtained in FY-1983 an extensive literature survey was conducted on techniques to model fracture systems. The search indicated fractures are not monolithic and are best modeled as a

system of fractures with a log normal distribution. Borehole televiewer data of the Raft River test well were analyzed and five major fracture areas were identified. Each of the major areas had discrete fracture within them. The major fracture areas correlated with spinner data on areas of flow entry.

Two FRACSL models were developed, each for a vertical model plane centered on the hydrofracture which lies in a plane including the well centerline. The smaller model included only a narrow zone along the vertical extent of the hydrofracture. This model included only the fractures observed at the wellbore and was used to scope the effective fracture apertures and to study the drawdown response. The larger model was for a 500 ft by 500 ft section and a fracture system synthesized partially from the statistics of the observed fractures. Hydraulic and dispersion characteristic studies on this model will be completed in FY-1985.

Analysis of self-potential (SP) data obtained at East Mesa during FY-1983 has shown that reservoir fluid movement was not detected. The changes which were reported previously[1] were due to potentials induced by fluids flowing in the supply pipelines. It is concluded that SP has little potential to detect reservoir fluid movement at the depths of the East Mesa wells.

4.0 DISCUSSION

4.1 Historical

The injection test program was initiated at the Raft River Geothermal field in southern Idaho in September of 1982. A series of eight short-term injection and backflow tests followed by a long-term injection test were conducted on one well in the field. Tracers were added during injection and monitored during backflow of the well. In December of 1982 a Request for Proposal (RFP) was issued to obtain an industrial partner to obtain follow-on data on the injection/backflow technique in a second field and to study any alternate advanced concepts for injection testing which the industrial community might recommend. Republic Geothermal, Inc. and the East Mesa Geothermal Field were selected for the second test series. Two wells were utilized for testing, and a series of ten tests were conducted in July and August of 1983 aimed principally at further evaluation of the injection/backflow technique. When the test series was completed both wells at East Mesa were injected with tracer laden fluid to determine the effect of a long term quiescent period. In February of 1984 the two wells were backflowed. Test data are available in References (2) and (3) on the Raft River test series and the first test series at East Mesa. Results of the backflow tests after six months quiescence are described in this report. Papers on technical analysis of the data are reported in References (4-12).

To support the test program and assure that the techniques which evolve from the work have a sound theoretical basis, laboratory work has been initiated by EG&G Idaho and ESL/UURI. At EG&G Idaho during FY-1983 and FY-1984, a series of laboratory fracture flow experiments were conducted to obtain basic data for assisting in the analysis of the Raft River mixing and flow data. Technical reports, presentations and equipment descriptions on the laboratory work are summarized in References (13-16).

At ESL/UURI, basic studies were conducted to determine tracers which might be used in the field tests and to screen those which reacted adversely with the geothermal fluids. An extensive effort has been required to develop improved analytical techniques to analyze test results(17).

4.2 Test Program

During FY-1984, analysis has been concentrated on the test results obtained at East Mesa. Two wells were chosen for the injection-backflow experiments at East Mesa -- Republic Geothermal Wells 56-30 and 56-19. These wells were selected for comparative tests because their temperature and fluid compositions differ and because they produce from different depths. Well 56-30 produces a 174°C sodium chloride fluid having a total dissolved solids (TDS) content of 1700 ppm from a depth of 1820 m (5970'). Well 56-19 produces a 126°C (259°F) sodium chloride fluid having a TDS content of 4900 ppm from a depth of 910 m (2985 ft). The well used to supply the injectate was Republic Geothermal Well 38-30. Fluid from this well is similar in temperature and composition to that from Well 56-30. The two wells, 56-30 and 38-30, are believed, as a result of pressure transient tests, to be in hydraulic communication. Average chemical analyses of fluid from these wells are listed in Table 1.

Fluid from Well 38-30 was transported approximately 0.8 km (0.5 mi) in iron pipe to the 56-30 well site, where it was flashed at atmospheric pressure. Calcite scale inhibitor was added immediately prior to flashing. The flashed fluid was then transported via centrifugal pump to either the 56-30 or the 56-19 well head. The tracer solution, made up beforehand using fluid from Well 38-30, was injected into the flowline ahead of the centrifugal pump, using a positive displacement pump, at a rate of .06 to .12 l/s. The flow rate of tracer injection was controlled manually. The flow rate of the total injected fluid was controlled by an automatic flow-control loop downstream of the tracer injection.

A complete summary of tests conducted at East Mesa is shown on Table 2. The broad objective for the tests on Well 56-30 were, 1) obtain baseline hydraulic data by conducting flow tests at 2 rates, 2) obtain a baseline injection backflow test to characterize the reservoir around the well and 3) conduct a long-term tracer performance test to assess reservoir drift. The test program on Well-56-19 had similar objectives and in addition, parametric studies were conducted on flow rate and injection volume. These data are needed to confirm theoretical approaches being developed for analyses of reservoir characteristics.

TABLE 1. AVERAGE CHEMICAL COMPOSITIONS OF FLUID FROM REPUBLIC GEOTHERMAL WELLS 56-30, 56-19, AND 38-30.

	Well 56-30			Well 56-19			Well 38-30		
	$\bar{X}$	$\frac{100\sigma}{\bar{X}}$	n	$\bar{X}$	$\frac{100\sigma}{\bar{X}}$	n	$\bar{X}$	$\frac{100\sigma}{\bar{X}}$	n
Na	585	2	34	1848	0.9	23	647	2.6	8
K	23	5	34	44	1.8	23	26	3.9	8
Ca	6	0	18	17	3.0	10	6	8.1	8
Mg	<.5	0	34	2.7	17	23	<.5	0	8
SiO_2	176	4	34	91	4.8	23	210	3.2	8
Sr	.72	5	34	2.59	1.8	23	.78	5.4	8
Li	.45	4	34	1.99	1.4	23	.61	6.7	8
B	.98	23	34	8.38	1.1	23	n.d.	-	-
Cl	519	2	31	2280	1.3	21	n.d.	-	-
F	2.3	5	20	2.3	5.5	13	n.d.	-	-
TDS	1760	1	15	4840	.6	6	n.d.	-	-
pH	6.4	2	21	6.7	1.8	12	6.12	.9	7
HCO_3	581	5	19	1120	3.1	13	n.d.	-	-
SO_4	171	1	20	33	4.5	13	n.d.	-	-
I	<.1	0	4	.5	14	5	<.1	0	8
SCN	<.5	0	4	<.5	0	4	<.5	0	8
Br	<.2	0	4	2.2	4.4	4	n.d.	-	-

TABLE 2. SUMMARY OF EAST MESA INJECTION BACKFLOW TESTS

Test Designation	Injection Well	Injection Rate (l/sec)	Injection Volume (l)	Quiescence Period	Production Rate (l/sec)	Produced Volume (l)
1(-30)	56-30	none	none	none	18.9	1.6×10^6
2(-30)	56-30	none	none	none	28.4	2.5×10^6
3(-30)	56-30	18.9	7.6×10^5	12 hr.	18.9	4.5×10^6
4&5(-30)	56-30	18.9	7.6×10^5	6.5 mo.	18-32	1.1×10^7
1(-19)	56-19	none	none	none	18.9	1.6×10^6
2(-19)	56-19	none	none	none	31.5	2.7×10^6
3(-19)	56-19	18.9	8.1×10^5	12 hr.	18.9	3.6×10^6
4(-19)	56-19	31.5	8.1×10^5	12 hr.	31.5	5.4×10^6
6(-19)	56-19	31.5	1.5×10^6	12 hr.	31.5	5.4×10^6
8&9(-19)	56-19	31.5	7.9×10^5	5.5 mo.	18-31	1.3×10^7

4.3 Geochemistry/Tracer Development

The objectives of the geochemistry tracer development work are to identify tracers for use during injection, conduct screening laboratory tests to evaluate the various tracers and to develop techniques for sampling and analyzing the tracers both in the field and in the laboratory.

The tracers used at East Mesa were anions chosen for their conservative nature based on our experience at Raft River[9]. These tracers were bromide (Br), iodide (I), chloride (Cl), fluorescein, thiocyanate (SCN), and borate (reported as B). With the exception of Cl, the tracers were the sodium salt of the anion. Cl was obtained as LiCl and KCl in order to evaluate the behavior of these cations in geothermal fluids. The quantities and species of tracers used for each test are listed in Tables 3a and 3b.

The original tracer plan was to use LiCl and KCl in Well 56-30, tests where there would be no natural Cl contrast between injected and native reservoir fluid. Unfortunately, these tracers were not delivered at the anticipated time, and difficulties were encountered with the tracer injection pump rate. For these reasons, sulfate (SO_4), naturally present in the injected fluid, was used as a tracer in Test 3(-19) rather than the added tracers listed in Table 3.

Either one or two of the tracers, Br, I, and Cl, were continuosly added to Well 38-30 fluid during each injection. In addition, disodium fluorescein plus either B or SCN were injected at high concentrations for a period of five minutes during each injection as a 'point source' or slug. The combination of tracers was based in part on analytic considerations. For example, titration of Br will also titrate SCN, so the sets used were Br + B and I + SCN. Continuous tracers were always Br or I, and slug tracers were consistently B or SCN.

4.3.1 Sampling Procedure. Samples were collected at the 56-30 well site during tests on both Wells 56-30 and 56-19. Fluid from Well 56-30

TABLE 3a. TRACER INJECTION PARAMETERS, TESTS 3, 4 AND 5 WELL 56-30.

TEST	TRACER	TRACER TANK			TRACER INJECTION					
		SOLUTION		QUANTITY OF	AVERAGE	START		STOP		VOLUME OF TRACER
		VOLUME (gallon)	FROM WELL	TRACER ADDED (lbs.)	PUMP RATE (gpm)	DATE (mo/day/y)	TIME (hrs:min)	DATE (mo/day/y)	TIME (hrs:min)	SOLUTION INJECTE (gal)
3	KCl	740	38-30	1700	1	7/24	13:50	7/25/83	1:20	690
	$Na_2Fl.$	250	38-30	0.008	300	7/24	14:55	7/24/83	15:00	1300
	Borax	1750	38-30	2500	300	7/24	14:55	7/24/83	15:00	1300
4	NaSCN	2000	38-30	62	300	7/29/83	11:10	7/29/83	11:15	1470
4	$Na_2Fl.$	2000	38-30	3.5	300	7/29/83	11:10	7/29/83	11:15	1470
4	NaI	740	38-30	170	1-0.94[2]	7/29/83	10:10	7/29/83	22:10	706

[1] Calculated from change in depth of liquid in the tracer tanks.

[2] Due to an irregular flow rate on the tracer pump the flow was decreased to 0.94 gal/min during the final 8 hours of injection.

TABLE 3b. TRACER INJECTION PARAMETERS, TESTS 1, 2, 3, 4, 6, 8 and 9 WELL 56-19.

TEST	TRACER[1]	TRACER TANK			TRACER INJECTION					
		SOLUTION		QUANTITY OF	AVERAGE	START		STOP		VOLUME OF TRACE
		VOLUME (gallon)	FROM WELL	TRACER ADDED (lbs.)	PUMP RATE (gpm)	DATE (mo/day/y)	TIME (hrs:min)	DATE (mo/day/y)	TIME (hrs:min)	SOLUTION INJECT (gal)
1	NaCl	108	56-19	50	13.4	8/3/83	18:24	8/3/83	18:29	67
1	$Na_2Fl.$	108	56-19	.114	13.4	8/3/83	18:24	8/3/83	18:29	67
2	NaCl	148	56-19	130	13.7	8/7/83	11:59	8/6/83	12:07	110
2	$Na_2Fl.$	148	56-19	.36	13.7	8/7/83	11:59	8/6/83	12:07	110
3	LiCl	740	38-30	1100	1.0	8/8/83	12:21	8/9/83	00:17	728
3	NaI	740	38-30	170	1.0	8/8/83	12:21	8/9/83	00:17	728
3	$Na_2Fl.$	2000	38-30	3.5	341	8/8/83	14:21	8/8/83	14:26	1703
3	NaSCN	2000	38-30	62	341	8/8/83	14:21	8/8/83	14:26	1703
4	NaBr	740	38-30	200	1.5	8/12/83	12:34	8/12/83	19:56	678
4	$Na_2Fl.$	2750	38-30	7	506	8/12/83	14:35	8/12/83	14:40	2530
4	Borax	2750	38-30	2500	506	8/12/83	14:35	8/12/83	14:40	2530
6	NaI	740	38-30	200	.7	8/17/83	10:28	8/18/83	00:56	622
6	NaSCN	2750	38-30	120	547	8/17/83	12:23	8/17/83	12:27.5	2406
6	$Na_2Fl.$	2750	38-30	7	547	8/17/83	12:23	8/17/83	12:27.5	2406
8	NaBr	740	38-30	400	1.5	8/21/83	07:31	8/21/83	14:46	674
8	$Na_2Fl.$	2750	38-30	7	494	8/21/83	09:18	8/21/83	09:23	2470
8	Borax	2750	38-30	2500	494	8/21/83	09:18	8/21/83	09:23	2470

[1] Abbreviations: $Na_2Fl.$ = disodium fluorescein; NaI = sodium iodide; NaCl = sodium chloride; NaSCN = sodium thiocyanate; NaBr = sodium bromide.

[2] Calculated from change in depth in liquid of tracer tank, includes amount directed to pit until continuous tracer flow stabilized.

was drawn from the wellhead through 12 m of 0.64 cm stainless steel tube at an average rate of 0.1017 l/s. Fluid from Well 56-19 was first transported 5 m from the main pipeline in a 2.54 cm iron pipe at an average rate of 1.14 l/s, and then drawn through 5 m of 0.64 cm stainless steel tubing at 0.017 l/s. Downhole samples were taken using a Kuster downhole sampler. Fluid sampled during both tests was cooled below 40°C, prior to sampling, to prevent evaporative cooling loss.

Prior to initiating the injection-backflow tests, an experiment was conducted to determine the extent of fluid mixing in the 1.8 km pipeline connecting the wellhead of 56-19 and the sampling point at well site 56-30. A 5 minutes slug of NaCl + Na_2fluorescein was injected into the pipeline near Well 56-19 during the background flow tests (1-19) and 2(-19). The fluid was sampled immediately downstream of the slug injection point as well as at site 56-30. The slug was found to retain its integrity during flow from site to site. Thus, it was considered acceptable to obtain samples for tests of both wells at site 56-30.

Sample intervals varied from one minute to eight hours, and were determined by the rate of change of electrical conductivity and/or fluorescence of the test fluid. The samples were analyzed for the tracer suite or a multi-element suite, consisting of Na, K, Mg, Fe, SiO_2, Sr, Li, B, HCO_3, SO_4, Cl, F, TDS, pH and relevant tracers. Ca was not analyzed by ESL for a majority of the samples due to contamination, discovered after the tests, from black phenolic resin caps used on the sample bottles. However, a concurrent investigation by Republic Geothermal[2] on calcite scaling during injection has provided reasonable coverage of Ca concentrations during the tests.

Estimates of analytical precision, detection limits, and sample preservation methods are listed in Table 4. A more comprehensive explanation of the analytic techniques used can be found in Reference (17).

A summary of recovery percentages is presented in Table 5. The recovery percentages were calculated for the test as a whole and also for

TABLE 4. METHODS OF GEOTHERMAL WATER ANALYSIS

ELEMENT	SAMPLE PREPARATION[a]		ANALYTIC TECHNIQUES	DETECTION[h] LIMITS	PRECISION[i] (%)	LABORATORY[c]
	FILTERED[a,b]	PRESERVATION[a]		(mg/l)		
Na	Yes	20% HNO_3	ICP[e]	1	.66	ESL
K	Yes	20% HNO_3	ICP	2	1.03	ESL
Ca	Yes	20% HNO_3	ICP	0.2	1.19	ESL
Mg	Yes	20% HNO_3	ICP	0.5	4.5[j]	ESL
Fe	Yes	20% HNO_3	ICP	0.1	1.93	ESL
B	Yes	20% HNO_3	ICP	0.1	2.07	ESL
SiO_2	Yes	20% HNO_3	ICP	1	1.02	ESL
Sr	Yes	20% HNO_3	ICP	.01	.93	ESL
Li	Yes	20% HNO_3	ICP	.05	1.24	ESL
Cl	No	None	Mohr Titration[f]	2	.90	ESL
F	Yes	None	Specific Ion Electrode[k]	0.1	2.81	ESL
$SO_4^{=}$	Yes	2% HCl	Gravimetric	2	1.80	ESL
HCO_3^- , $CO_3^{=}$	Yes	None	H_2SO_4 Titration	1	1.44	ESL, Field
I^- [d]	No	None	Specific Ion Electrode[k]	0.2	2.81	ESL
Br	No	None	Titration	1	1.55	ESL
SCN^-	No[m]	None	Colorimetric[g]	.5	2.26	ESL
pH	No	None	pH electrode[a]	±0.1	[j]	Field
TDS[l]	Yes	None	Gravimetric	5	.48	ESL
Na_2Fluorescein	No[m]	None	Colorimetric	0.02	[j]	ESL

a. Completed immediately after sample collection.
b. 0.45 μ membrane filter.
c. ESL = Earth Science Laboratory, University of Utah Research Institute; Field = East Mesa test site, field laboratory.
d. Iodate analyzed for and not present.
e. ICP = Inductively Coupled Argon Plasma Spectrophotometry.
f. Corrected for I, Br and SCN.
g. Ferric iron complex.
h. The detection limit is defined as the point at which precision is approximately ± 100% of the given value with a confidence level of 95%. At ten times the detection limit the precision is ± 10% (Christensen et al., 1980).
i. Precision determined by East Mesa repeat analyses.
j. Not determined.
k. Method of additions.
l. Total dissolved solids.
m. Sample filtered only if cloudy.

TABLE 5. INJECTATE RECOVERY PERCENTAGES

Tracers used to calculate recovery for each test are in parentheses.

Test	Borehole Tracer % Recovery		Whole Test Tracer % Recovery*		Quiescence
	Continuous	Slug	Continuous	Slug	
3(-30)	99(Cl)	--	104(Cl)	70(B)	12 hrs.
4&5(-30)	8(I)	--	96(I)	64(SCN)	6.5 mos.
3(-19)	100(SO_4)	--	100(SO_4)	82(SCN)	12 hrs.
4(-19)	99(Cl)	--	100(Cl)	102(B)	12 hrs.
6(-19)	99(Cl)	--	98(Cl)	115(SCN)	12 hrs.
8&9(-19)	40(Br)	--	7(Br)	2(B)	5.5 mos.

* (Kg tracer backflowed/Kg tracer injected) x 100

only the portion of fluid that remained in the wellbore during the test. The recovery percentages for each test as a whole reflect losses or gains of the tracers to the formation. Since the fluid that remained in the wellbore never contacted the formation, a wellbore recovery percentage close to 100% reflects a high precision of chemical analyses and flow rate control for injection versus blackflow.

Flow rates from Well 56-19 were difficult to maintain because of excessive gas production, resulting in gas blockage at high points along the pipeline. The blockage was relieved by installing valves at the high points of the pipeline. Combined gas/liquid samples were taken to identify the gas constituents. These constituents, primarily Co_2, are listed in Reference (12).

4.3.2 Calculation of Recovery Curves. The recovery curves wre constructed by plotting the fraction of injectate in recovered fluid versus the cumulative volume of fluid recovered. The fraction if injectate is calculated from the relationship:

$$X = \frac{C - C_R}{C_I - C_R} \qquad (1)$$

where x = fraction of injectate in the recovered fluid,
C = concentration of conservative tracer in the recovered fluid,
C_R = concentration of conservative tracer in the reservoir fluid, and
C_I = average concentration of (conservative) tracer in the injected fluid.

The total mass of tracer recovered was also determined and compared with the mass of tracer injected to help determine whether or not the tracer had undergone reaction in the reservoir, i.e., whether or not the tracer was conservative. The mass of tracer recovered (M) was calculated using the equation(9).

$$M = \sum_{i=0}^{n} 1.2\,(T_{i+1} - T_i)(C_I X_i + C_I X_{i+1})R_i \qquad (2)$$

where T_i = relative collection time of the ith sample;
R_i = average flow rate during time interval T_i to T_{i+1}, and
n = number of samples.

Fluctuations in the chemistry of the injectate or reservoir fluid can result in an injectate fraction somewhat greater than one or less than zero. In these cases $C_I x_i$ is replaced by C_I in Equation 2.

4.3.3 Total Tracer Recovery. Chemical analyses of fluid samples taken during the East Mesa injection testing are listed in Reference (12). Average background chemical concentrations for Wells 56-19, 38-30, and 56-30 are listed in Table 1. Borehole and whole-test tracer recovery percentages are listed in Table 5. Borehole recovery percentages of the continuous tracers were also excellent, ranging from 96% to 104%. Whole-test slug recovery percentages ranged from 70% to 115%. The low percentages indicate a loss of tracer, while the high percentages indicate a gain of tracer.

4.3.4 Recovery Curves. The slug and continuous tracer recovery curves are shown for each test in Figures 1 through 6. For comparison, recovery curves for the 12-hour quiescence tests are also presented in Figure 7 (continuous tracers) and 8 (slug tracers). Inspection of these figures shows that continuous tracer levels in all 12-hour quiescence tests, except Test 3(-19), return to background concentrations after recovery of approximately two injection volumes. Test 3(19) reaches the background level at 3.45 injection volumes. The continuous tracer recovery curves for Tests 4(-19), 6(-19) and 3(-30) are very similar. In contrast the slug recovery curves differ in amplitude. Test 3(-19) (Figure 5) displays a flattened continuous tracer recovery curve and a multiple peak slug tracer recovery curve. The positions of the slugs in both the injected and recovered fluids are listed in Table 6.

The long-term quiescence tests, 4&5(-30), Figure 5, and 8&9(-19), Figure 6, were backflowed for 16 and 18 injection volumes, respectively. Tracer levels in Tests 4&5(-30) returned to background concentration after recovery of 16 injection volumes. Borehole recovery was 8% for the

TABLE 6. RELATIVE POSITION OF SLUG DURING INJECTION AND BACKFLOW

	Injection $(1 - \frac{V_S}{V_I})$	Backflow $(\frac{V_B}{V_I})$
3(-30)	.89	.82
4(-30)	.89	7.7, 10.0
3(-19)	.70	.61, 2.2
4(-19)	.69	.74
6(-19)	.85	.92

V_S = Volume of injected fluid from beginning of continuous injection to beginning of slug injection.

V_I = Volume of fluid injected into formation.

V_B = Volume of fluid backflowed until slug peak was reached.

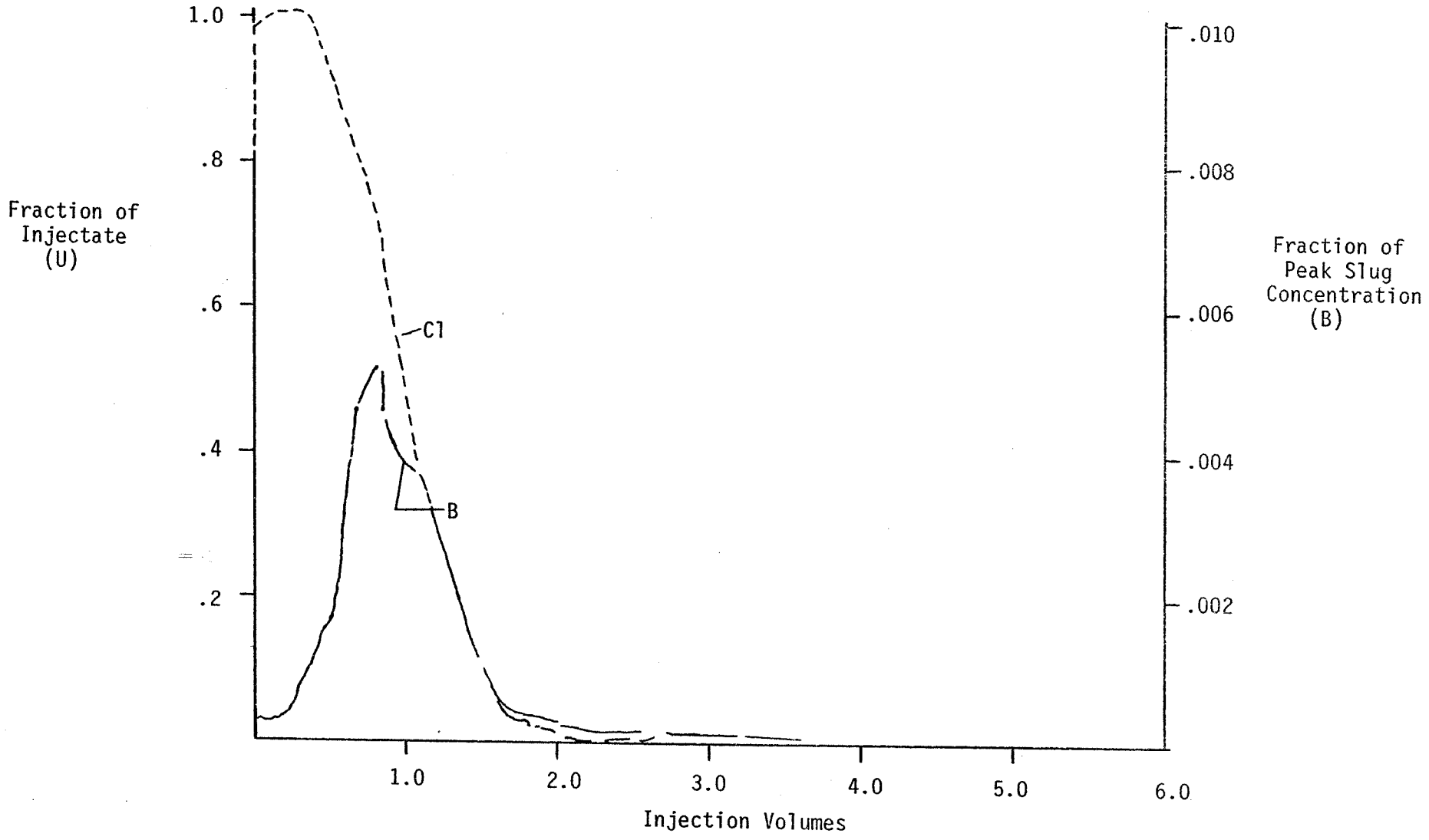

Figure 1. Recovery Curve for Test 3, Well 56-30.

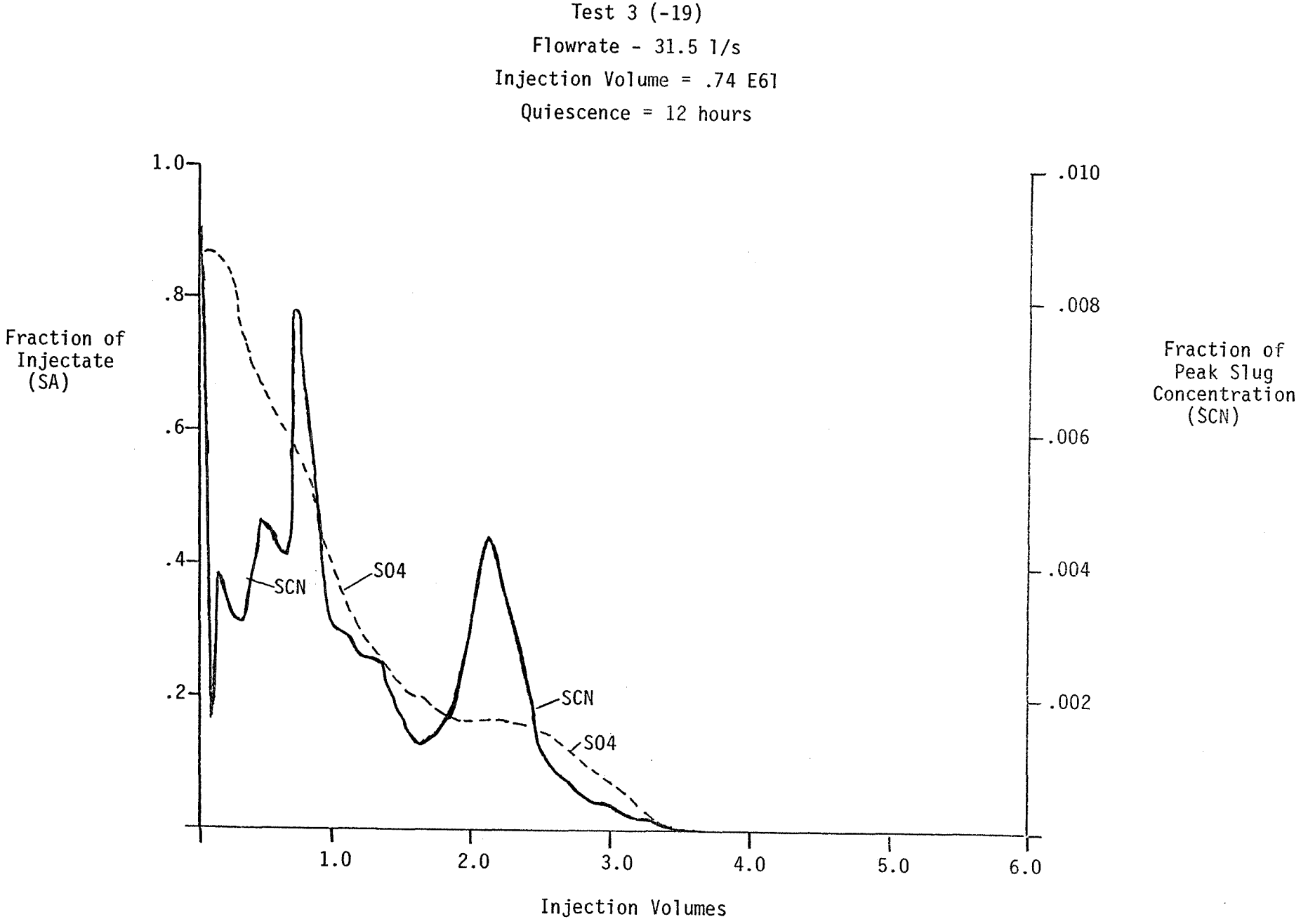

Figure 2. Recovery curve for Test 3, Well 56-19.

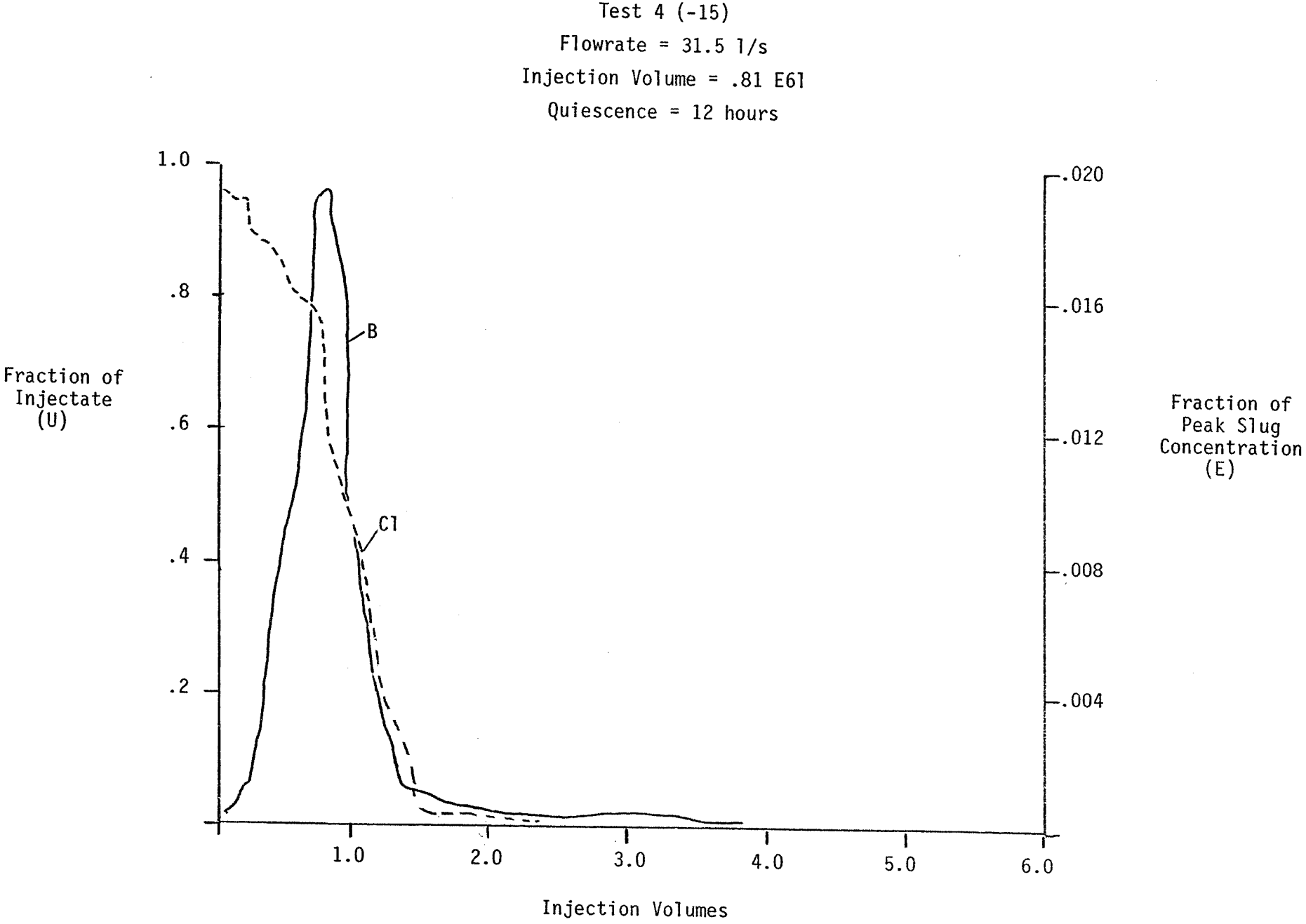

Figure 3. Recovery Curve in Test 4, Well 56-19. The tracers used were cl (continuous) and B (slug).

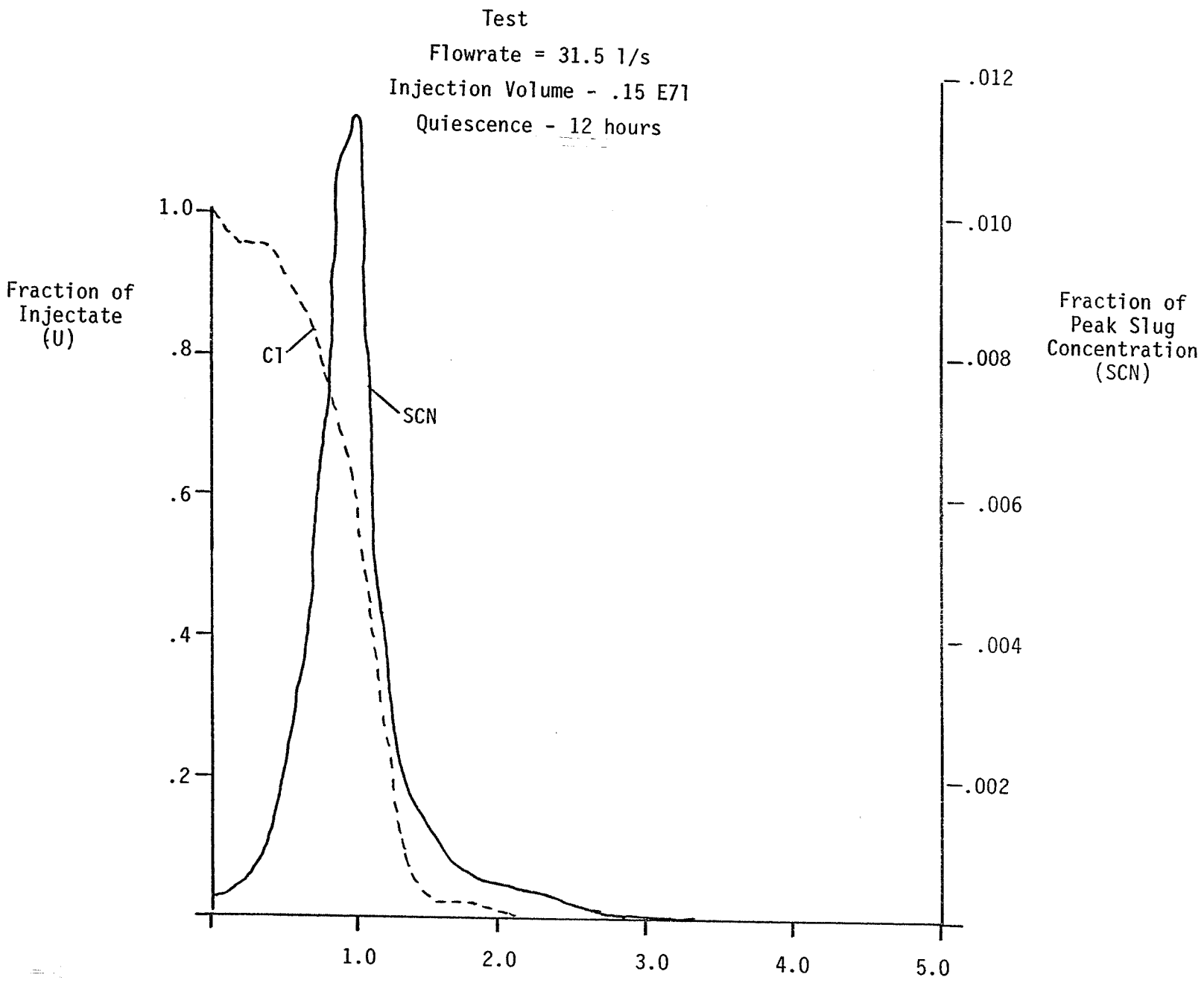

Figure 4. Recovery curve for Test 6, Well 56-19. The tracers used were CP (continuous) and SCN (slug).

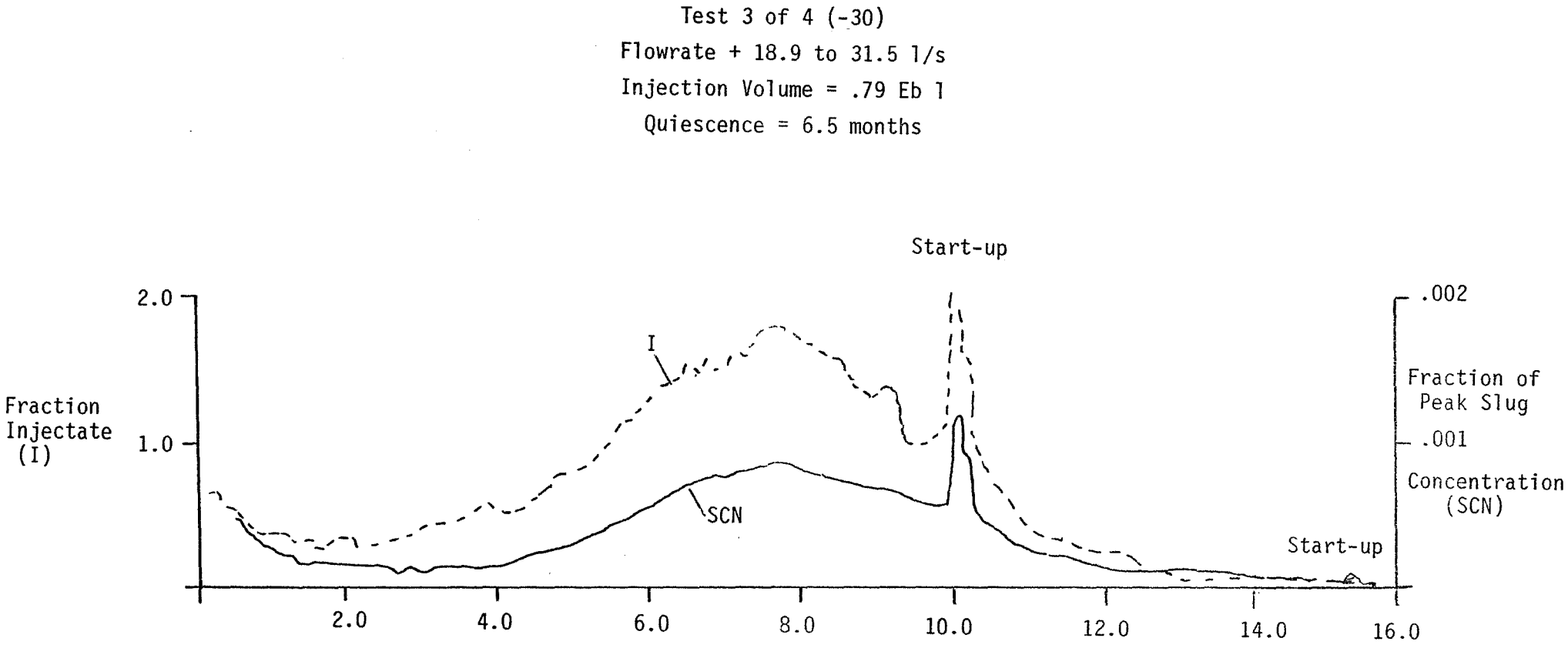

Figure 5. Recovery curve for tests 4 and 5, well 56-30.

Test 8 & 9 (-19)
Flow rate - 20 l/s to 31.5 l/s
Injection Volume = .79 E6 l
Quiescence = 5.5 months

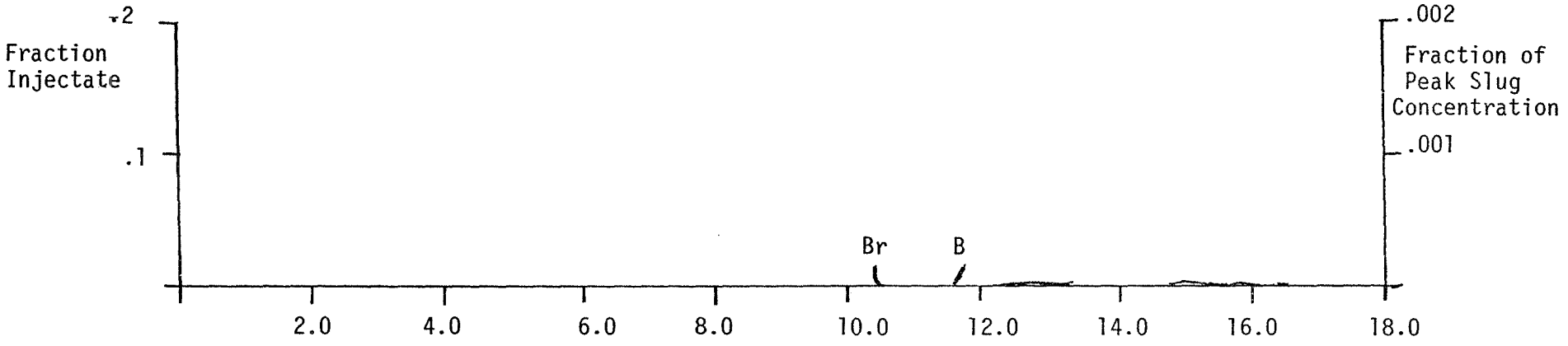

Figure 6. Recovery Curve for Test 8 and 9, Well 56-19.

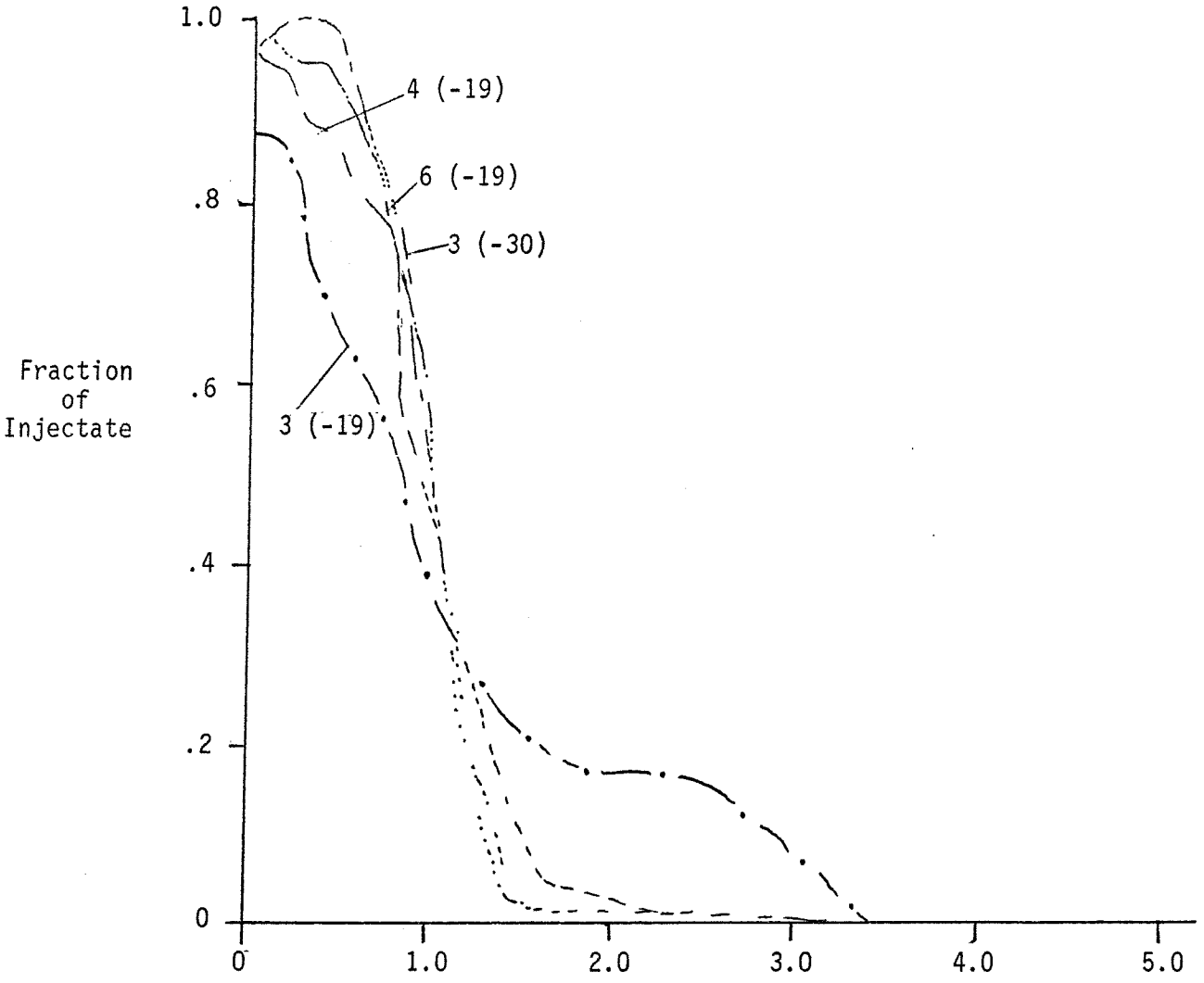

Figure 7. Recovery curves for all 12-hour quiescent tests at East Mesa.

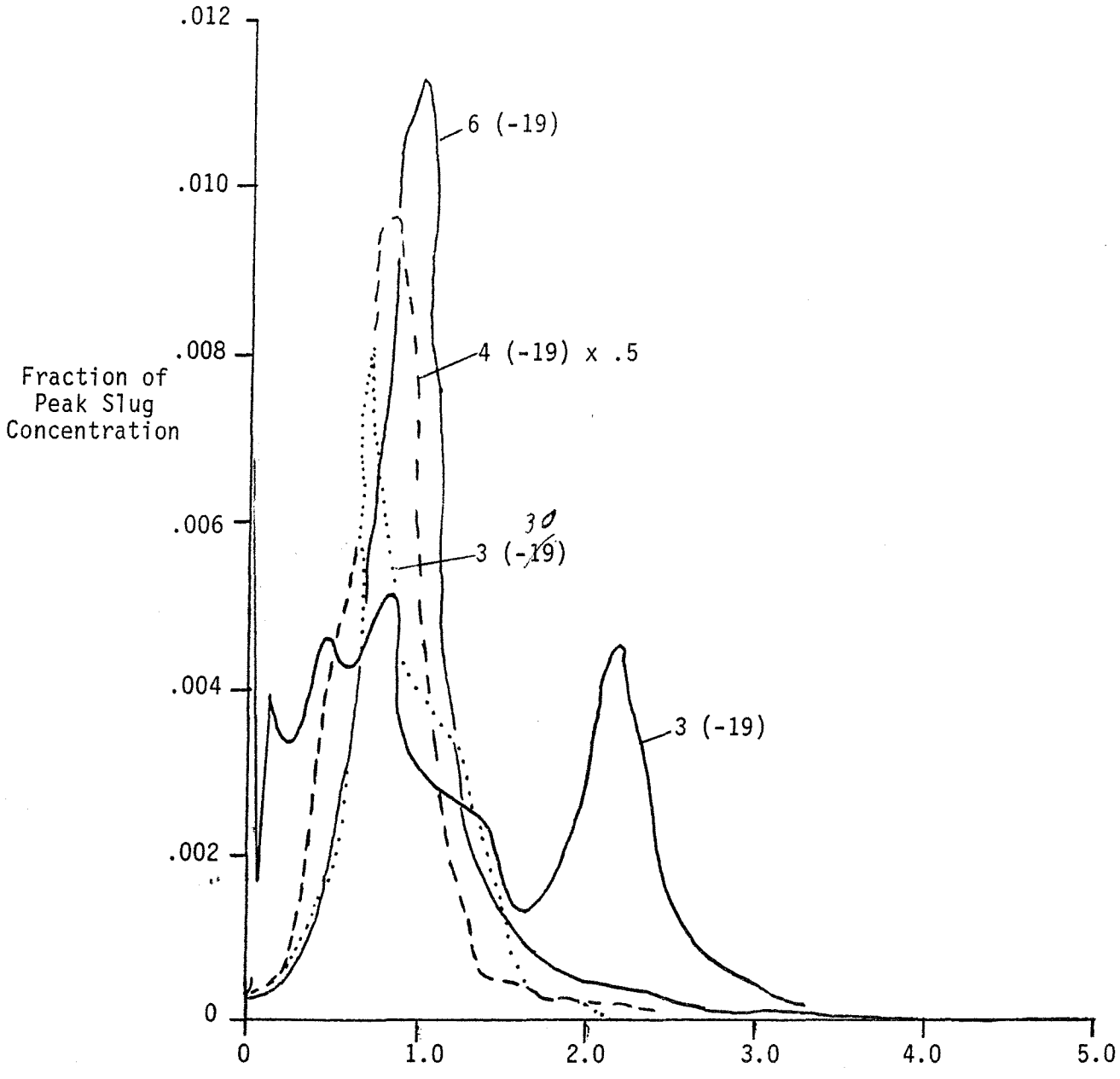

Figure 8. Slug tracer recovery curves for all 12-hour quiescent tests at East Mesa.

continuous tracer, indicating incursion of reservoir fluid into the wellbore during the quiescent period. The fact that slug tracer was also found in the wellbore, whereas in other tests the slug was completely in the formation, also indicates incursion of reservoir fluid. Whole-test recovery percentages were 96% for the continuous tracer and 64% for the slug tracer. The recovery curve displays a single broad peak, with subsidiary shape peaks occurring after each of the two times the well was shut-in and then restarted. These interruptions of the backflow were not planned as part of the experiment and did not occur during the 12 hour quiescence tests. None of the fluid injected into the formation during Test 8&9(-19) was recovered, although the well was backflowed for 18 injection volumes. Wellbore recovery percentages were 40% for the continuous tracer and 10% for the slug tracer.

4.3.5 Chemical Reactions. Preliminary interpretation of the chemical data shows that the halogens Cl, Br, and I behaved conservatively. Sulfate, which was already present in the geothermal fluid, also behaved conservatively. Silica and calcium, however, were precipitated in the formation. The actual concentrations of silica and calcium in the recovered fluid are illustrated in Figure 9 and 10, respectively. Also shown in these figures are the predicted concentrations of silica and calcium calculated from the conservative elements, based on the assumption of no mineral precipitation. These figures show that silica precipitated rapidly when the injectate was introduced into the formation. It is not known at this time whether the minimum levels of silica within the injectate were controlled by kinetics or equilibrium. The minimum concentrations within the injectate in each test are close to the value predicted by equilibrium with chalcedony. The silica concentration in the undisturbed reservoir is controlled by quartz.

Another factor common to each test is a hump in the silica curve which appears when 1 to 1.5 injection volumes have been recovered. This hump appears to be due to the dissolution of the metastable silica mineral precipitated from the injectate. The dissolution would be a result of contact with higher temperature formation fluid during recovery.

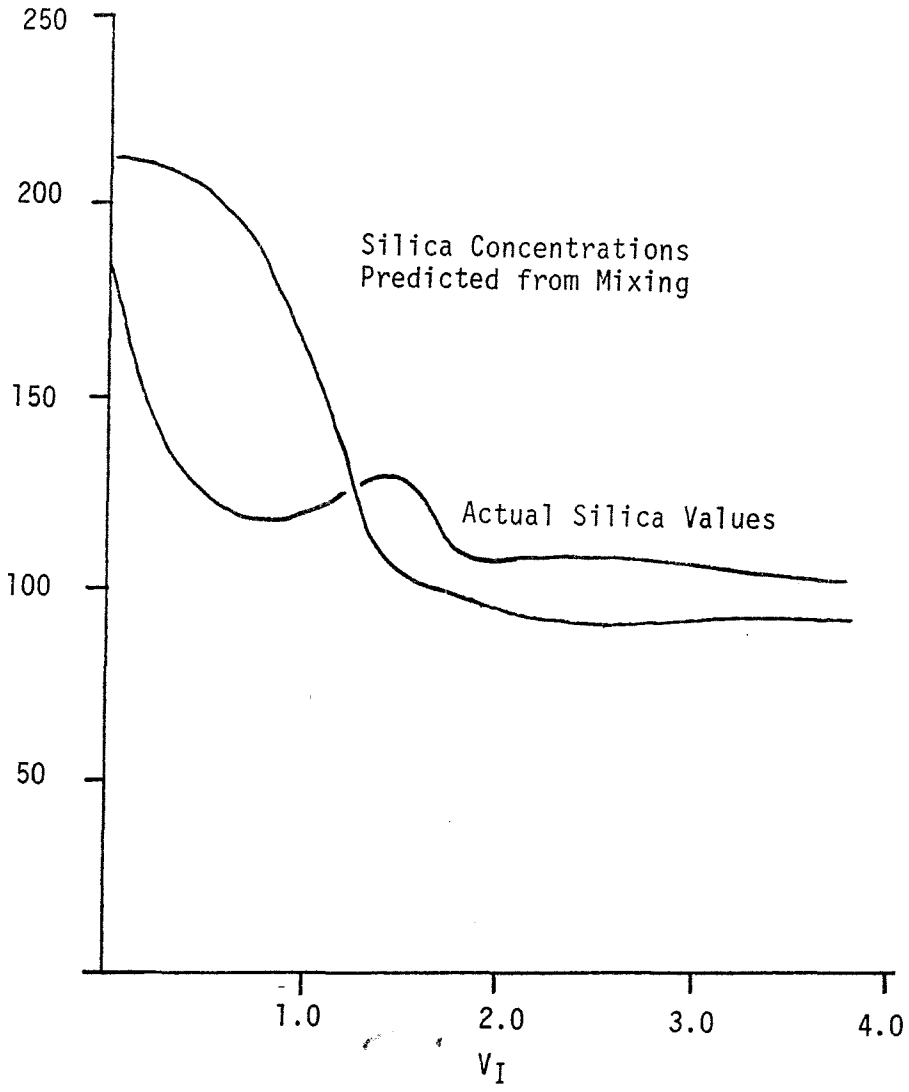

Figure 9. Silica Recovery, Test 6, East Mesa, Well 56-19

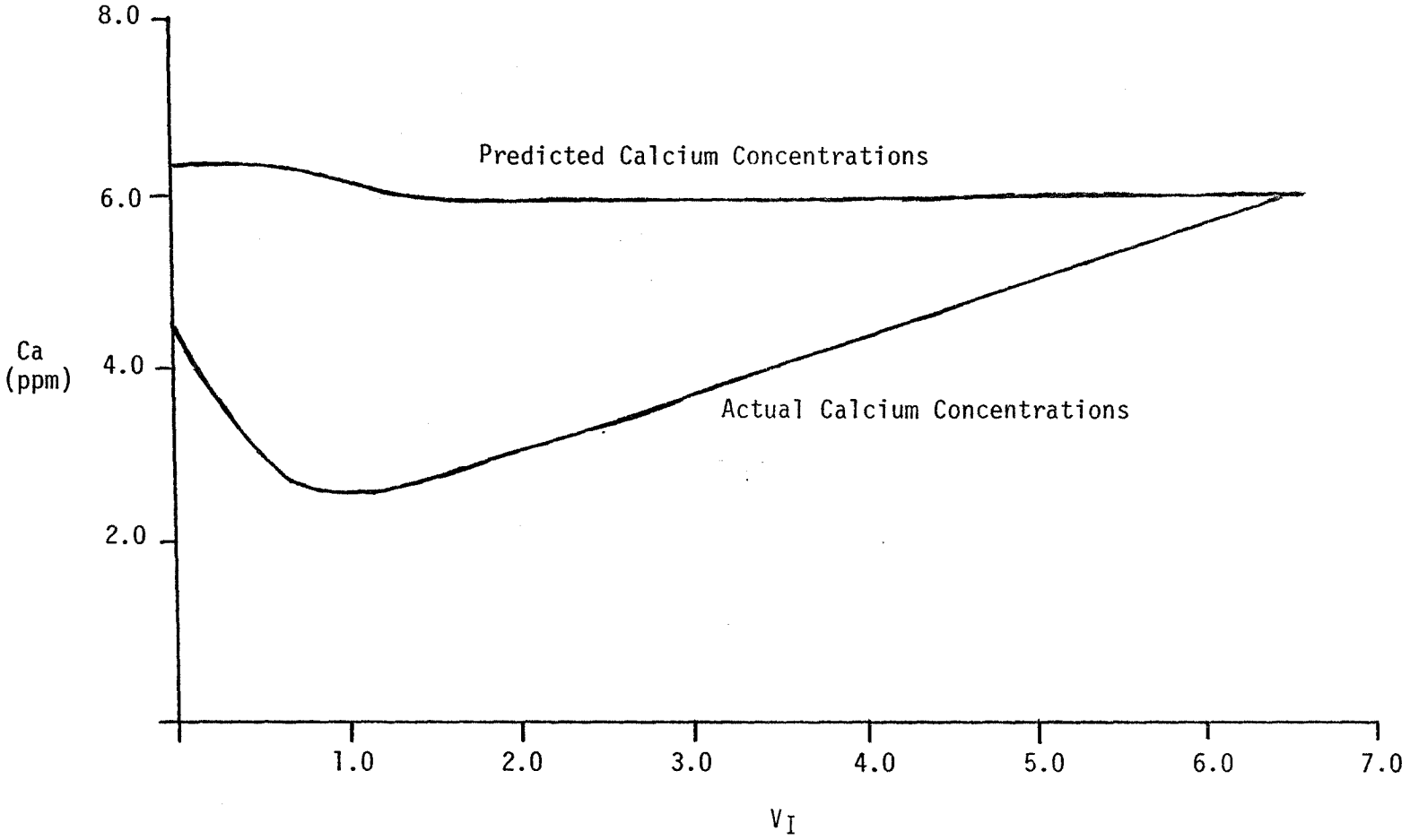

Figure 10. Calcium Recovery, Test 3, East Mesa, Well 56-30

The calcium curve (Figure 10) shows similar behavior. Calcium was lost in the body of the injected fluid and recovered from the precipitate by the formation fluid recovered. However, calcium was still being lost from formation fluid in which no injectate was present. This phenomenon was much more pronounced in the test of Well-56-30. The most probable explanation for the loss of Ca from the reservoir fluid is nucleation on newly-formed calcite precipitated from the injectate. Michels[2] has presented an extensive analysis of the calcium data. In his report he analyzed the effectiveness of the precipitation inhibitors used during the testing and was able to estimate a half-life for effectiveness of the inhibitor. The data were invaluable in that they indicated the inhibitor retained its effectiveness for a sufficient time to indicate there would be no plugging problem in the formation.

4.4 Reservoir Analysis

The overall objective of the reservoir analysis is to find means to predict the movement of fluid away from an injection well. It is hoped to meet this objective from an interpretation of the fluid mixing heat transfer and drift data which can be obtained from injection backflow testing.

To meet the overall objective of the reservoir analysis, five specific objectives were established for each well test. These objectives were directed at evaluation of:

1) Downhole flow distribution during various backflow and injection conditions.
2) Well pressure responses to various injection and backflow conditions.
3) Interference effects between the test well and adjacent observation wells.
4) Wellbore and formation heat transfer to production and injection fluids.
5) Dispersion of fluids in the reservoir.
6) Drift of the native reservoir fluids.

Results of analyses on each of these objectives is provided in the following sections.

4.4.1 Downhole Flow Distribution. The test plans prepared for Wells 56-30 and 56-19 were directed at the determination and evaluation of the following flow distribution parameters:

1. Well production zone(s).
2. Change in the production zone(s) with time.
3. Effect of flow rate on downhole production.
4. Well injection zone(s).
5. Change in the injection zone(s) with time.
6. Effects of injection of a "cool" fluid on the production zone(s).

Data to address these objectives were collected by using a borehole spinner tool and an isotope flow meter (56-30 only) to generate a set of borehole flow logs. In addition, downhole temperature data were collected and used to assist in the interpretation of downhole flow distribution. Interpretation of these logs was complicated by the irregular wellbore diameter outside the slotted liner and by difficulties with the instrumentation.

Well 56-30. A total of seven spinner and four isotope flow meter logs were run. As shown in Figure 11, the borehole flow data collected during the backflow phase were well defined and consistent for the different production rates. Approximately 90% of the flow is contributed from three primary zones. The remaining 10% comes from undefined zones. The major production zones for both flow ratres closely correspond, suggesting no difference in the producing zones for the different production rates and volumes. No good data were obtained during injection. Consequently, no findings can be presented with regard to the flow response of the reservoir during the injection phase.

Temperature and differential temperature logs were conducted during the backflow phase to complement the borehole flow data. The temperature increase and high temperature differential readings correlate with the production zones indicated by the spinner logs. It could not be

Figure 11. 56-30 Well Production Zones

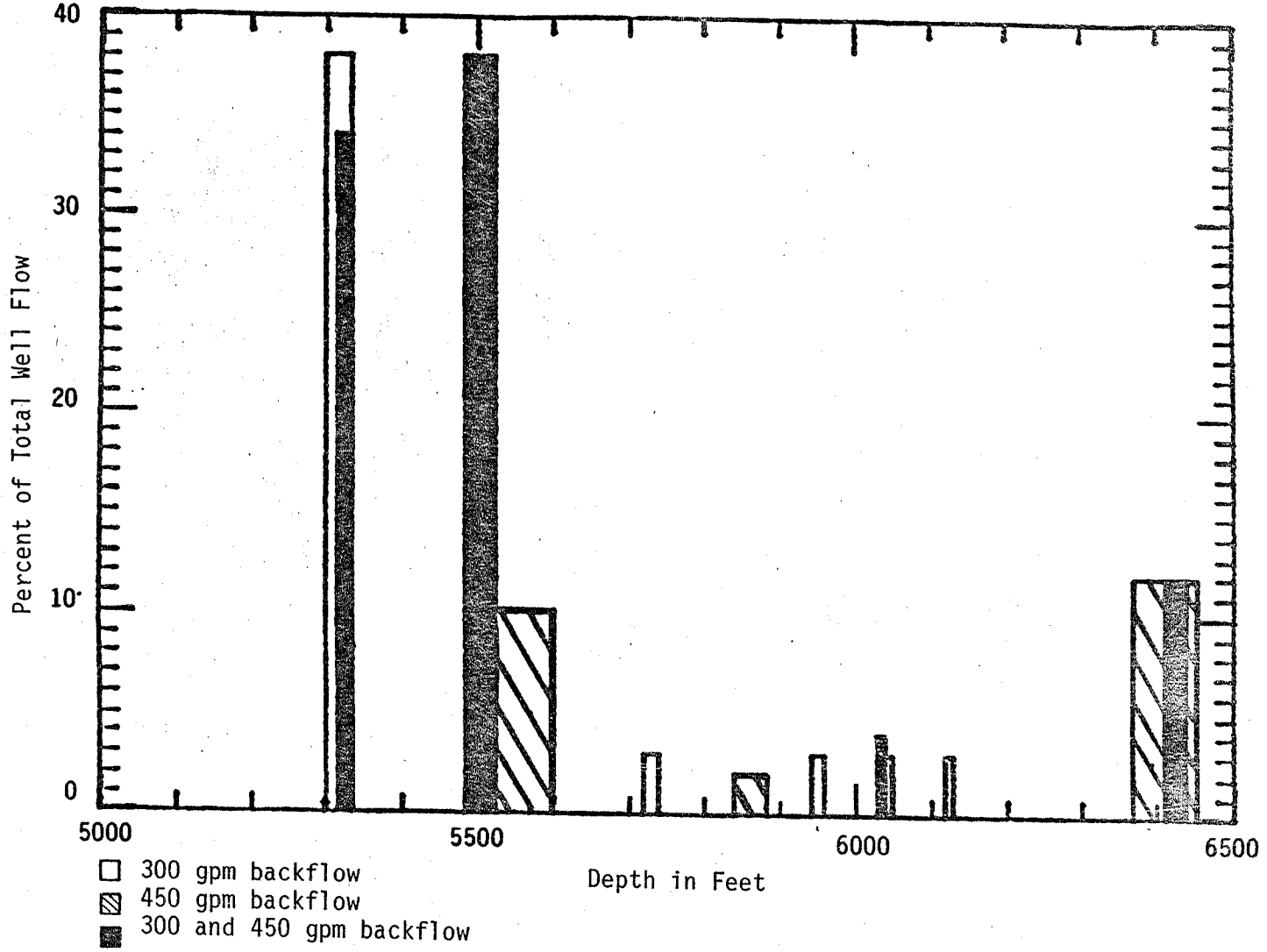

determined if the production zones are changing with the production time and rates, and if the injection zones correlate with the production zones due to the limited number of logs and relatively low sensitivity of the tool.

The spinner data collected was insufficient to determine if the production and injection zones change significantly with time or if the injection of a "cool" fluid affects the reservoir productivity or injectivity.

Well 56-19. Eight downhole spinner surveys were conducted during the different phases of testing. Four spinner surveys conducted during the backflow phase of testing were used to determine if the production zones are affected by a change in flow rate and/or production volume. Analysis of these spinner surveys, as shown in Figure 12, indicate that there are five primary production zones. Within the limits of the tool employed, a reasonable correlation of the spinner surveys demonstrate that changing the flow rate and production volume had no significant effect on the five production zones. Production from these zones constitute approximately 70% of the total; the other 30% is produced from various zones that could not be correlated between tests.

Three spinner logs were conducted during the injection phase of testing. Two primary injection zones were identified from this set of surveys. These zones appear to have a higher capacity than the production zones in the same depth interval. There are some indications there may be interzonal flow in Well 56-19 (See Section 4.4.4) and this may be associated with the changes in flow distribution.

The spinner logs conducted during shut-in well conditions failed to detect vertical movement within the wellbore. However, the spinner has a limited sensitivity and it would miss low flow rates.

Temperature and differential temperature logs were not conducted in this well due to problems with the equipment.

The data collected from the spinner surveys indicate that the production and injection zones do not change with time. The effect of the "cool" fluid injection on the production zones could not be measured,

Figure 12. 56-19 Well Production Zones

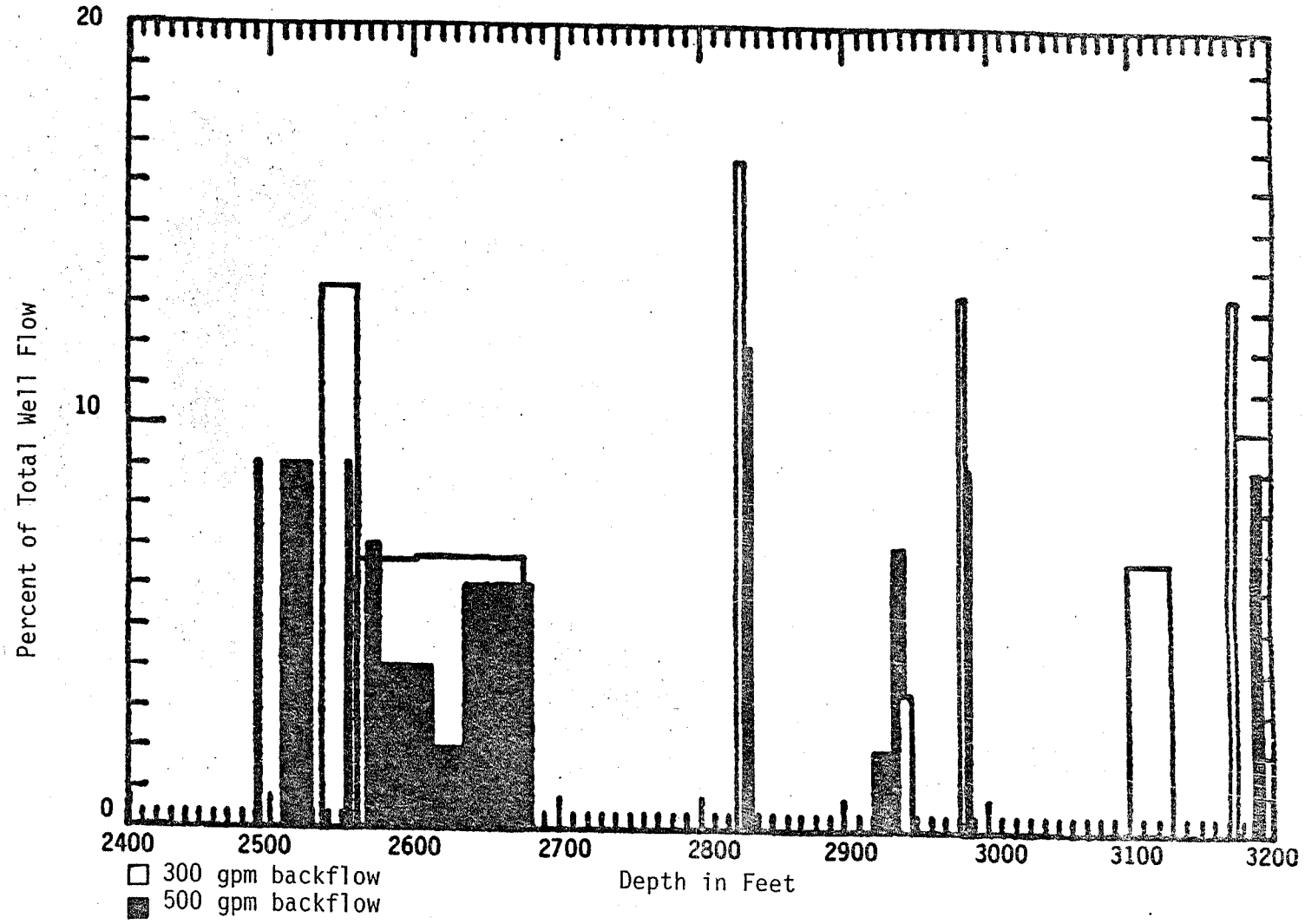

however, transmissivity calculations (See Section 4.4.2 and Figure 16) suggest that the cool fluid injected affected the production zone(s).

Comparison of Test Wells. The flow distribution in Wells 56-30 and 56-19 varied substantially. Well 56-30 has three production intervals contributing approximately 90% of the total flow. The total thickness of the producing intervals for 56-30 is about 140 feet. Well 56-19 has five production zones contributing about 70% of the total flow and several less significant producing zones. The flow distribution data provided valuable information for the evaluation of the tracer data and the computer simulations.

4.4.2 Pressure Response. The well response to injection and backflow are recorded during geothermal well testing to provide the necessary data to calculate the hydraulic parameters of the reservoir. Wellhead and downhole temperature/pressure measurements were made at pre-determined time/intervals to satisfy the requirements of this test objective. The downhole measurements were taken to record the effect of hydrostatic pressure changes within the wellbore which are difficult to assess with wellhead instrumentation alone. Wellhead temperature/pressure data were continuously recorded and the downhole temperature/pressure data were collected during the intitial phases of each test sequence (i.e., initiate backflow, terminate backflow, initiate injection, etc.). The objectives for taking these measurements are to:

1. Obtain baseline drawdown and recovery data.
2. Obtain drawdown and recovery data at a second flow rate.
3. Compare measured reservoir characteristics during injection with data obtained during production.
4. Determine if cold water injection affects the well flow characteristics.
5. Determine the maximum flow rates for wells 56-30 and 56-19 at which flashing will not occur.
6. Determine if the increased injection flow rate affects the well flow characteristics of Well 56-19.

Well 56-30. Two baseline production/recovery and two injection/backflow tests provided data for the calculation of reservoir transmissivity. The baseline tests were conducted at 300 and 450 gpm flow rates. The injection tests were run at 300 gpm. A summary of the calculated transmissivity (kh) values for these tests is presented in Figure 13. Pressure responses to the 300 and 450 gpm blackflow tests and the 300 gpm backflow tests after cold fluid injection, measured at 5,000 feet are presented in Figure 14. The pressure response for the 300 and 450 gpm flow rates provided expected results and comparable drawdown data. However, the pressure response recorded, following the 300 gpm cold fluid injection, results in a decrease in calculated reservoir transmissivity values (see Figure 13, Note 1). This data suggests that cold fluid injection affects the reservoir characteristics, decreasing the transmissivity.

Well 56-19. An extensive test program was conducted at Well 56-19. Two production/recovery tests and four injection/backflow tests were run during the test program at this well. The first two flow tests were repeated because of problems encountered with gas production and flow control. Attempts to mitigate these problems were not successful; consequently, the pressure and temperature measurements, particularly at the wellhead, are considered unreliable. In addition, numerous mechanical problems with the downhole pressure/temeprature tool were encountered, apaprently due to turbulent wellbore conditions. This problem is believed to have resulted from a rupture in the casing at depth.

The backflow and injection tests for Well 56-19 were conducted at 300 and 500 gpm flow rates. Pressure responses to the 300 and 500 gpm injection flow rate measured at a depth of 2450 feet are presented in Figure 15. Pressure buildup for the 300 gpm rate is greater than for the 500 gpm injection test. The 300 gpm test also gave a different tracer response and analysis is in progress to determine if the reason for this anomoly can be found.

Pressure data for different phases of testing for a 500 gpm flow rate were used to calculate reservoir transmissivity values. Calculated values

Figure 13. 56-30 Well Transmissivity

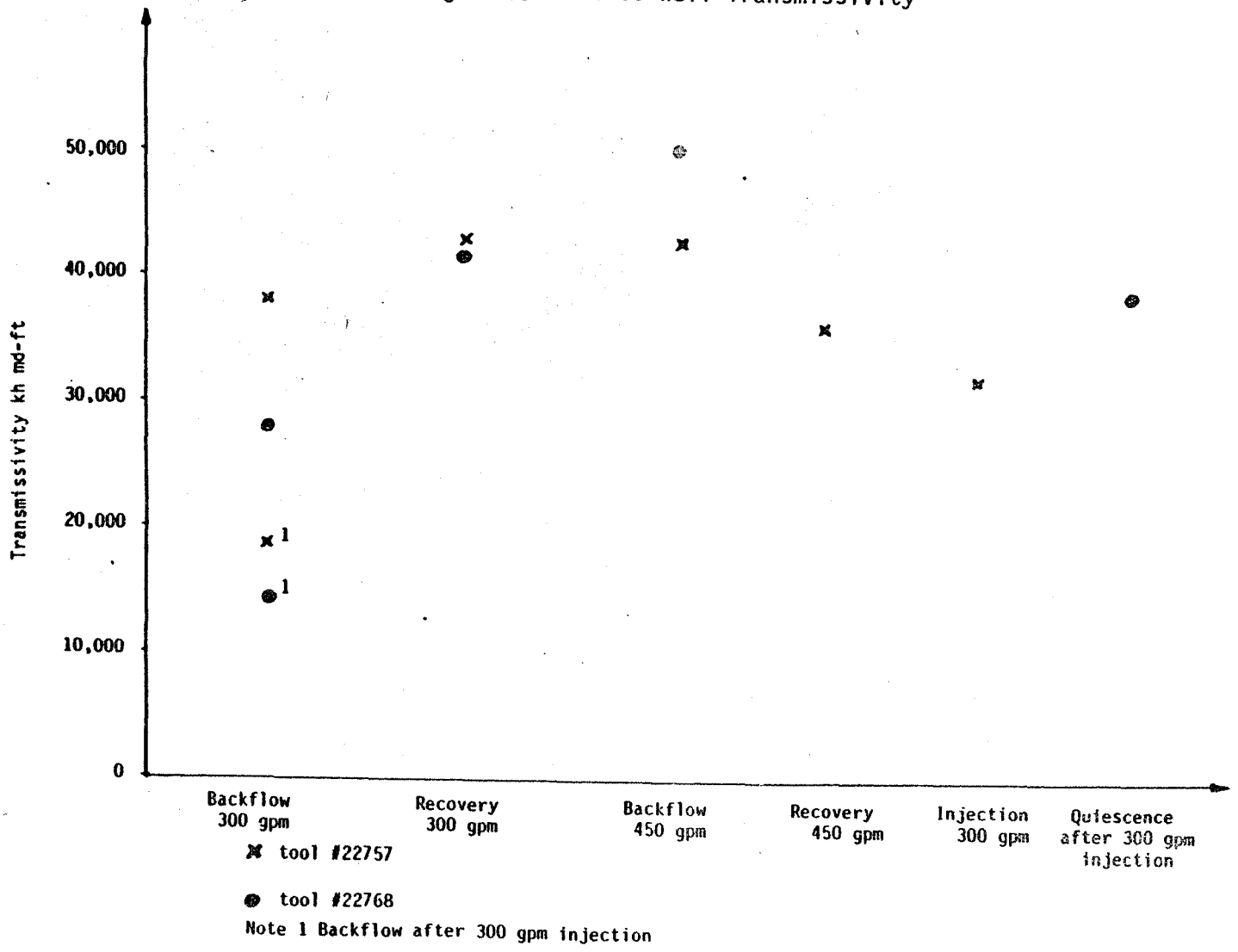

Figure 14. 56-30 Downhole Pressure Response to Backflow

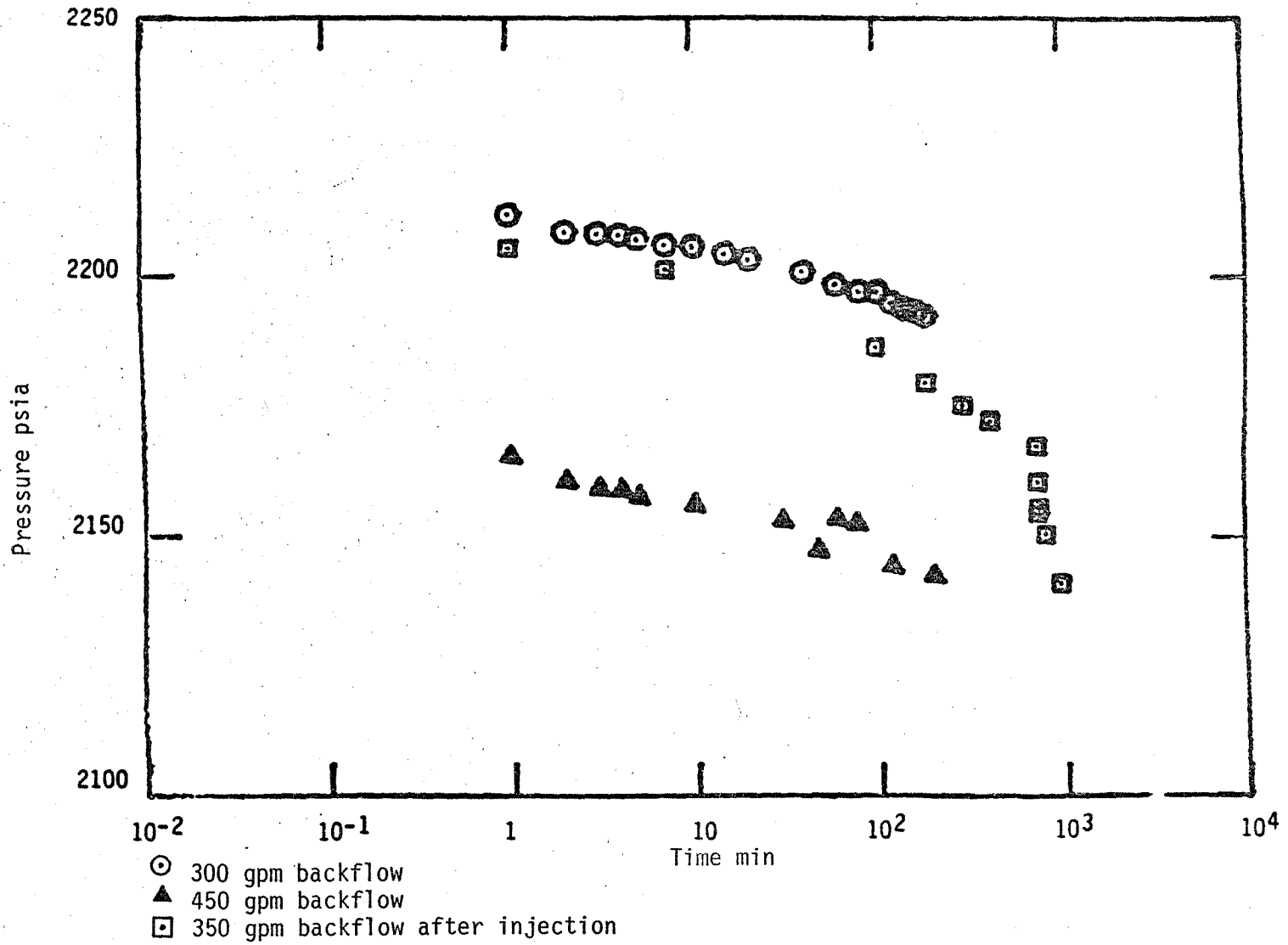

Figure 15. 56-19 Downhole Pressure Response to Injection

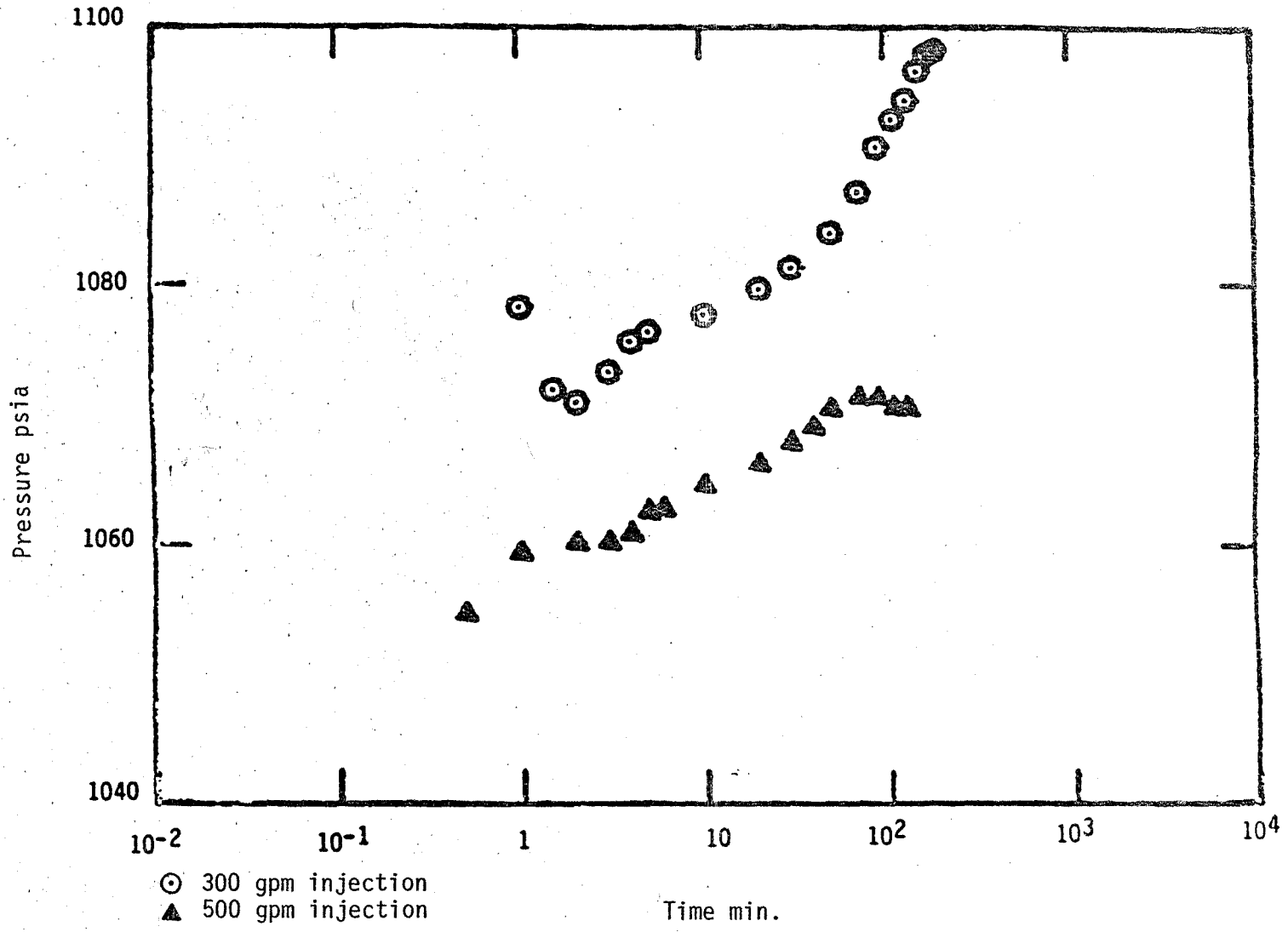

are presented in Figure 16. The values are widespread and inconsistent. The inconsistency is attributed to mechanical and interpretation problems with the downhole temperature/pressure tools, and off-gasing at the wellhead making it difficult to accurately measure pressure and control the flow. The values obtained from the injection tests are lower than those measured for the conventional production/recovery tests. The cold water injection appears to affect the reservoir hydraulic characteristics by decreasing the calculated transmissivity values.

4.4.3 Well Field Interference. This objective was designed to collect data to determine the effect of injection/backflow testing on nearby observation wells. In particular, this test objective provided a potential opportunity to conduct a conventional tracer breakthrough test and to compare the interpretation of data obtained from the tracer breakthrough with the interpretation of data from the injection/backflow test sequence.

Wellhead pressure data were collected from ten wells during the conduct of the test program in order to detect any interference effects. The location of the test wells and nearby wells monitored are shown in Figure/7. No interference effects could be detected as a result of any of the tests.

4.4.4 Wellbore and Formation Heat Transfer. Downhole and wellhead temperatures were measured and recorded to assist in the evaluation of wellbore and formation heat transfer. The downhole data were required in order to isolate formation heat transfer from that occurring in the wellbore.

The set of data for Well 56-30 has been used because its production temperature and production-minus-injectate temperature differential are much greater than those of Well 56-19. The downhole temperature was measured with the downhole temperature probe coupled with the pressure tool. The tool was lowered to a depth of 5000 feet, immediately above the slotted liner, for all downhole measurements used in this analysis.

Figure 16. 56-19 Well Transmissivity

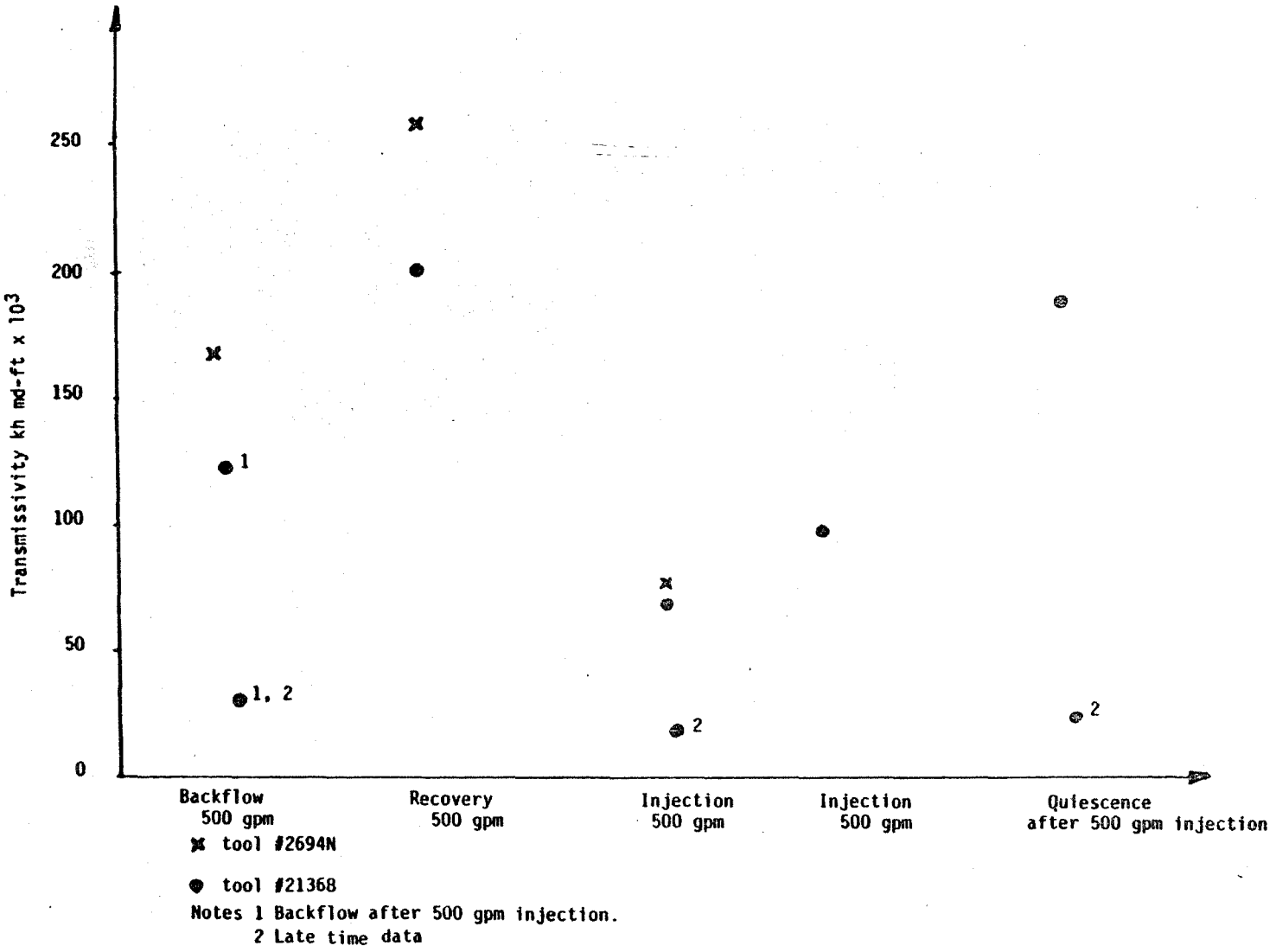

Figure 17. Location Map

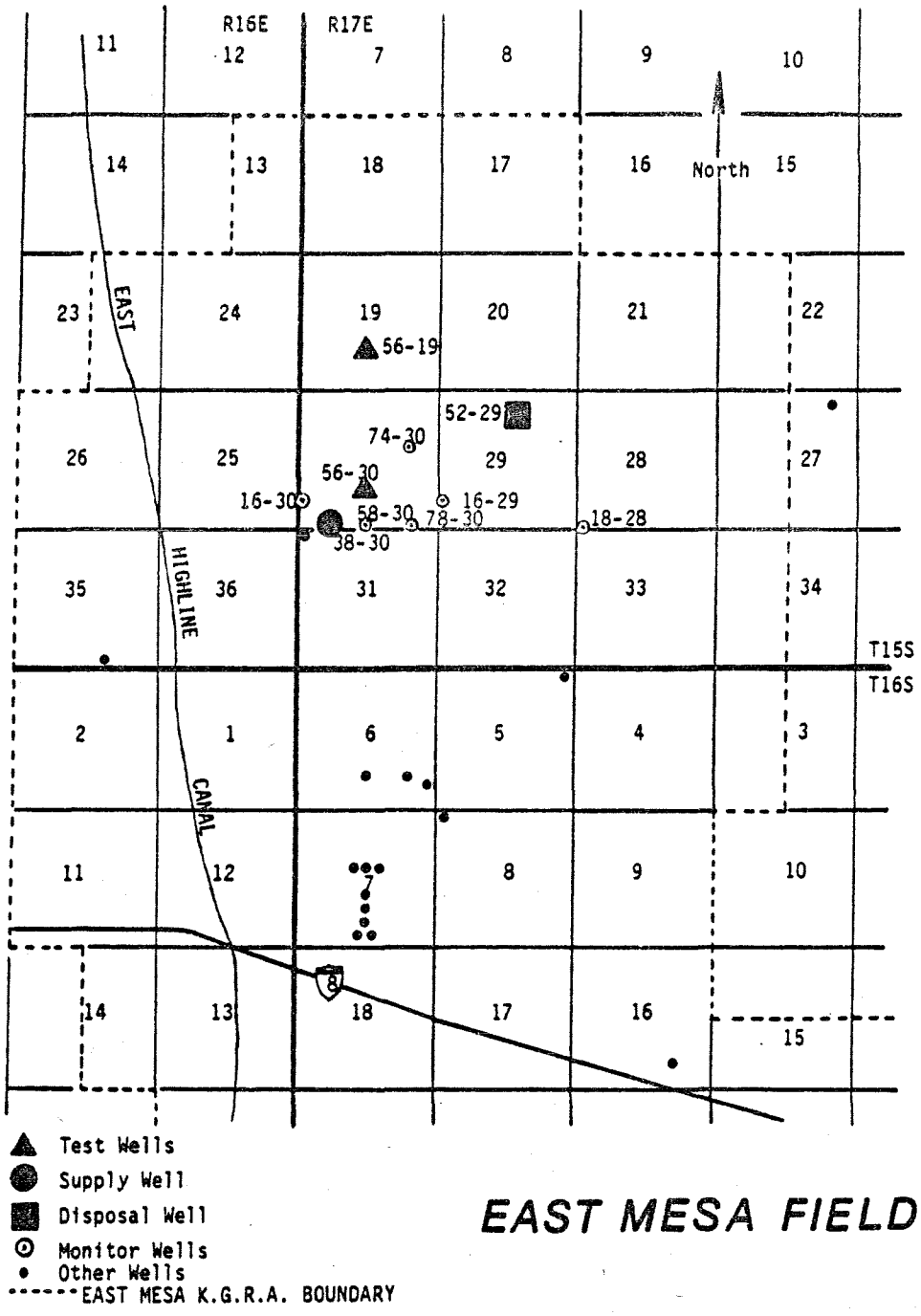

The initial production/recovery tests provided the opportunity to measure thermal losses within the wellbore by comparison of the downhole temperatures with those recorded at the wellhead. As expected, the wellhead temperature was lower than that at depth. After the wellbore had warmed to approach/obtain thermal equilibrium, this temperature differential was approximately 17°F. Assuming the rate of thermal loss is assumed to be linear, the rate of loss is 0.34°F/100 ft.

Heat transfer from the reservoir formation to the mixture of injected and native fluids was determined from the conduct of injection-quiescence-backflow tests. The downhole temperature measurements were taken immediately prior to the termination of injection, during quiescence, and during the initial backflow periods. The downhole thermal data for the injection/backflow tests with quiescent periods of twelve hours and six months are shown in Figure 18.

As can be seen in the figure, the fluid injected during Test 56-30-3 was at 207°F when it reached the 5,000 feet level. It began to increase in temperature immediately after termination of injection and continued to increase through the quiescent period. The temperature increased approximately 65°F, up to 272°, due to convective circulation of warmer water moving up the wellbore.

When backflow was initiated, the measured temperature dropped to 242°F (see Figure 18). This drop represents the replacement of convection mixed wellbore fluid with that drawn from the adjacent formation. The increase from this point has been extrapolated to the native fluid temperature of 320°F at approximately 22 hours of backflow. The dotted line on Figure 18 shows the temperature the fluid should have been if there were heat transfer. This was calculated using the mixing data from Figure 1. The difference in temperature between the two curves is the heat transferred from the reservoir rocks. To conduct detailed heat transfer analysis results from the FRACSL code prediction of fluid movement in the reservoir will be used.

Figure 18.
Thermal Response Temperatures at
5000 ft Depth, Well 56-30

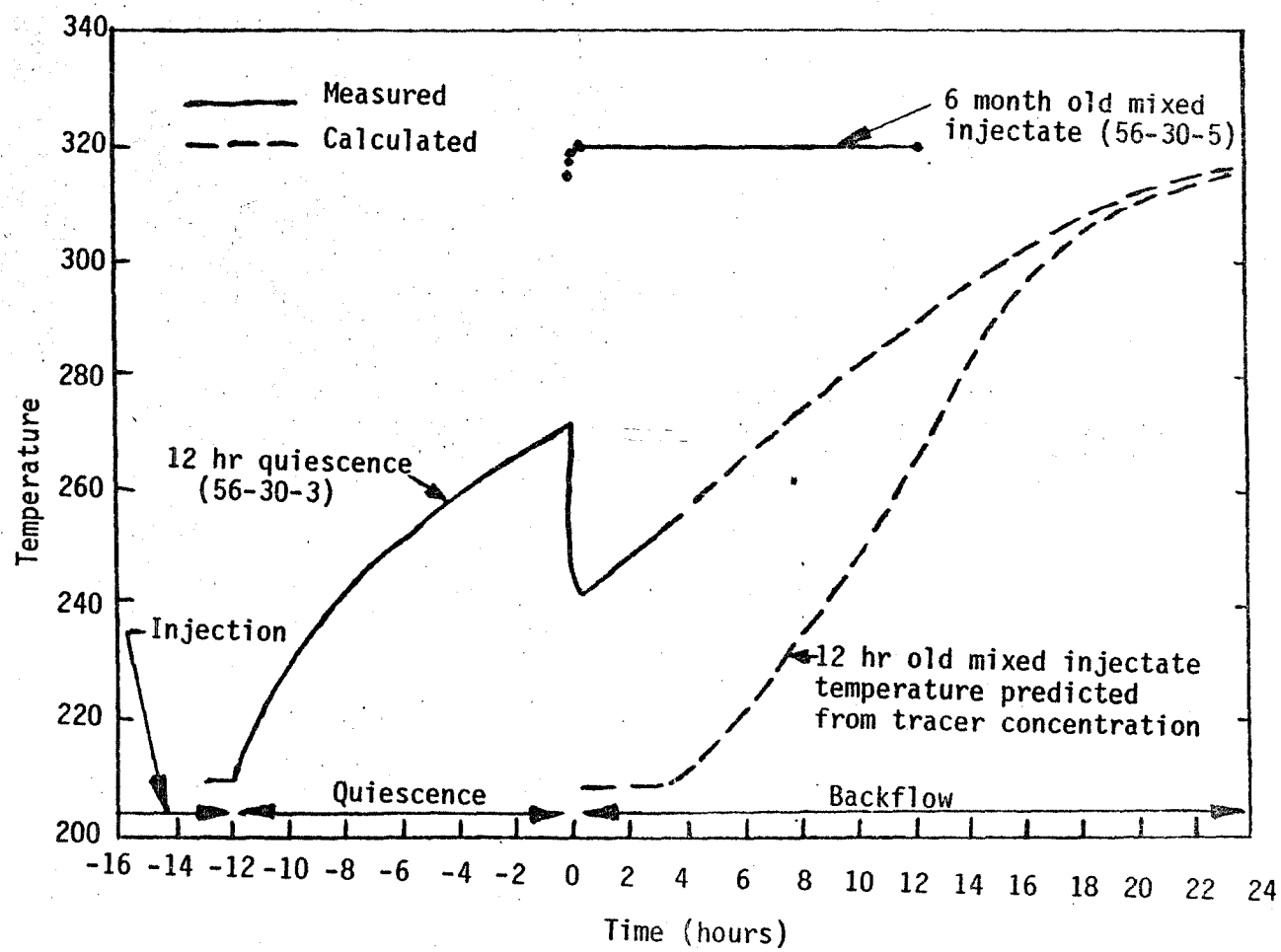

The temperature data for the fluid returning after the 6 month quiescent period are also shown. The fluid is at the reservoir temperature, however, the drift discussed in Section 4.4.6, indicates the initial fluid returning was not injected fluid and heat transfer analyses are not possible.

4.4.5 Analysis of Fluid Dispersion. Analysis of fluid dispersion in the East Mesa test wells was conducted using the FRACSL code. Details of the model input and operation for this study are summarized in Reference 18. Basically, the studies were conducted by developing a model using all available geology, wellbore, and reservoir engineering data. The reservoir was simulated as a single flat porous homogeneous area with a thickness determined by well log information and the horizontal size determined by the problem under study. The model was input with measured flows, both during injection and backflow. The dispersion was initially estimated by a technique described in Reference 18 and then adjusted until a best fit with observed mixing data was obtained. Dispersivity coefficients were then determined for both continuous tracers and slug tracers. It was found that one dispersivity coefficient for each well could be used to simulate both slug and continuous tracer data. The theoretical significance of the dispersivity coefficient is fully discussed in Section 4.5.3.

Specific objectives for the dispersion studies were to 1) compare the dispersivities of Wells 56-19 and 56-30 to determine if this information could be used to help plan field development, 2) to parametrically study the effect of injection volume to determine if theoretical concepts for dispersion in homogeneous models are applicable at East Mesa and 3) to parametrically study the effect of a change in injection rate for the same reasons as Objective Number 2.

Representative matches of predicted slug and continuous tracer return using FRACSL and test data are shown on Figure 19 and 20.

In general, good agreement was obtained from all tests illustrating that FRACSL has adequate capability to analyze dispersion data in a homogeneous reservoir.

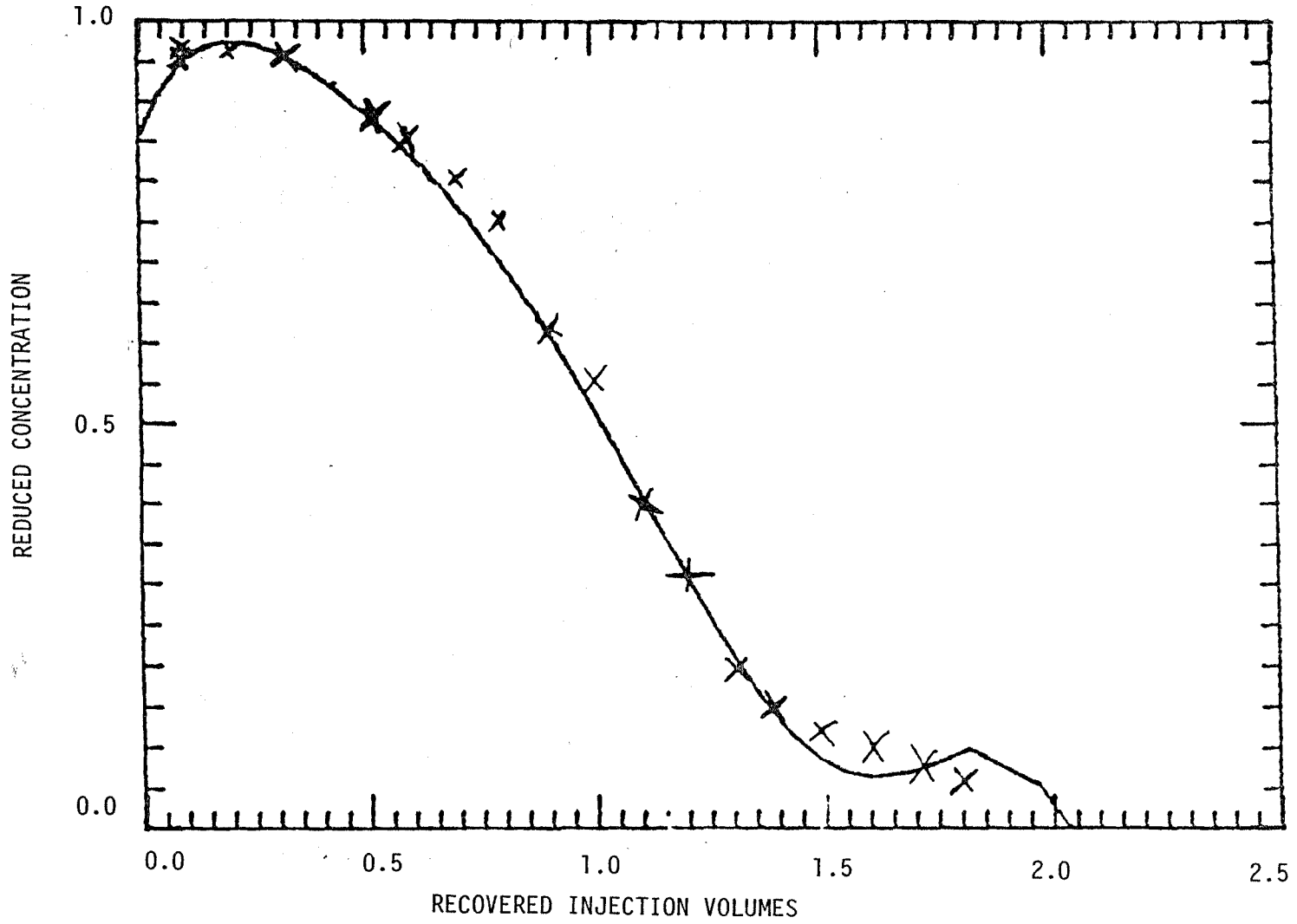

Figure 19. Comparison - FRACSL and Data Test 6 Well 56-19

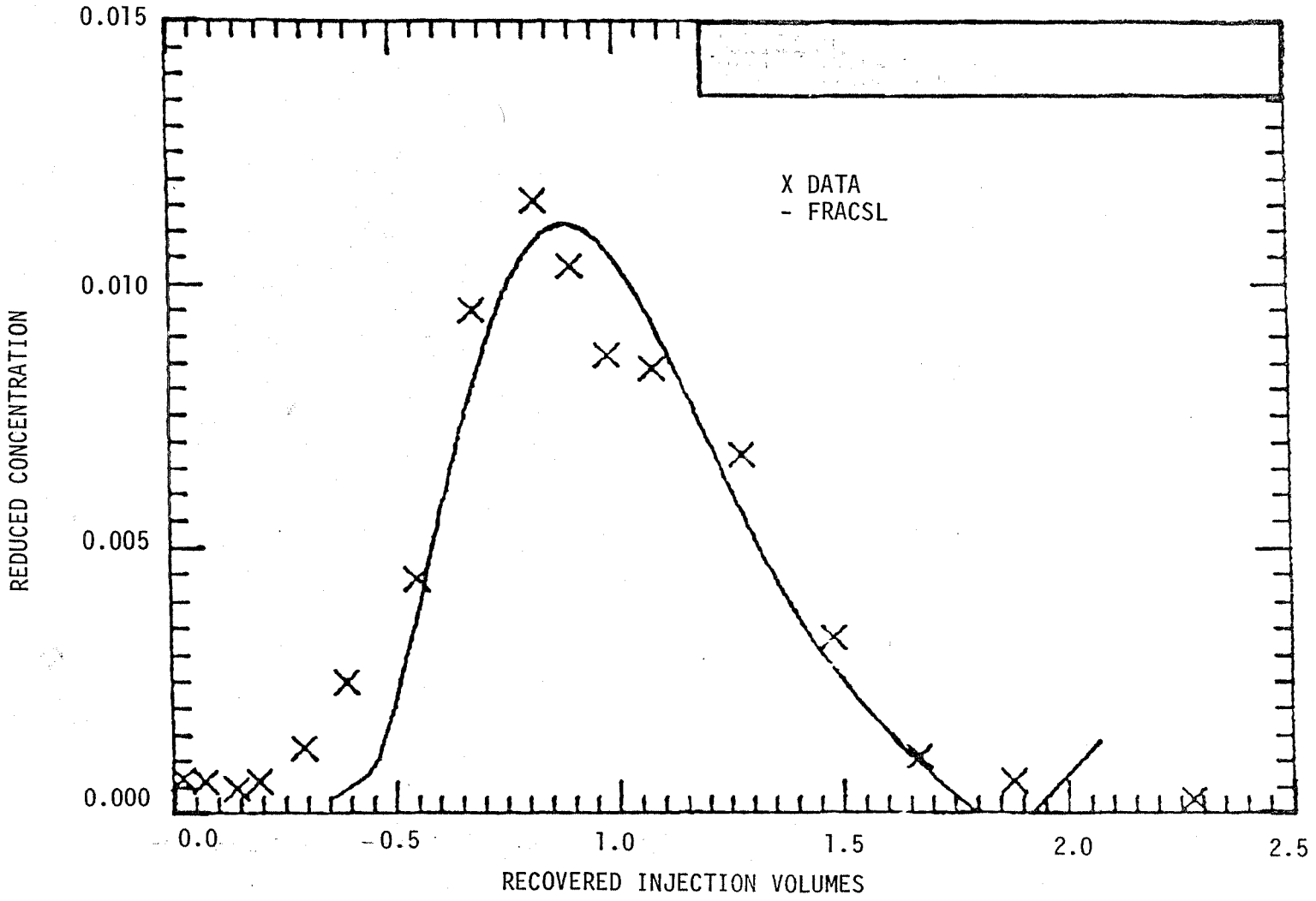

Figure 20. Comparison FRACSL and DATA Test 3 Well 56-30.

The following are conclusions relative to the objectives:

1) Comparison Wells 56-19 and 56-30. A dispersion coefficient of 0.29 was obtained for Well 56-30 and 0.54 for Well 56-19. The known information about the East Mesa reservoir does not indicate any particular reason why the dispersion coefficients should vary between the wells. It is suspected that the fact that the reservoir was simulated as a single porous layer rather than multiple layers may be the cause of the problem. Particularly on Well 56-19, this assumption may be a problem. The spinner data and pressure data (See Sections 4.4.1 and 4.4.2) indicate differences between injection and backflow which could cause the assumption of a single equivalent flow area to be in error. Additional studies are planned in FY-85 to assess this theory.

2) Effect of Increased Injection Volume. The same dispersion coefficient was obtained with injection volume varied by a factor of 2 (Tests 4 and 6, Well 56-19). This close agreement verifies the theory for mixing in homogeneous systems which suggest that the dispersion coefficient should not change.

3) Effect of a Change in Flow Rate. The tracer return shape from the 300 gpm injection test at Well 56-19 was vastly different in character than for any of the other injection backflow tests at East Mesa. The data obtained from this test could not be matched adequately by FRACSL simulations.

   It is possible that the data could be matched with a multiple layer approach in which the injection flow split between layers differs from the backflow flow split. Differences in flow split could be caused by a nonhydrostatic pressure distribution in the reservoir layer. This theory, however, does not readily explain why the effect was observed at 300 gpm and not at 500 gpm. Additional work is planned on this anomoly.

4.4.6 Drift of the Native Reservoir Fluids. Drift was studied in both Wells 56-19 and 56-30 by conducting a baseline injection backflow test with a 12 hour quiescent period between injection and backflow and then

repeating the test with approximately a six month quiescent period. This was accomplished with Tests 8 and 9 at Well 56-19 and Test 3 and 4 at Well 56-30 (See Table 2).

Almost no tracer returned in Well 56-19 and a significant delay in the return of tracer was obtained at Well 56-30. This can be seen by comparing Figure 1 which had the 12 hour quiescence with Figure 5 which had the 6 month quiescence.

Five possibilities can be visualized as a cause for the delayed return of the tracer from Well 56-30.

1) Adsorbtion of the tracers in the reservoir.
2) Change in the reservoir flow characteristics.
3) Thermal gradients with each reservoir flow zone.
4) Flow between zones in the reservoir due to thermal or hydraulic gradients.
5) Natural convection in the reservoir.

The following summarizes conclusions relative to each of the possibilities:

1) Adsorbtion. Adsorbtion of the tracers into the rocks is not considered to be a reasonable possibility for two reasons; 1) if the tracers had absorbed into the rocks it is most likely they would have desorbed in an exponential decay, i.e., a gradual decline in tracer return rather than the peak observed, 2) it is considered highly unlikely that both the slug tracer and continuous tracer would have desorbed in an identical manner as shown on Figure 5.

2) Change in Reservoir Flow Characteristics. The reservoir thermal data obtained clearly show that thermal equilibrium had not been obtained after 12 hours of quiescense (See Figure 18). After 6 months the data show thermal equilibrium for the fluid surrounding the wellbore. Conceivably, the thermal effects could change the flow chracteristics but no reason can be visualized for the thermal effects to selectively push the injected fluids out into the reservoir.

3) Thermal Gradients Within a Flow Zone. The injected fluid is cool and convection could cause hotter fluids to flow over cooler fluids resulting in a dilution. This, however, should result in a stretch out in the return of the tracer not the peaking which was observed.

4) Interzonal Flow. Hydraulic or thermal gradients could cause tracer to be removed from one layer and flow into a second layer. This could result in a delay in the return of tracer with a gradual increase and decrease in the tracer concentration. This is not considered a good possibility for Well 56-30 because the slug tracer should return with two peaks. The first peak being the slug removed from the exhausted zone and the second peak from originally injected fluid.

   At 56-19 interzonal flow is a possibility. A double peak in slug return was noted in Test 56-19-3 (See Figure 2) and the return of the continuous tracer was stretched out relative to other tests. However, the failure of this phenomenon to be demonstrated in other 56-19 tests makes this a very tentative conclusion.

5) Natural Reservoir Convection. Natural reservoir convection is considered the most likely possibility for Well 56-30. This conclusion is based on the orderly return of the continuous and slug tracers and a FRACSL analyses which demonstrated the feasibility of a drift in the injected plume. The FRACSL run was made by injecting fluid into the reservoir and adding a constant flow of reservoir fluid into one side of the 56-30 model while removing the same volume of fluid from the other side. The crossflow of fluid was adjusted until the peak of the tracer return from FRACSL matched the observed data. A comparison of the FRACSL prediction and the observed data is shown on Figures 21 and 22 for the continous and slug data, respectively. In order get FRACSL to match the shape of the curves it was necessary to assume that the injection plume was elliptical in shape and that it moved in a direction perpendicular to the major axis of the ellipse. Actual position and shape of the drifted elipse is shown on Figure 23. The data are the marker particles used by FRACSL to simulate injected fluid. 00 on Figure 23 represents the wellbore and the particles surrounding the 0-0 coordinate represent the shape of the fluid plume

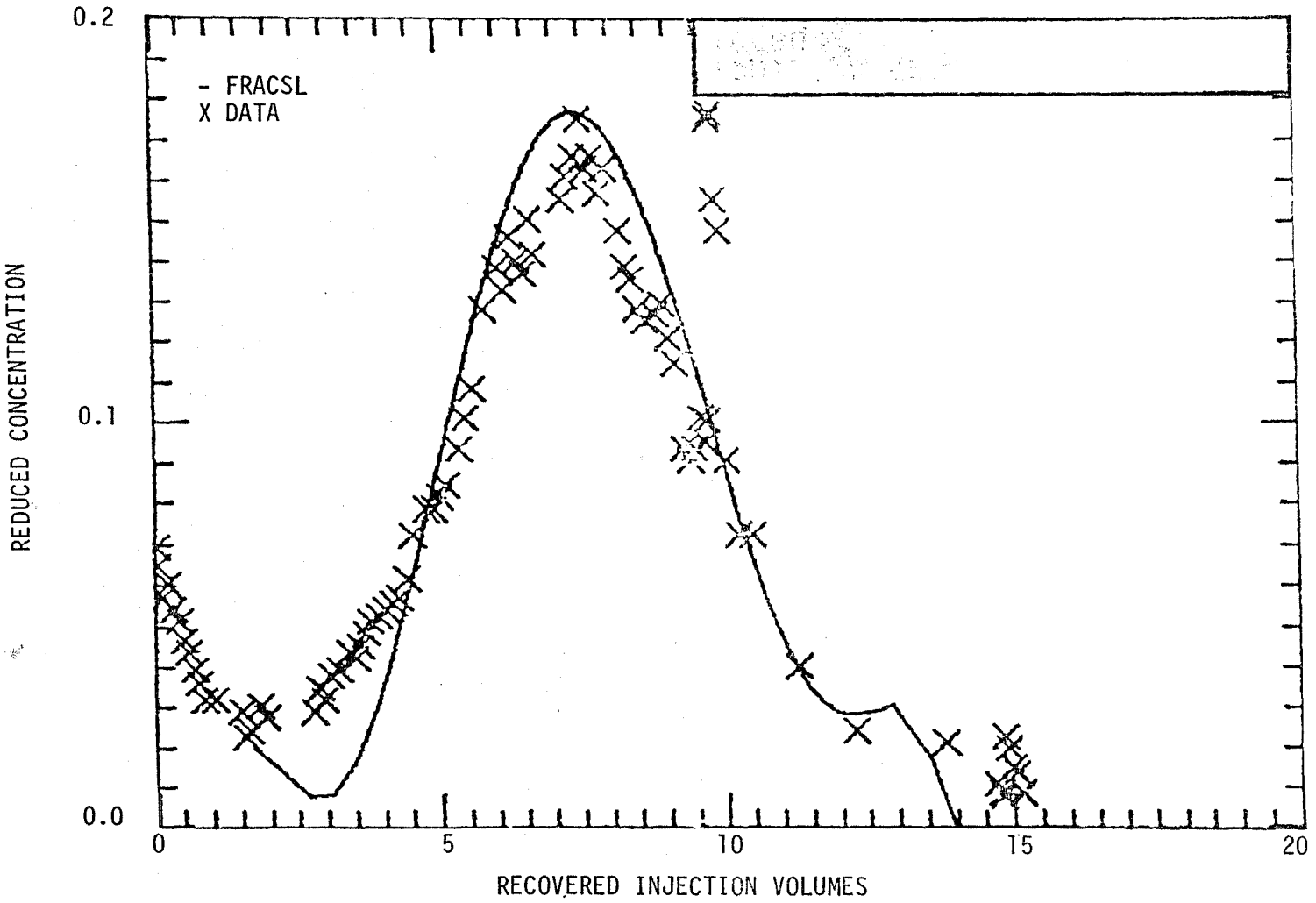

Figure 21. Comparison FRACSL and Continuous Tracer Return Test 4 and 5, Well 56-30.

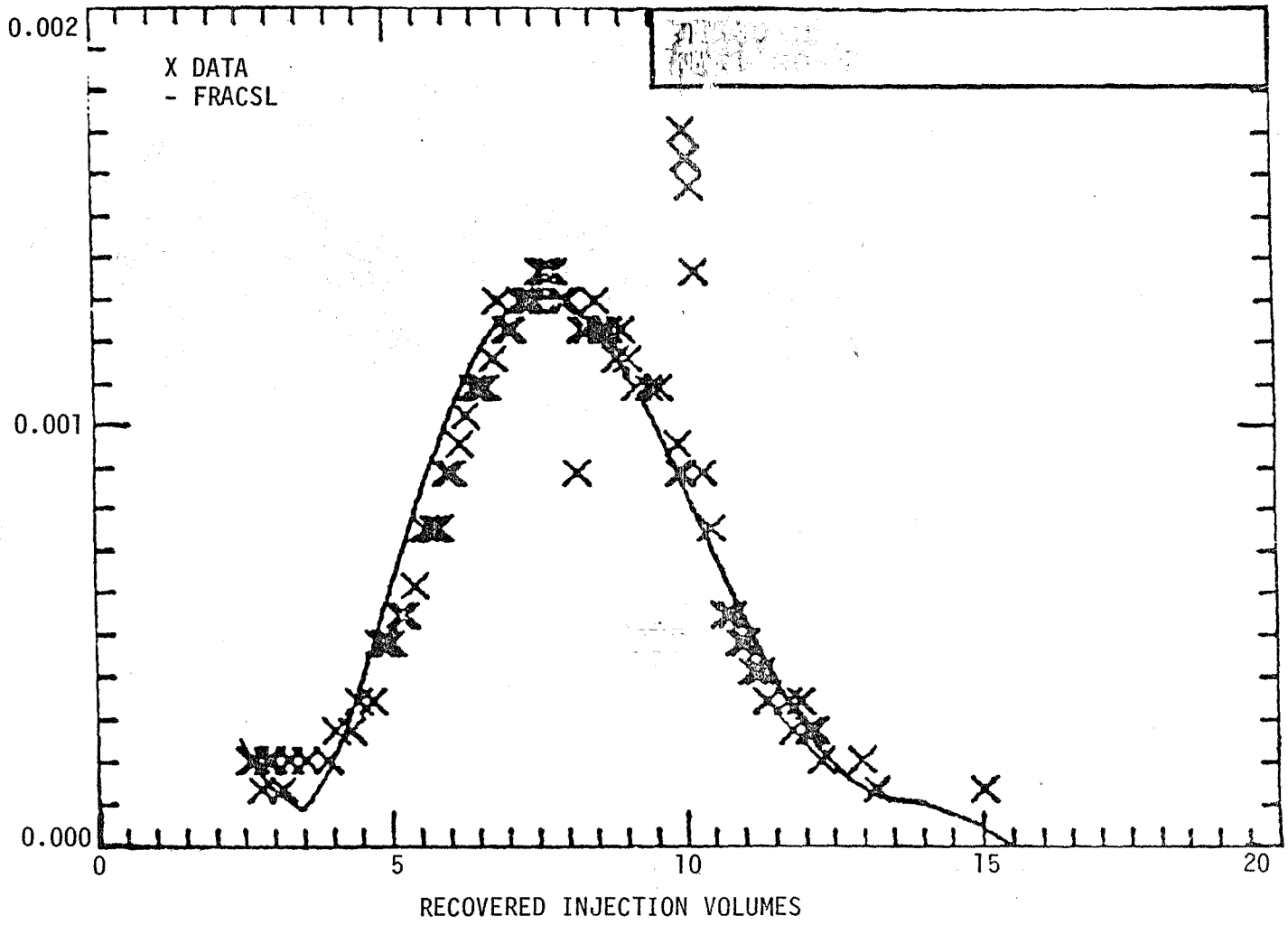

Figure 22. Comparison FRACSL and DATA Test 4 and 5, Well 56-30.

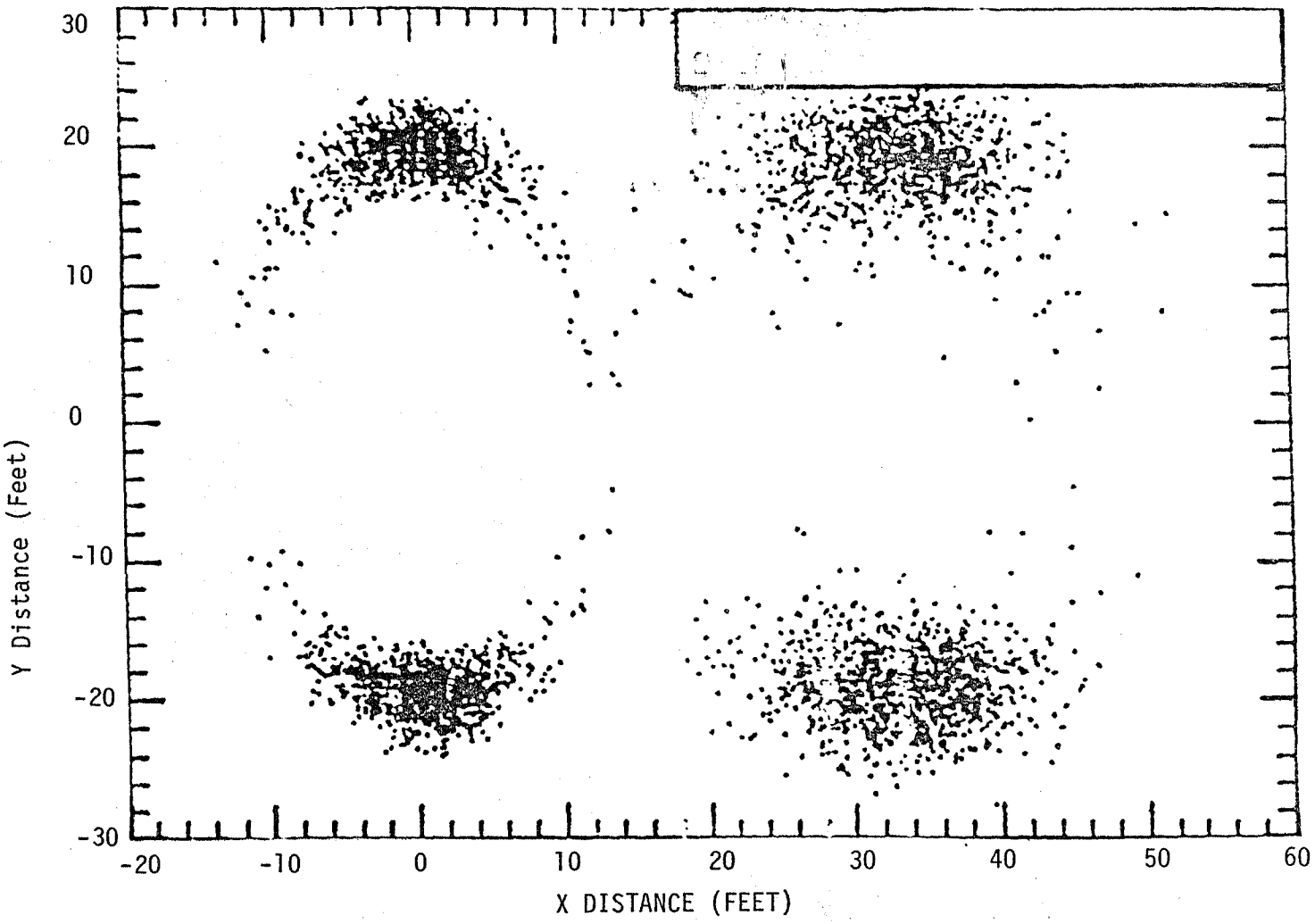

Figure 23. FRACSL Comparison Marker Particle Position After 6 Month Drift - Well 56-30

shortly after injection. The particles centered at the 0-32 coordinate represent the drifted injection plume. 32 is the estimated distance in feet that the plume has moved and the increased scattering of the particles represent the dispersion which occurred while the plume was drifting.

The hydraulic gradient calculated by FRACSL to move the fluid is .014 ft/ft. This is considered to be an unreasonably high gradient to exist over an entire field. East Mesa, however, has a number of vertical fractures which may result in regional hydraulic gradients which in turn could give localized fluid movement similar to that calculated to exist at Well 56-30.

4.5 Physical Model Studies

4.5.1 Purpose. The purposes of the laboratory scale fracture network experiments are to study mechanisms controlling solute transport under conditions of known fracture parameters, to evaluate injection-backflow test procedures under conditions of known reservoir parameters, and to acquire data for validation of numerical models. Validation of computer codes against laboratory data collected under controlled conditions, provides reassurance that the codes deal with important processes in a realistic manner.

4.5.2 Overview of Models. Five physical models are being used to study fracture flow:

1) Single fracture model
2) Fracture junction model
3) Multiple fracture, multiple junction model
4) Porous media block model
5) Dual permeability, multiple fracture model

The first three models are made of plexiglass, which allows visual observation of tracer movement by using a dye added to solutions. Plexiglass is easy to work with, impermeable, and nonconductive of electricity. Sheets of plexiglass ranging from 1 cm to 2.54 cm have been used. The fractures are cut into the plexiglass using a milling machine. Fractures are not cut through the plexiglass, which precludes the need for sealing the bottoms of the fractures. The tops of the fractures are sealed with thin plexiglass cut to match the shape of the fracture or fracture network, producing a lattice effect. With the lattice structure, glue (ethelyne dichloride) is pulled under the cover plate by capillary action, giving a good seal.

Two solutions are used in the models to study the mixing characteristics between miscible fluids. The native fluid consists of distilled water dyed yellow with food coloring. Tracer solution is a dilute solution of KCl in distilled water with blue food coloring added. Thus, movement and mixing of the two solutions can be monitored both visually by observing

the color changes, and by measuring the resistivity of the fluid. The distillation process deaerates the water, and air bubble formation during testing has not been a problem. Entrapment of air during the initial filling operation can be a problem, however. Physical models are purged with carbon dioxide gas prior to filling, which flushes all air out of the model. Any carbon dioxide gas bubbles trapped in the model during subsequent filling operations are rapidly dissolved.

Piezometers are installed in fractures to measure pressure distributions. Holes are drilled through the cover plate of the model directly over fractures, and copper tubing, 2 cm long and 1.5 mm in diameter cemented flush with the upper wall of the fracture.

Platinum electrodes, 3.2 mm in diameter, are imbedded in upper and lower fracture walls to measure fluid resistivity. This permits very precise measurement of tracer concentration changes in the fractures without disturbing the flow field.

The fourth and fifth models are made of porous polyethylene. The porous polyethylene has a pore size of 40 microns and can be machined easily. It is somewhat like a sandstone in properties, with a porosity of 25% and an estimated permeability of 0.6 cm/min.

The small matrix block model is being constructed to determine hydraulic and dispersivity characteristics of the porous polyethelene for use in computer simulations of the dual permeability fracture network. The block is 15.25 cm long and 10.2 cm wide. Manifolds on two sides give constant head boundaries to control flow through the block. Flow tests will be conducted where pressure drop and flow rate are measured.

The fifth model is also under construction. A fracture network has been designed (Figure 24) and the pieces have been cut. Tolerances in the machining are ± 125 microns. Fractures are planned to be 380 microns, which is dictated by the smallest saw blade available to make the deadend fractures. The model will include one inlet and one outlet port, and will be fully instrumented with conductance and pressure probes when completed.

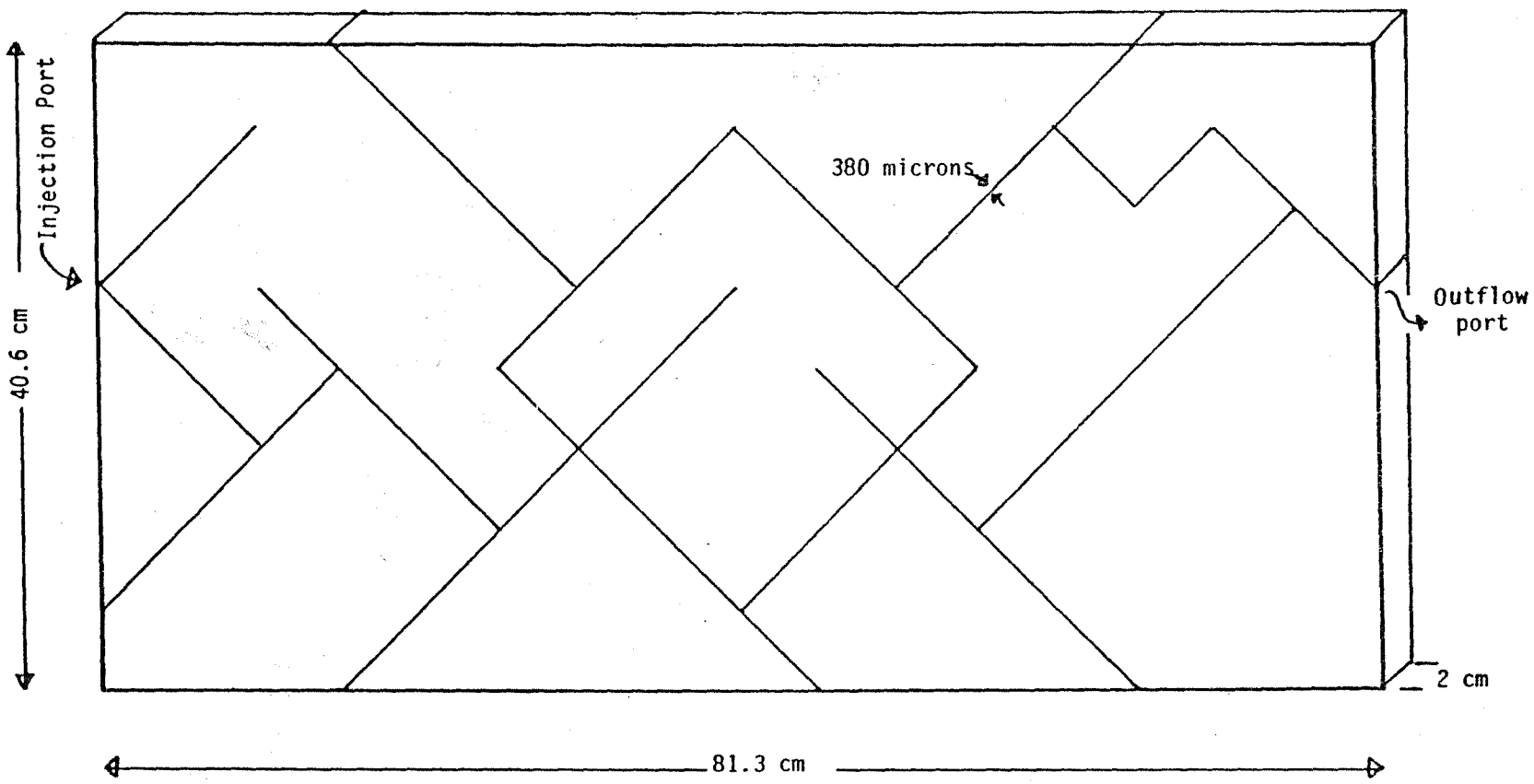

Figure 24. Design of fracture system dual porosity model.

4.5.3 Literature Survey. An extensive literature survey has been conducted to develop basic concepts for analyzing the fracture flow data obtained from the laboratory models. Most approaches to dispersion in fractures are based on parallel plate theory. Dispersion is related to the parabolic velocity profile that develops due to friction against fracture walls. This is the most commonly used approach, and the one that has been adopted for current modeling studies, both numerical and in the laboratory. Ogata and Banks[19] derived an analytical solution for concentration in one dimension for constant concentration boundary conditions and a step input:

$$C/C_o = 0.5 \text{ erfc } \left(\frac{1 - T}{2\sqrt{T/Pe}}\right) + e^{(Pe)} \text{ erfc } \left(\frac{1 + T}{2\sqrt{T/Pe}}\right) \quad (1)$$

where

Co = initial concentration
C = concentration at distance x
erfc = complementary error function
Pe = Peclet number ux/D_l
D_l = longitudinal dispersion coefficient
T = dimensionless time, ut/x.
x = distance
u = mean velocity

The Peclet number is an important parameter in that it defines the shape of the breakthrough curve which will be obtained when a solute moves through a permeable medium. To use the generalized concentration equation, it was necessary to develop an equivalent form of the Peclet number for fraction flow.

Hull[20] derived an expression for the Peclet number for fracture flow and defined limitations for its use:

$$P_f = \frac{D_m x}{ub^2} \quad (2)$$

where

P_f = fracture Peclet number
D_m = coefficient of molecular diffusion

X = distance

b = fracture aperture

u = mean velocity

Hull showed that for Peclet numbers less than 157, the one-dimensional assumption is not valid and Equation 1 cannot be used. These criteria provided a basis for designing and analyzing data from the models.

4.5.4 Computer Codes. Three computer codes are used for analysis of the laboratory data:

1) PNLFRAC for simulation of flow in single fractions
2) SALE for study of fracture flow in junctions
3) FRACSL for simulation of flow in fracture systems

4.5.4.1 PNLFRAC--PNLFRAC is derived from the Prickett, Naymik and Lonnquist 'Random Walk" model[21] modified to simulate flow and transport in fractures. Velocities at nodes are calculated from analytical solutions to the velocity equation between parallel plates (2-D) or for flow in rectangular channels (3-D). Both two-dimensional and three-dimensional velocity fields can be employed, giving capabilities for both infinite parallel plates and rectangular channels, such as in the physical models. The code can handle single fractures only. Solute transport is by particle tracking. Advection is calculated from the velocity at the particle position in the fracture times the time step. The lateral position of the particle is changed by transverse diffusion within the fracture. This approach allows easy simulations in both two and three dimensions, and is valid over the entire range of laminar flow velocities. Because of symmetry, only one-half or one-quarter of the fracture need be simulated. There is no explicit treatment of dispersion, dispersion is handled on a mechanistic level by velocity profile and diffusion.

4.5.4.2 SALE--The SALE code is a fluid dynamics code from Los Alamos National Laboratory, written by Amsden et. al.[22]. The acronym for this code stands for Simplified Arbitrary Lagrangian Eularian. Both two-dimensional and three-dimensional versions are available, although all simulations carried out to date have been with the two-dimensional

version. The code had no provisions for solute transport, and so the same particle tracking algorithm used in the PNLFRAC code was adapted to the SALE code. The SALE code was initially used for single fractures until it was confirmed that an analytical solution to the flow equation would produce the same results. Most of the use of SALE has been to simulate single fracture junctions.

4.5.4.3 FRACSL--FRACSL is under development at EG&G. It is a reservoir level simulation code for dealing with flow in porous media, discrete fractures, and dual permeability media. It is described more fully in section 4.6.

4.5.5. Single Fracture Model Studies. A series of four runs were made in the single fracture flow model at velocities of 0.1, 0.3, 1.0 and 3.0 cm/min. These correspond to Peclet numbers of 110, 37, 11, and 3.7, respectively as calculated from equation 2. The results are shown on Figures 25-28. Good agreement was obtained between the predictions of PNLFRAC and the single fracture model. These results show that the theoretical concepts developed for analyzing flow in fractures are correct and the multidimensional effects which typically cloud laboratory studies have been properly accounted for. It also shows that the partical tracking routine used in all three simulation codes properly predicts the dispersion which will be obtained in fractures.

4.5.6. Fracture Junctions. A series of runs were made in the fracture junction model at varying flow rates. Within the ability to control flow, essentially no mixing was obtained. The laboratory runs were simulated with the SALE code and good agreement was obtained. Figure 29 shows a photograph of a laboratory test and Figure 30 shows a SALE simulation of the same test.

A conclusion from the laboratory studies and SALE simulations is that the conditions under which complete mixing at junctions will occur are limited, and a computer code that assumed complete mixing in its algorithm would cause increased latteral dispersion of tracer, and consequently decreased concentration peaks in the direction of flow.

Figure 25. Comparison PNLFRAC and DATA Single Fracture Model 3 cm/min

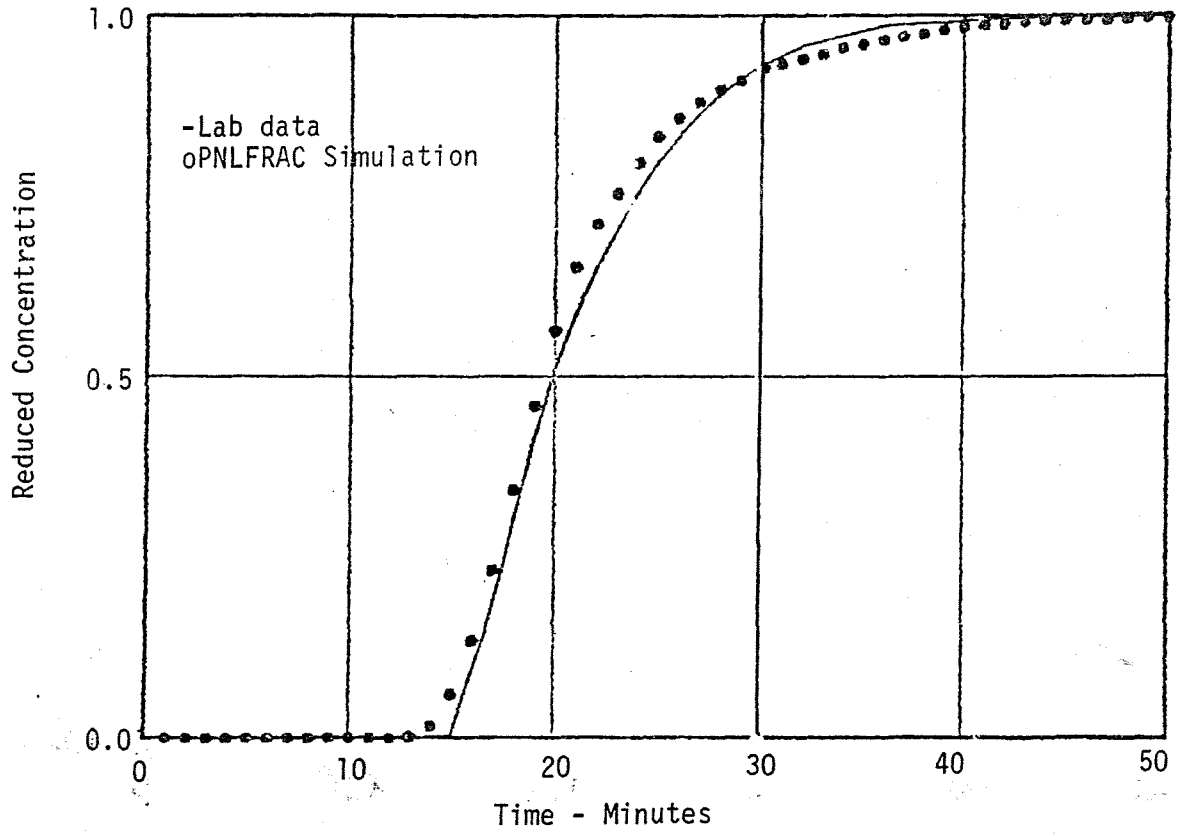

Figure 26. Comparison PNLFRAC and DATA Single Fracture Model 1.0 cm/min.

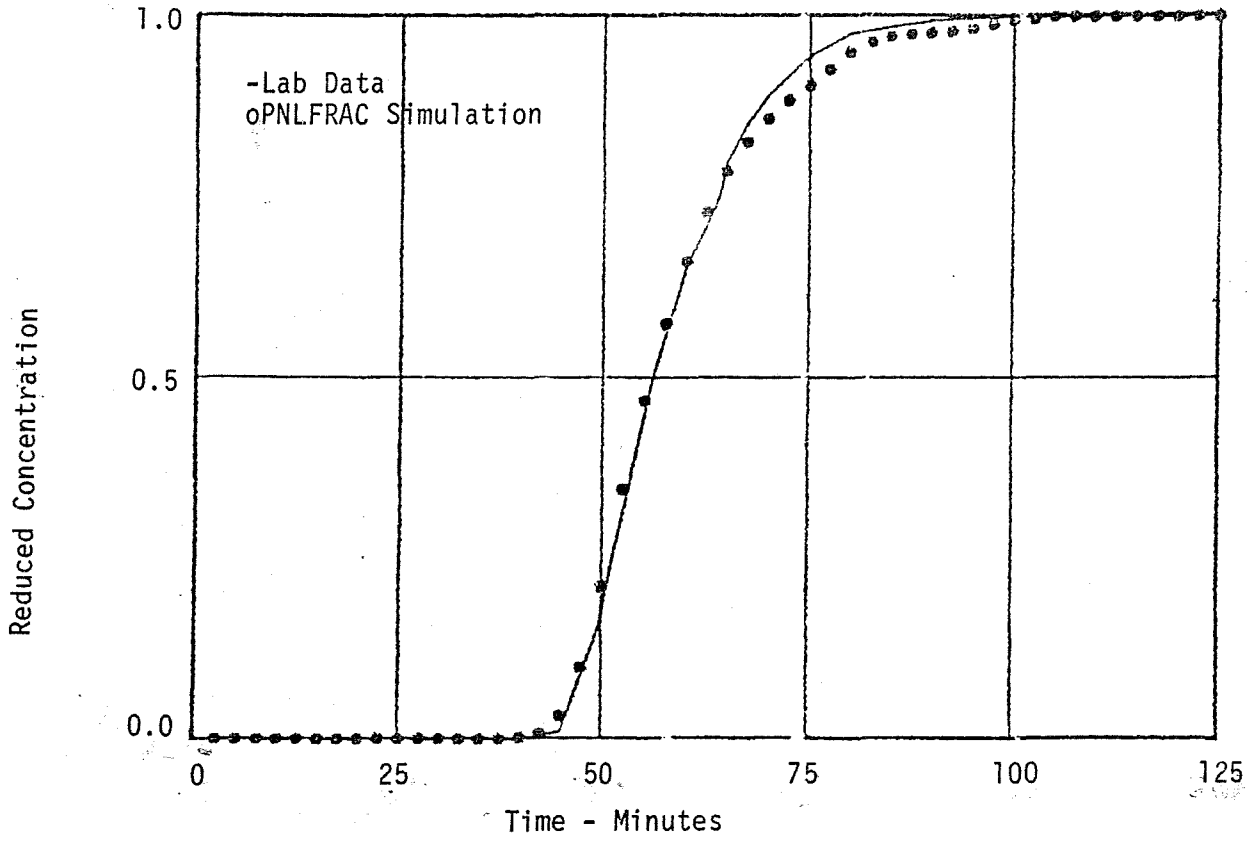

Figure 27. Comparison PNLFRAC and DATA Single Fracture Model 0.3 cm/min.

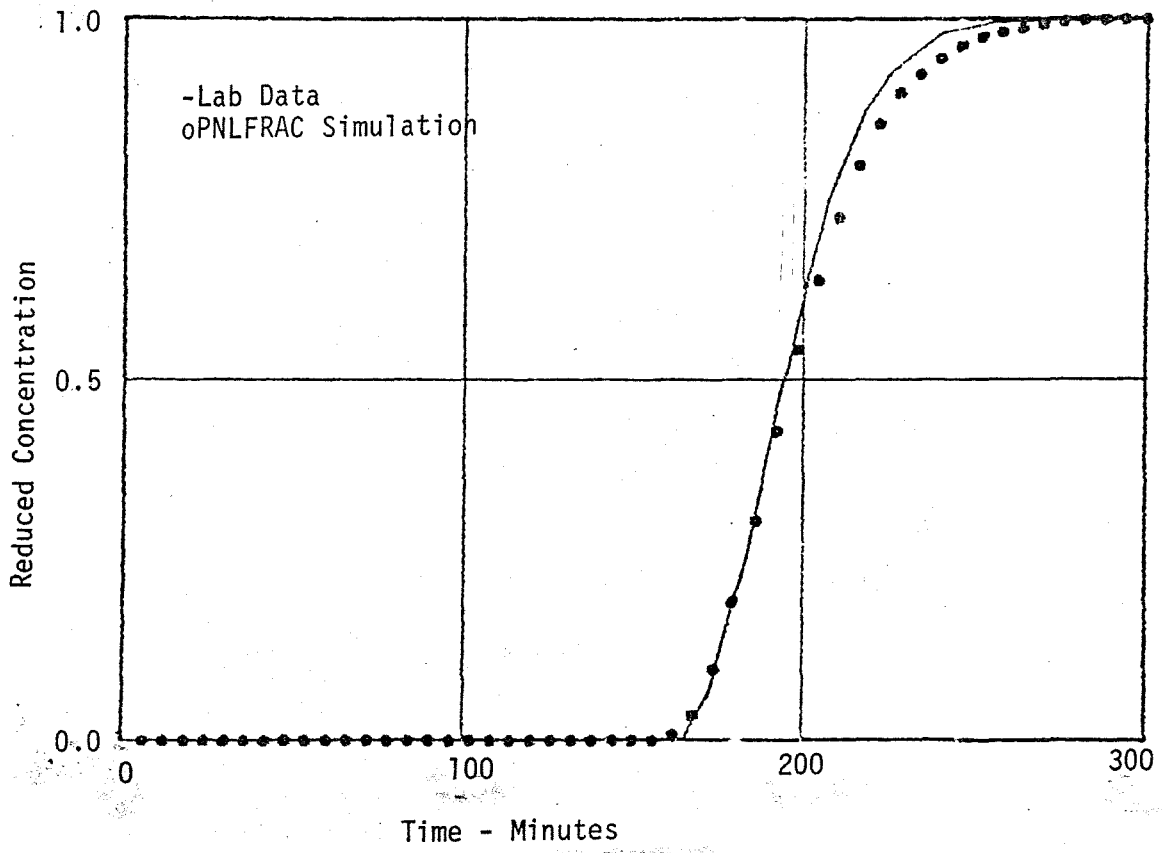

Figure 28. Comparison PNLFRAC and DATA Single Fracture Model 0.1 cm/min

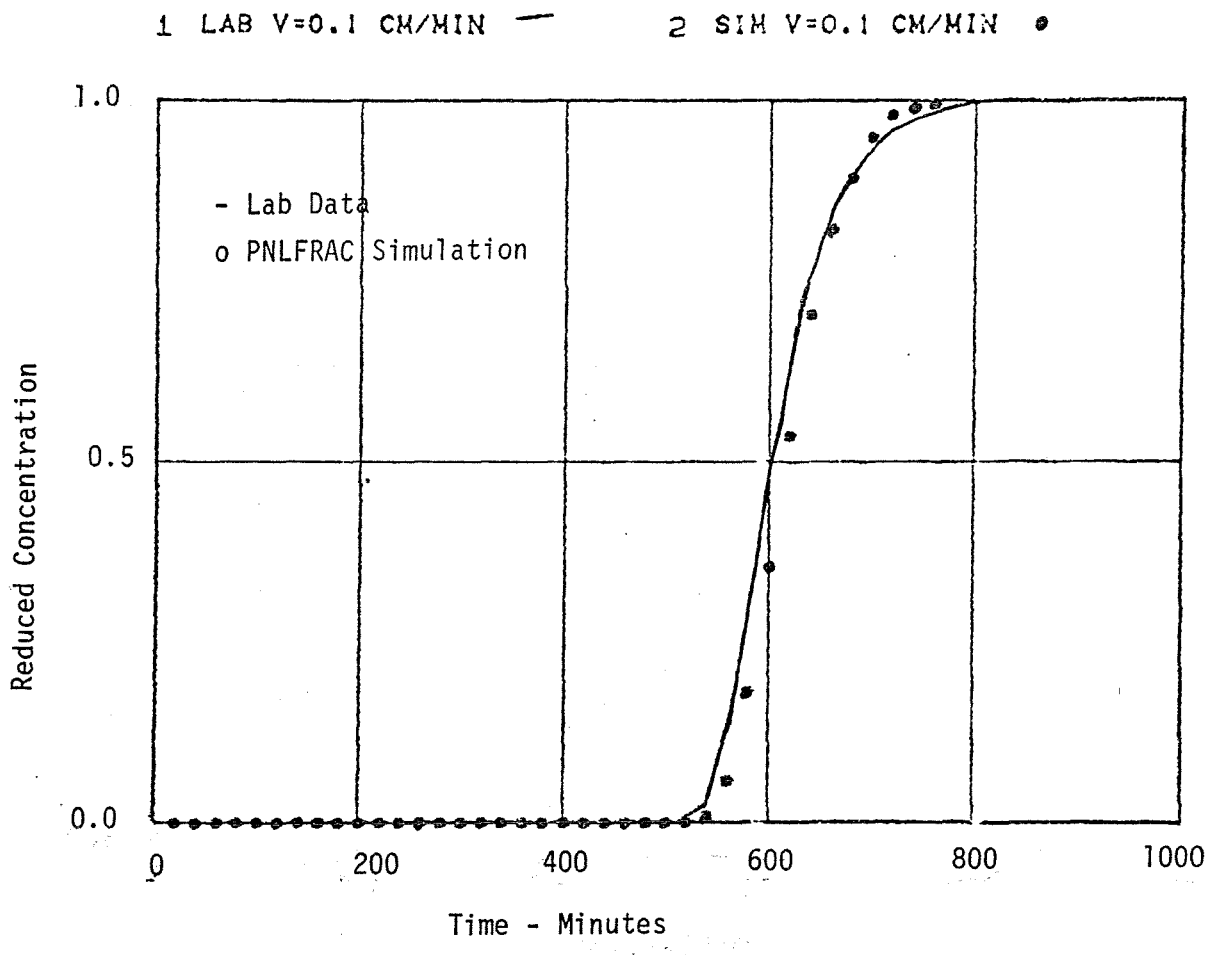

Fig 29

tube

Supply

in

Reproduction

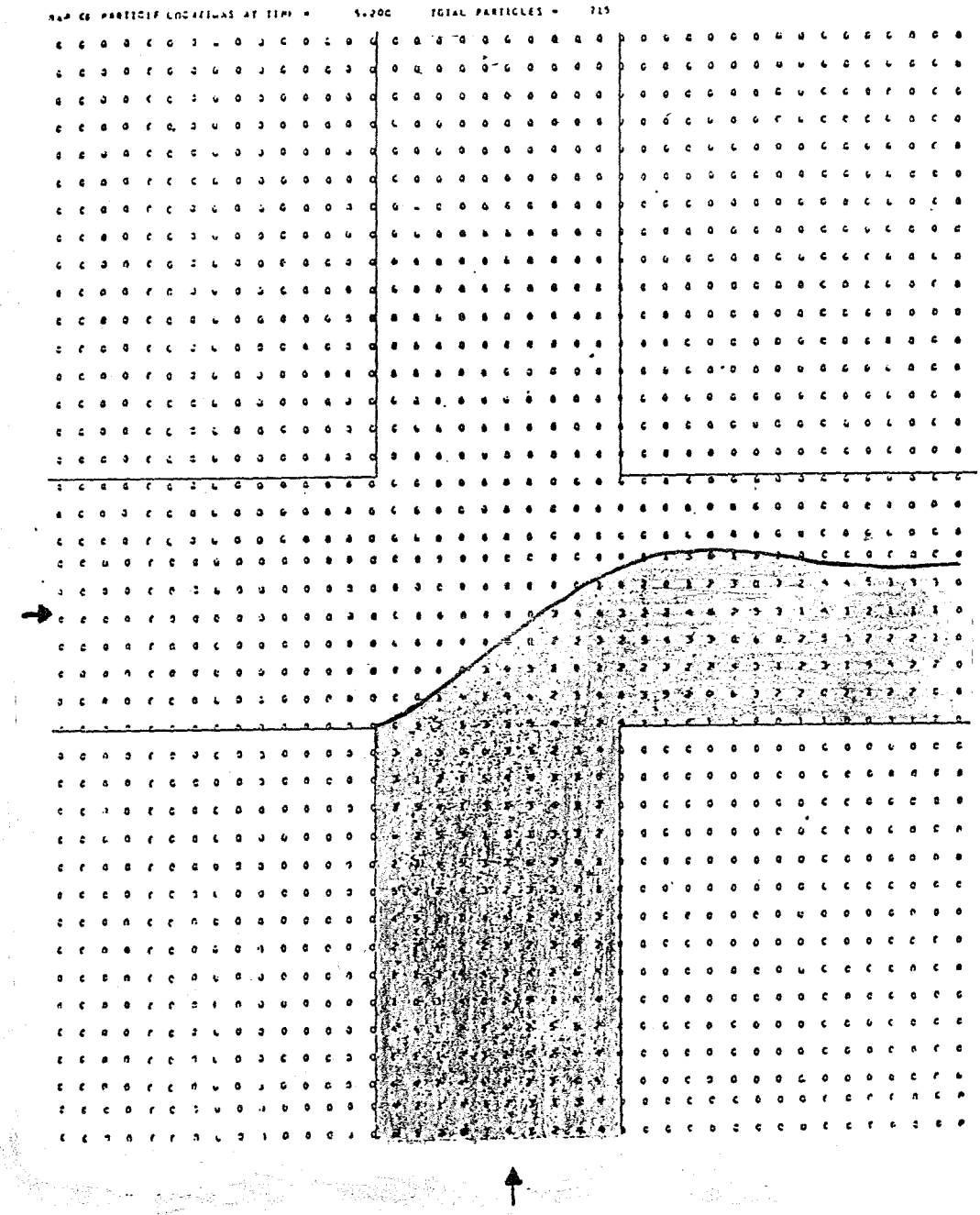

Figure 30. Flow Distribution SALE Code Prediction Equal Flow Rates

4.5.7 Multiple Fracture Model. In FY-83, results of runs were reported with the multiple fracture model[1]. The results reproduced again on Figures 31 and 32 show that as the injected volume was increased, the normalized backflow curves fall on top of each other. A similar result was obtained at Raft River. Classical dispersion theory indicates this should not happen and an effort was expended in FY-84 to explain the observed results. Consider what would be expected to happen according to classic dispersion theory. As the volume of fluid injected increases, the tracer front moves further from the wellbore. This increases the value of the Peclet number (ux/D_1) by increasing the value of x. This assumes that there is constant dispersion coefficient that describes the mixing of the injected and native fluids. The effects of increasing the Peclet number are illustrated in Figure 31. In Figure 31b, the absolute spread in the tracer front increases with distance travelled. However, Figure 31c shows that the reduced tracer breakthrough curves become steeper as the Peclet number increases. While the spread of the tracer front increases with distance travelled, the relative spread compared to the total distance travelled decreases.

For the tests conducted in the fracture networks at Raft River and in the laboratory, the reduced tracer recovery curves did not become steeper as the distance the tracer front travelled increased. This indicates that, at least in the classical sense, that the Peclet number remained constant. This requires that the dispersion coefficient also increased. Increasing dispersion coefficients with the distance over which they are measured is commonly observed in measurement of dispersion coefficients for porous media. An alternative explanation is more plausable for studies in fractured media.

The coincidence of the reduced tracer recovery curves for the injection-backflow tests conducted in the fracture systems can be explained by the hydrodynamics of flow between parallel plates. When flow rates in fractures are fairly high, classic dispersion theory is not valid, and the classic Peclet number cannot be used in these situations. That velocity profile effects were significant was clearly observed during testing of the laboratory model. Stringers of tracer moved rapidly up the center of fractures,

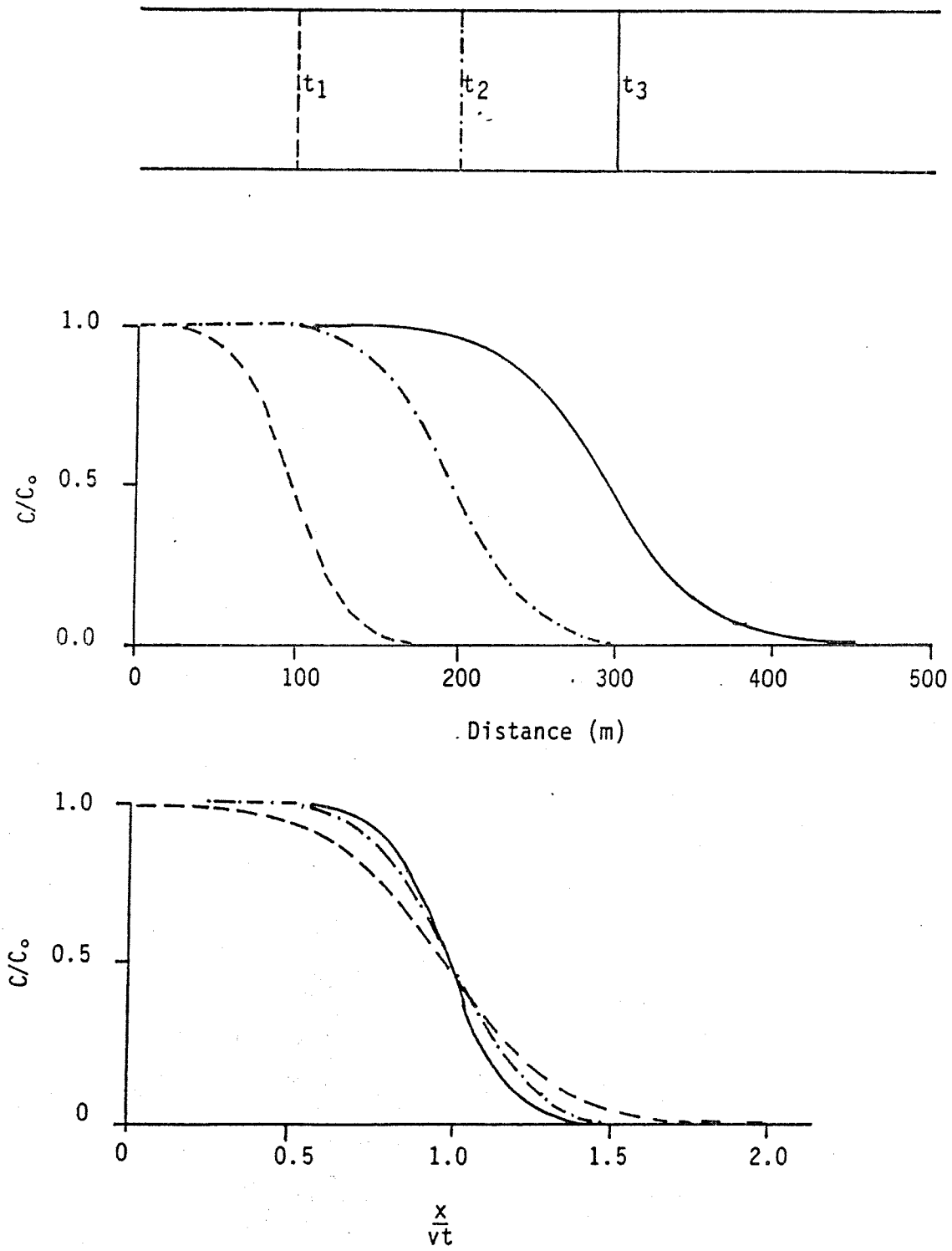

Figure 31. Changes in shape of a one dimensional tracer front for raw data and normalized data.

retaining their parabollic shape even when split at junctions. For classic dispersion theory, there is no constraint on the range of fluid velocities encountered, but the range rapidly takes on a Gaussian distribution with distance travelled. For flow in a parallel plate fracture, however, there are definite constraints on the range of fluid velocities encountered. In the center of the fracture, flow will travel 1.5 times the mean velocity (Figure 32). Along the fracture walls, the velocity will be zero. This then constrains any tracer to cover a range of fracture between a point of 0 and 1.5 ut (Figure 32). Normalizing any tracer breakthrough curve will generate a curve that connects these two points, irregardless of the distance the tracer front has travelled.

Naturally, it is not that simple. Transverse diffusion will cause tracer to move between streamlines, and therefore to move at a range of velocities. This will distort the shape of the breakthrough curve, by moving the $C=C_0$ point away from the origin of the fracture, and slowing the peak velocity to less than 1.5u. At the extreme, diffusion will homogenize the tracer, under which conditions, classic dispersion theory will be applicable to the fracture system. In the complete absence of diffusion, the recovery curve from an injection-backflow test would be a mirror image of the injection portion, with no spread in the data.

The shape of the recovery curve, therefore, represents the interaction of the distribution of flow velocity in the fracture with transverse diffusion homogenizing the tracer concentration. Thus, the tracer recovery curves from a series of tests can be used to estimate the fracture aperture based on an assumed geometry of the fracture. For diffusion to homogenize tracer within a fracture requires a dimensionless time of 2.0 as calculated from $D_m t/b^2$. Based on measured apertures of the major fracture zone at Raft River of 0.3 to 1.5 meters, gives homogenization times of 52 to 1300 days. Thus, homogenization would not be expected to have occurred during the tests conducted at Raft River. Lengths of tests to be conducted for future injection-backflow field experiments can be calculated from estimates of fracture aperture from downhole measurements dimensionless time. A range of tests covering dimensionless times of 1.0 to 3.0 would provide sensitivity in estimating fracture apertures.

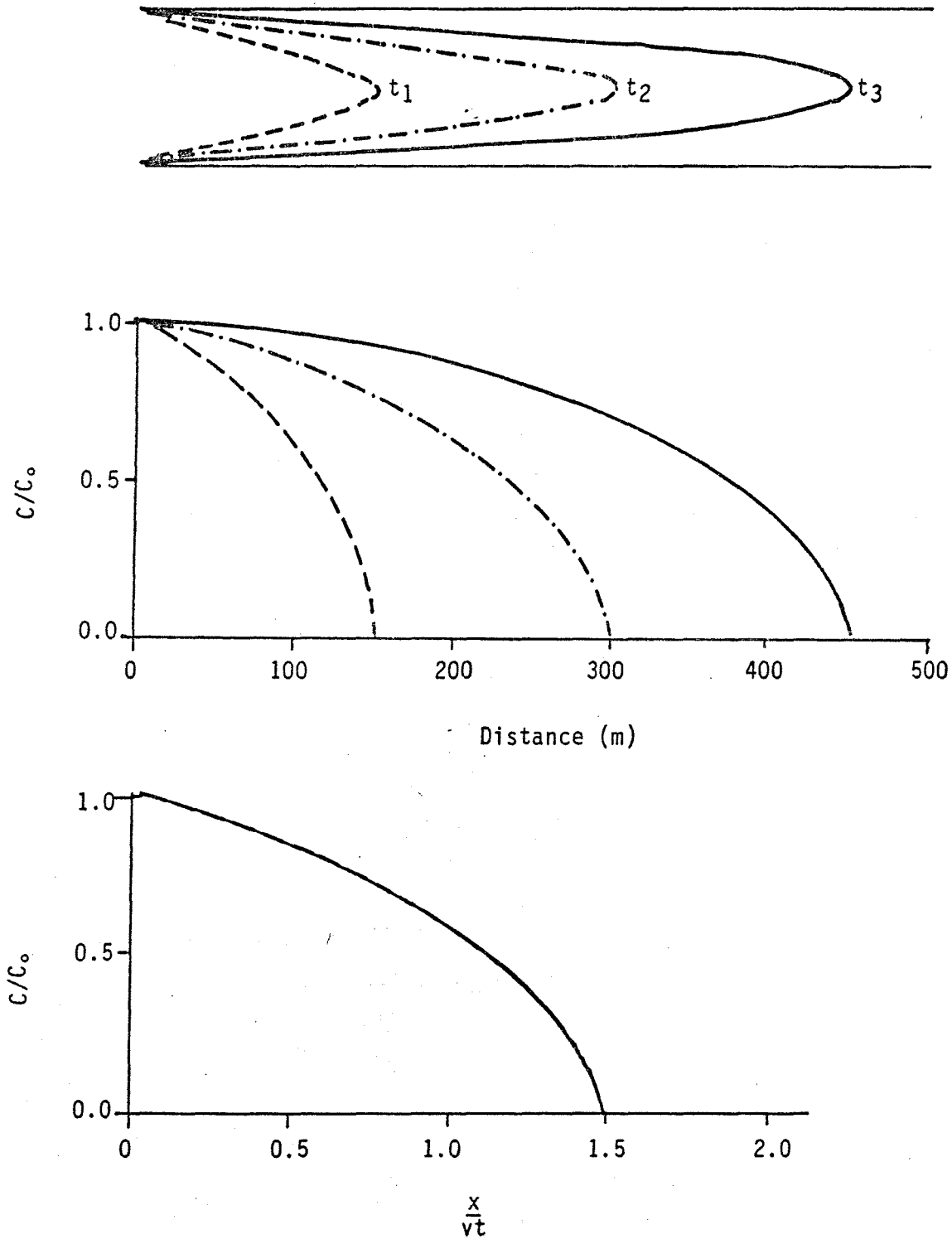

Figure 32. Changes in shape of a tracer front moving through a fracture and dispersing due to a parabolic velocity profile.

Results from the Raft River field site provide an example of dispersion within single fractures producing important effects in tracer breakthrough. Ignoring the effects of microdispersion would make interpretation of these test results difficult. Also, the Raft River results provide a field example where parallel plate theory provides a good explanation of observed behavior of a natural fracture system.

4.6 FRASCL Reservoir Simulation Code

FRACSL is being developed by EG&G to simulate injection-backflow tests in fractured reservoirs. FRACSL is capable of dynamically simulating wellbore pressure responses to injection or withdrawal of fluid from a well. The code can also simulate the movement within a reservoir of contaminant material injected from the test well.

Parameters defining a FRACSL reservoir model are linked to physical characteristics of the reservoir. When the results of FRACSL simulations are sensitive to changes of modeling parameters, these can be used to evaluate the physical characteristics of the reservoir by matching FRACSL results to physical testing data. FRACSL has already been used to model greatly varying reservoirs from unfractured East Mesa to a bench scale physical model of a fracture system. These models are all required to conform to the same basic structure.

A FRACSL reservoir model is composed of a base of reservoir media called the matrix upon which is superimposed a fracture network. A rectangular grid structure defines the borders of the matrix cells. Matrix material parameters are porosity, hydraulic conductivity, specific storage and dispersivity. Nodes exist at the intersections of the grid lines. Fractures are limited to line segments connecting neighboring nodes. Fractures are defined by position and width.

Pressure is the state variable of FRACSL. Pressures are defined at each node. The nodes interact hydraulicly along the grid lines through the matrix and via fractures. A node's fluid storage capacitance is obtained from a quarter of the capcitance of each adjoining matrix cell and half of each connecting fracture.

The driving function for FRACSL is supplied at a well node. The well node simulates a well by introducing a time varying flow rate into the reservoir. Presently, FRACSL has two possible boundary conditions. A fixed flow rate may be specified at each node. The other boundary condition is a connection from the nodes at the boundary to an infinite capacitance reservoir. The connection is supplied by a user specified conductivity.

The above definition, along with the laws of flow and conservation of mass, results in a two-dimensional isothermal simulation of laminar flow in a defined fracture system within a homogenous reservoir.

Simulation of tracer contamination within a reservoir is based on the concept of modeling a continuous process with discrete particles. In FRACSL, marker particles are introduced into the reservoir from the well node to simulate injection of contaminant tracers into the reservoir. These particles are moved about the reservoir in response to the flow determined from the hydraulic portion of the code. During a dynamic hydraulic simulation, marker particles are moved by a constantly changing flow solution.

The FRACSL models are implemented and solved using a continuous differential equation solver, the Advanced Continuous Simulation Language (ACSL).

Table 7 contains highlights of FRACSL's characteristics. These are explained in greater detail in the following sections.

4.6.1 Hydraulics. FRACSL assumes a laminar flow regime within the reservoir. The pressure gradient is assumed to be linearly related to the flow rate within both the fractures and matrix. Pressure changes at the nodes are determined from conservation of mass and the specific storage and size of the surrounding matrix. Flow between adjacent nodes is either across the intervening matrix or via a connecting fractures. Nodes can also be diagonally connected via fractures.

TABLE 7. FRACSL OVERVIEW

Scope: Simulation of pressure response and tracer transport within a fractured reservoir

Method: Hydraulics - lump parameter finite difference
Tracer - discrete particles

Capabilities:

Hydraulics - dynamic pressure response
-quasi-steady state pressure distribution
-flow distribution

Tracer -injection, movement, withdrawal
-matrix-fracture transfers
-dispersion
-diffusion

Boundary Conditions: -impermeable boundaries
-Fixed conductivity to an infinite reservoir

Limits: General -2D
-Isothermal
-Homogeneous reservoir media
-Rectangular geometry

Hydraulics -No inertia effects

Tracer -Conservative tracer
-2000 particles

The hydraulic solution for a given problem can be found either dynamically or in a quasi-steady state mode. Quasi-steady state refers to a fully developed pressure profile in which pressure rise or fall is at a constant rate throughout the reservoir.

4.6.2 Dynamics. The dynamic reservoir response is calculated by using one of two highly efficient variable time step, variable order, differential equation solvers. These are the Adams-Moulton and Gear's stiff integration algorithms.

The dynamic solution results in time varying pressure and flow which is more realistic than the quasi-steady state assumption. It provides the ability to determine the effects of flow changes on pressure and tracer transport. Fluid inertial effects, often referred to as "water hammer", are not modeled in the present FRACSL version.

Pressure responses calculated by FRACSL have shown the effects of reservoir size and boundary shape. One interesting feature is the distance over which the pressure response extends versus the penetration of injected fluid. Simulations of the unfractured East Mesa reservoir for 12 hours of injection yielded pressure sensitive to impermeable boundaries at 1000 feet distance while the injection fluid travelled to a distance less than 20 feet from the well. These effects bode well for the use of FRACSL in identifying major reservoir fractures, including large fractures and faults.

4.6.3 Quasi-Steady State. The quasi-steady state solution assumes a fully established flow regime and a constant rate of head change. The solution is determined by using a Newton-Raphson iteration scheme. This solution has the advantage of lower cost for long periods of constant flow. The steady state solution is sensitive to reservoir shape, but not to overall size. This is opposite to the dynamic case which requires a large reservoir and is insensitive to shape if large enough. Given enough time, the dynamic solution approaches the steady state solution for all geometries.

4.6.4 Marker Particles. Tracer movement is simulated through the use of discrete entities called marker particles. Computations using the calculated pressure distribution are performed to obtain base particle velocities. These deterministic velocities are adjusted to simulate stochastic dispersion and diffusion processes. Particles are moved discretely by a single derivative evaluation with a fixed time step. The flow chart in Figure 33 provides an overview of marker particle movement.

Marker particles are injected into the reservoir from the well node, either into a fracture or in the matrix. Placement is random within the fracture or matrix and apportioned randomly based on the fraction of flow entering each fracture or matrix cell.

4.6.5 Movement Within the Matrix. The pressure gradient at a particle position is found by calculating a local second-order pressure distribution. Figure 34 illustrates the calculation method. The pressure gradient in the x direction at point (x, y) is found in the following manner: pressures at the y locations are found by linearly interpolating between the corresponding nodal pressures. A term $\partial^2 P/\partial X^2$ is defined:

$$\frac{\partial^2 P}{\partial x^2} = \frac{2}{dx_1+dx_2}\left[\frac{P_{y_1}^1 - P_{y_2}^2}{dx_1} - \frac{P_{y_2}^2 - P_{y_3}^1}{dx_2}\right]$$

at point (x, y) $\partial P/\partial x$ is

$$\frac{\partial P}{\partial x} = \frac{P_{y_1} - P_{y_3}}{dx_1 + dx_2} + \frac{\partial^2 P}{\partial x^2} \cdot dx$$

where

$\frac{\partial^2 P}{\partial P^2}$ = 2nd derivative of pressure with respect to x

dx_i = width of matrix cell

$P_{y_i}^1$ = pressure at location Y_i

$\frac{\partial P}{\partial x}$ = pressure gradient in x direction at point (x, y)

dx^1 = distance, in the x direction, of (x, y) from node 22 (in this example, dx^1 is negative)

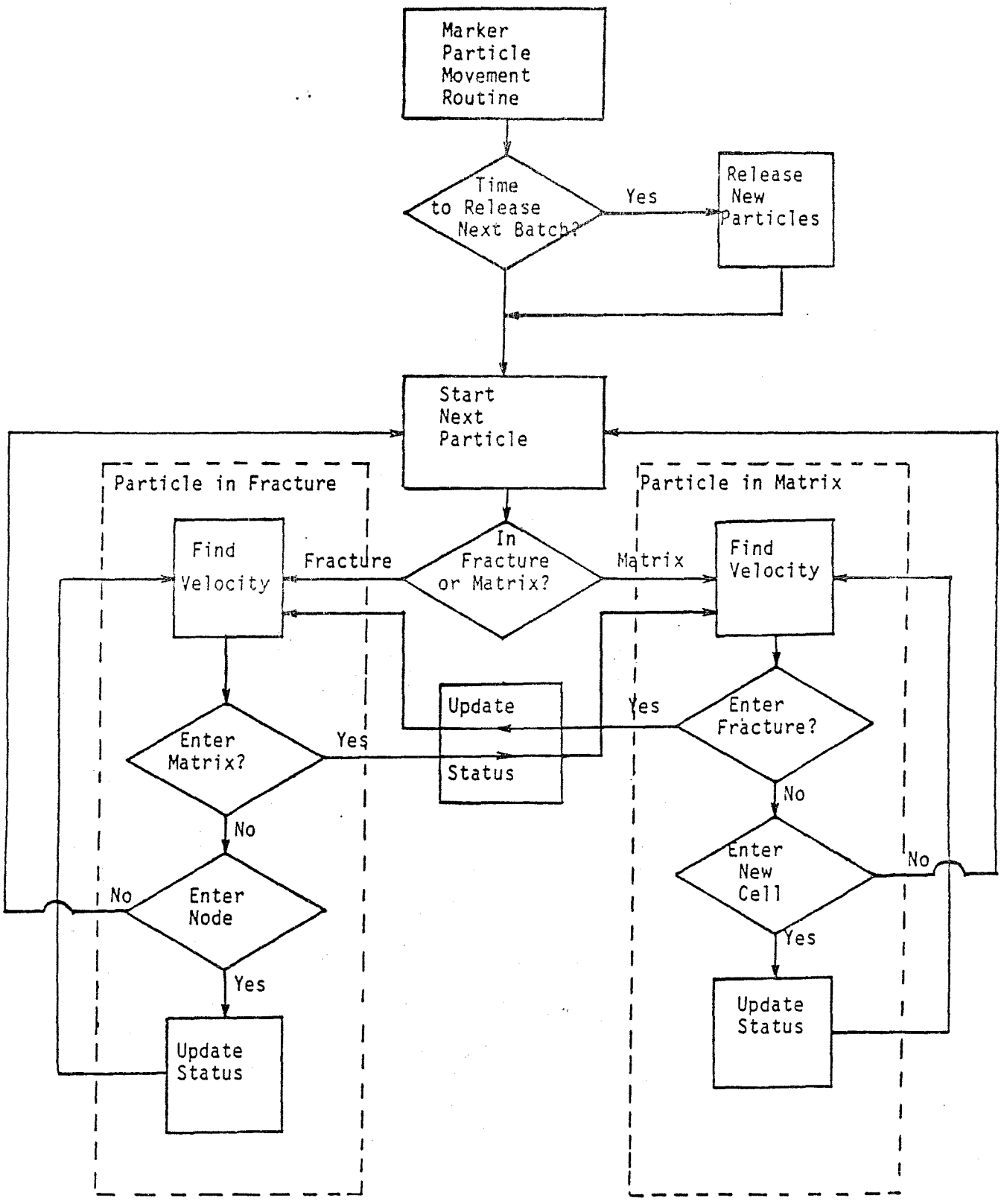

Figure 33. Flow Diagram Marker Particle Routine - FRACSL Code.

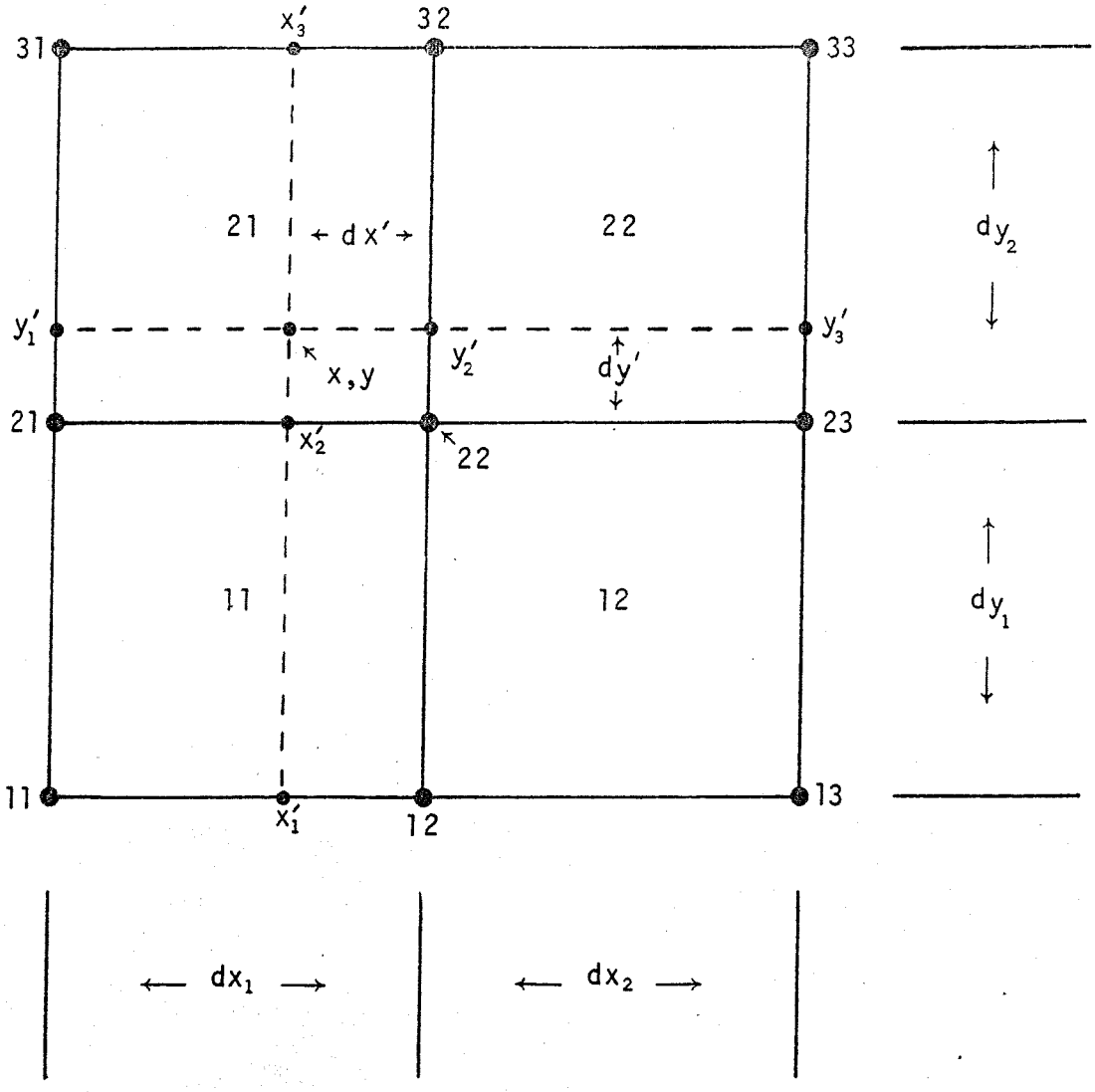

Figure 34. Marker particle and matrix cell schematic diagram

If the line containing $y\frac{1}{2}$ also contains a fracture, or a diagonal fracture exists in the cell, the pressure gradient is treated as a constant from the fracture to the opposing y^1 location.

Particle velocity is determined by multiplying the pressure gradient by the conductivity. Pressure gradients determined from nodes at the corners of a cell do not properly address accumulation of fluid within a cell. This is most evident if fractures, within or bordering the cell, are providing fluid to the cell. An additional velocity term has been introduced to account for fluid loss from the fracture, which has accumulated in the cell. This term is perpendicular to the fracture and diminishes with distance from the fracture.

Dispersive effects are simulated using a routine developed by Prickett, Naymik, and Lonnquist[21]. Dispersive movement is added to the advective (deterministic) movement. Dispersion is a Gaussian stochastic process of zero mean and a standard deviation equal to the square root of the product of the dispersivity and the advective distance travelled. Due to the Gaussian nature of the process, dispersion is a function of distance travelled only and not the number of time steps taken to get there.

Diffusion in the matrix is also modeled. FRACSL simulates diffusion in a manner similar to dispersion except that it is a function of time and not distance travelled. Like dispersion, diffusion is independent of the number of times steps taken.

Marker particle movement in a time step is constrained to single cell and not allowed to cross fractures. If a particle movement intersects a cell boundary or fracture, the time used to reach the boundary is calculated and the particle is transferred into the appropriate cell or fracture.

Since a particle's velocity is determined at the start of movement, movement within a changing pressure gradient introduces error. Limiting the distance travelled provides a more efficient control of movement error than time step control. Particle movement is broken into segments

within a cell. If particle movement exceeds a fixed fraction of a cell width, the velocity of the particle is redefined after moving the limiting distance. The remaining movement is calculated from this updated velocity.

4.6.6 Movement Within a Fracture. Particle velocities within a fracture are determined along and transverse to the fracture. The average longitudinal velocity in a fracture is determined from the nodal pressure difference and the cubic law. For laminar flow conditions, the average velocity is a function of fracture width squared.

The actual velocity of a particle is determined by applying a Poiseuille distribution across the fracture. The Poiseuille distribution has a maximum at the center of a fracture of 1.5 times the average and decreases to zero at the wall as a function of distance from the wall squared.

The transverse velocity of a particle is composed of two terms. One is the head driven fluid flux across the adjoining matrix element. The second term approximates the amount of fluid leaving the fracture which is stored by the cell. These are the same velocities a particle in the matrix would have if immediately adjacent to the fracture.

Diffusion is superimposed on the deterministic velocity in the same manner as was done in the matrix. There is no dispersive component in a fracture.

If a marker particle movement intersects a side of the fracture, the particle is transferred to the matrix. This is consistent with the assumption of laminar flow in a fracture permeated along the sides with smaller fractures carrying away flow.

When a particle reaches the end of a fracture, it is transferred to the ending node and then introduced into a connecting fracture carrying fluid out of the node. Fracture selection, when more than one fracture carries fluid out of the node, is done randomly proportional to the relative flows in each. Presently, the lateral position of the particle is retained in the new fracture. This is not considered realistic and studies will be made to find a more appropriate scheme.

Longitudinal movement in a fracture is constrained by time step only. Since velocity is dependent on lateral position, the amount of movement in the transverse direction is segmented as in matrix movement.

4.7 Raft River Fracture Characterization and Reservoir Simulation

Raft River Well RRGP-5BF was tested in September through November 1982. During the interim since the tests were completed, a significant effort has been expended in developing analytic, physical and numerical methods for analyzing flow and dispersion in fractured media. The initial objective of this effort is to correlate the data collected in the Raft River tests. This section summarizes the numerical modeling work and the fracture characterization research conducted to provide the required description of fractured media characteristics. The characterization work consisted of a survey of generic fracture literature, an analysis of borehole data leading to a partial description of the local fracture system and the synthesis of a stochastic fracture system in the vicinity of the borehole. The numerical modeling effort involved the development of a fractured media simulation code, the evolution of two numerical models and a scoping analysis using one of the models.

The generic fracture characterization study included the complete range of scale from microcracks to major faults. The distinction was made between the two categories of void space which together represent all of the water of interest in a fractured formation. The first, flow porosity, is the void space in which flow is the dominant transport mechanism. The second, diffusion porosity, include voids and small channels in which molecular diffusion is the dominant process.

The need for an understanding of the nature of a fracture system in terms of its geologic evolution is clear from the literature and from the existence of fracture patterns. The genesis of a fractured formation may include pluton emplacement and crystallization, tectonic cycles resulting in folding, fracturing and faulting and, finally, mineral and chemical alteration.

The geometric fracture characteristics described in detail include orientation, persistence (length), spacing and aperture.

Fracture orientation is measured from surface outcrops or from boreholes or tunnels. A statistically significant number of fractures and a variety of orientations of boreholes or exposed surfaces is desirable. A correction is available for the effect of non-random borehole orientations on the number of fractures of a given orientation. Bivariate normal and spherical normal distributions have been used to describe orientation sets. There are usually three or four and as many as six orientation sets in a rock mass.

The persistence or length of discontinuities has been defined using log normal, exponential and power law distributions. The effect of censored (one or both ends not visible) and truncated (small fractures not observed) data must be considered in developing length distributions.

The spacing of fractures within an orientation set has been observed to conform to negative exponential and log normal frequency distributions.

Fracture apertures are poorly defined because of spatial and stress induced variations. Microfracture apertures have been quantified using scanning electron microscopes.

Fractures are frequently partially or completely filled with minerals which affect the permeability, porosity and chemical reactions between fluids and the host rock. The minerology can be used to correlate fractures and to help determine emplacement and tectonic history.

Flow through individual fractures has been shown to be a function of normal stress, shear stress and fracture surface characteristics. Effective aperture is commonly measured in terms of a measured flow which is proportional to the cube of the effective aperture. The effect of variation of aperture in the transverse direction has been studied in the laboratory.

The Raft River characterization included driller's logs, borehole geophysical logs including acoustic televiewer surveys and borehole logging conducted during the test series. This data was analyzed to determine fracture orientation, spacing, correlation with producing/receiving zones and apertures.

Figure 35 shows the geology of the Raft River KGRA and sectional view of the wells in the field. Test well RRGP-5BF had a long and involved completion history. An initial leg produced 1000 gpm of fluid at 275°F. Drilling continued in an effort to locate a higher temperature aquifer. The drill stem twisted off and the leg was completed with salt and cement. Leg B was drilled at an offset and was cased to a depth below the major aquifer in leg A. The well was hydrofractured and propped with sand. Figure 36 shows a completion drawing.

An acoustic televiewer survey was made by the United States Geological Survey for a 495 foot borehole interval prior to well completion. A second survey was made of the production interval after the liner was installed and the well was hydrofractured. There were no discernible differences in the common interval attributable to the hydrofracture. The log providing the highest quality data was used in the open interval and the precompletion log was used to provide additional data for the upper interval.

Only 35 well-defined discontinuities and 12 additional apparent discontinuities were observed. The well-defined discontinuities were grouped into five orientation sets based on the stereonet contouring shown in Figure 37. This is a southern hemisphere projection in which a normal to the fracture plane is extended until it pierces the surface of the hemisphere. The fracture is represented by that point. The data was corrected for magnetic declination, borehole inclination and, using the Terzaghi correction, for orientation frequency. Sets 2, 4 and 5 form a band on the stereonet where the strike is approximately N9°W. The dip ranges along this band from 75°W to 36°NE, assuring that these discontinuities will intersect. Sets 1 and 3 bracket set 2.

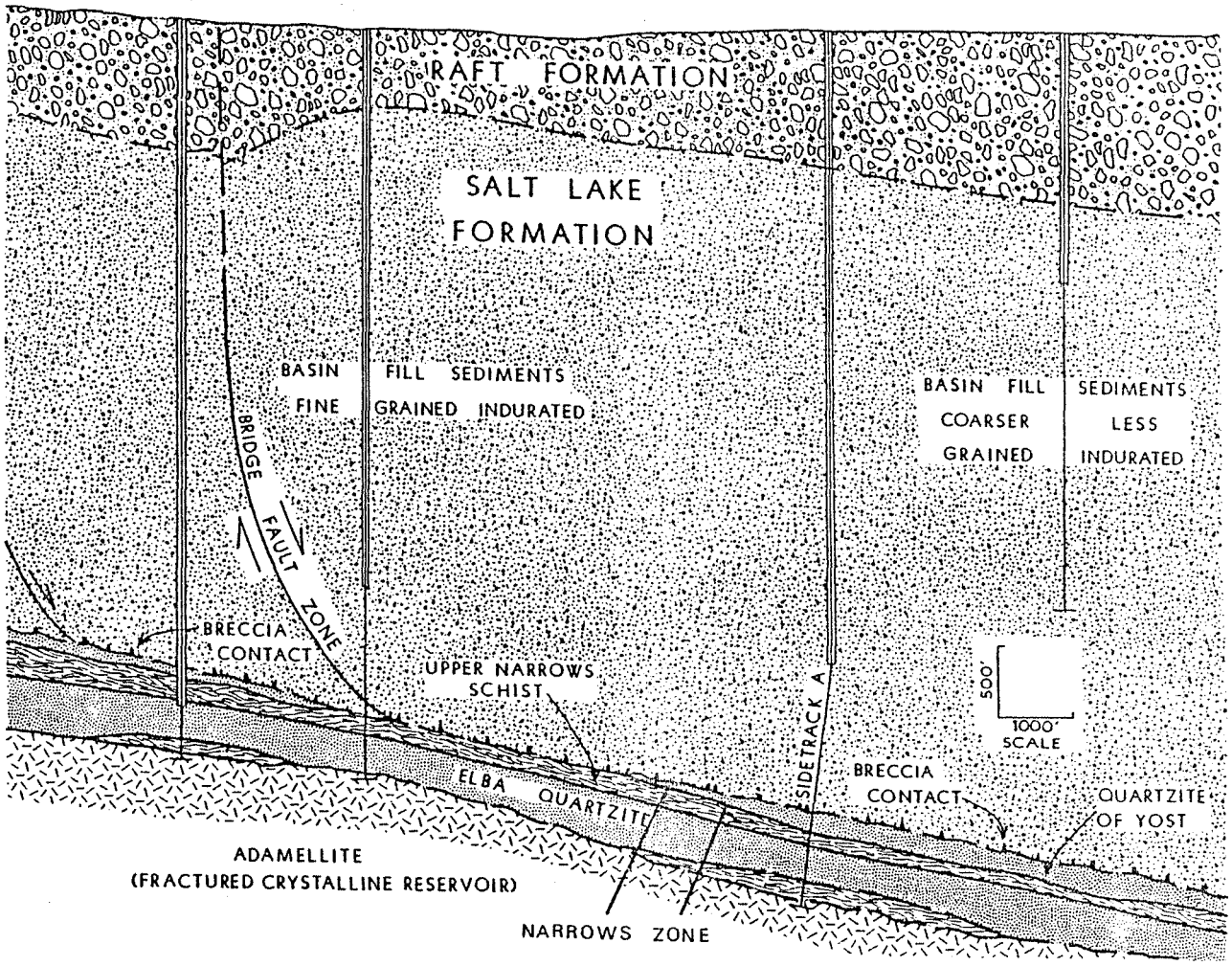

Figure 35. Raft River Geology

Figure 36. RRGP-5BF Well Construction

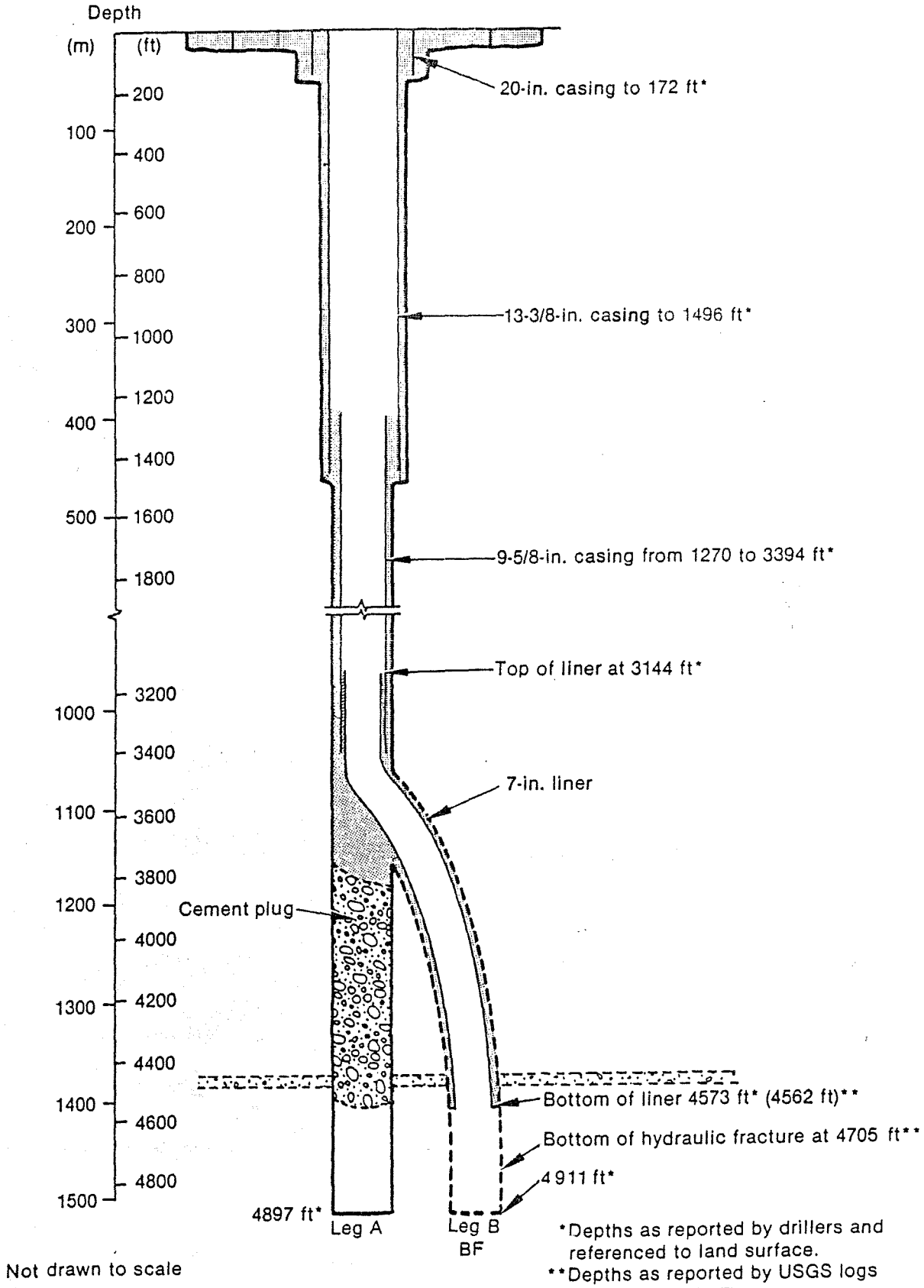

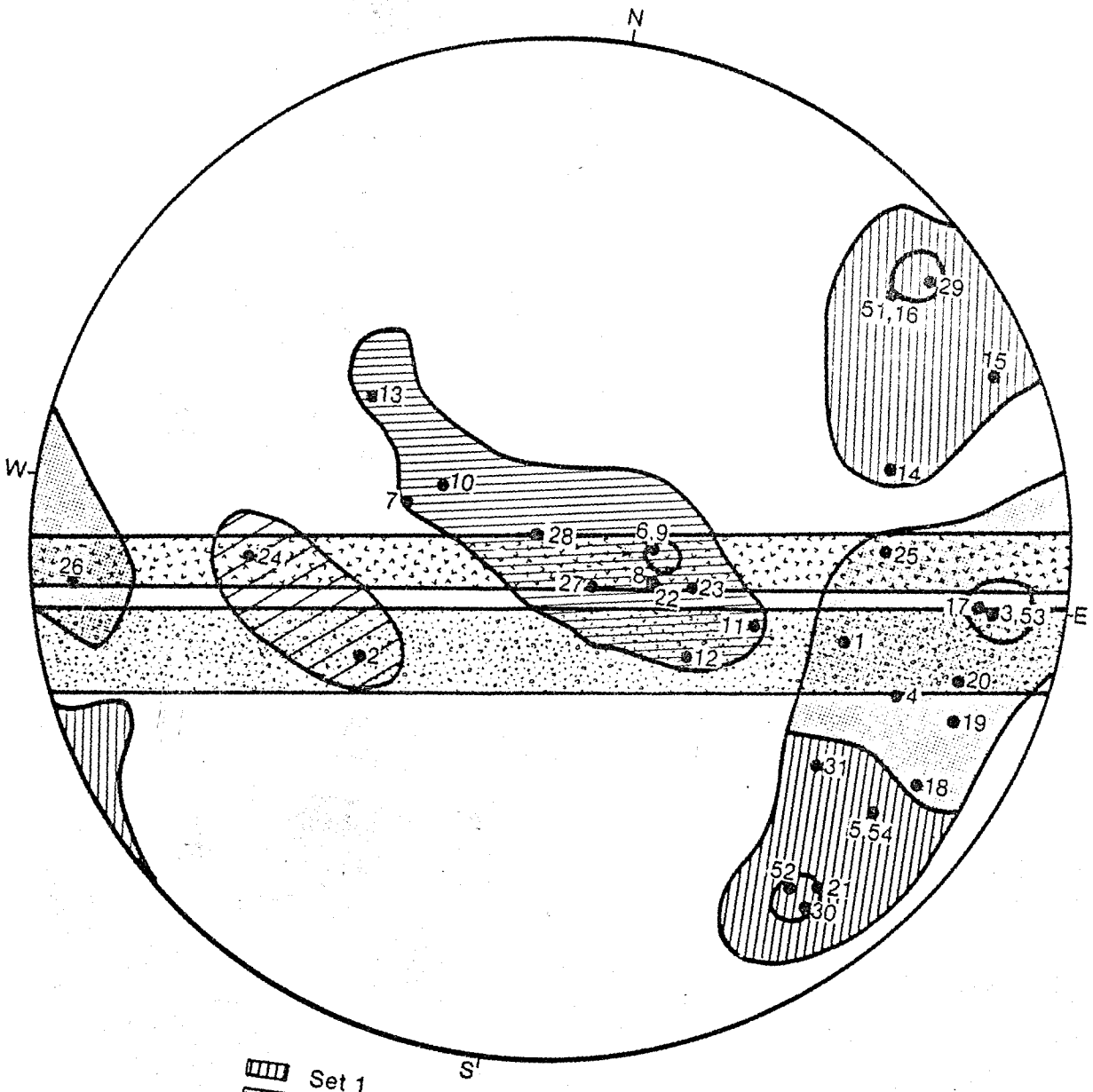

FIGURE 37. Equal area stereonet for 35 acoustic televiewer discontinuities in RRGP-5B between depths of 1341.1 and 1491.1m. (4400 amd 4895 ft.)

Figure 38 is a vertical profile showing the lithologic log, the fracture orientation, the discontinuity density and the cumulative discontinuity occurrence. The strike (azimuth of the intersection of the fracture plane with a horizontal plane) is indicated by the lateral position on the scale and the dip (steepest angle between the horizontal plane and the fracture plane) by the inclination from the horizontal of the tail.

After grouping the very closely spaced discontinuities of common orientation as a single feature, the borehole separations for the various sets were evaluated as follows:

Set	Maximum Density		Number	Separation Along Borehole - ft		
	Strike	Dip		Logarithm of mean	Logarithm of std dev	Mean Distance
1	N46°E	74°NW	6	1.768	.481	58.6
2	N	77°W	10	1.674	.298	47.2
3	N46°W	78°SW	5	2.154	.332	142.6
4	N5°W	18°W	12	2.137	.340	137.1
5	N23°W	41°E	2	-	-	319.

Apparent apertures, those inferred from the acoustic televiewer log, were classified in 0.5 inch intervals. The majority of apparent apertures range in width from 0.5 to 1.5 inch. Effective aperture, or even the existence of permeability, is much more difficult to determine. Figure 39 shows a correlation between the discontinuity locations and the production zones as shown by the spinner log. Within the resolution of the spinner log, all of the observed discontinuities appear to be flowing.

Computer models implementing these characteristics were developed using the FRACSL reservoir simulation code, described previously.

Two FRACSL models of the reservoir near RRGP-5BF have been developed. The smaller of the two is a vertical section centered on the hydrofracture and extending in an approximate E-W direction. This model is 189 feet

FIGURE 38. Vertical profile of discontinuity orientations and density for RRGP-5B.

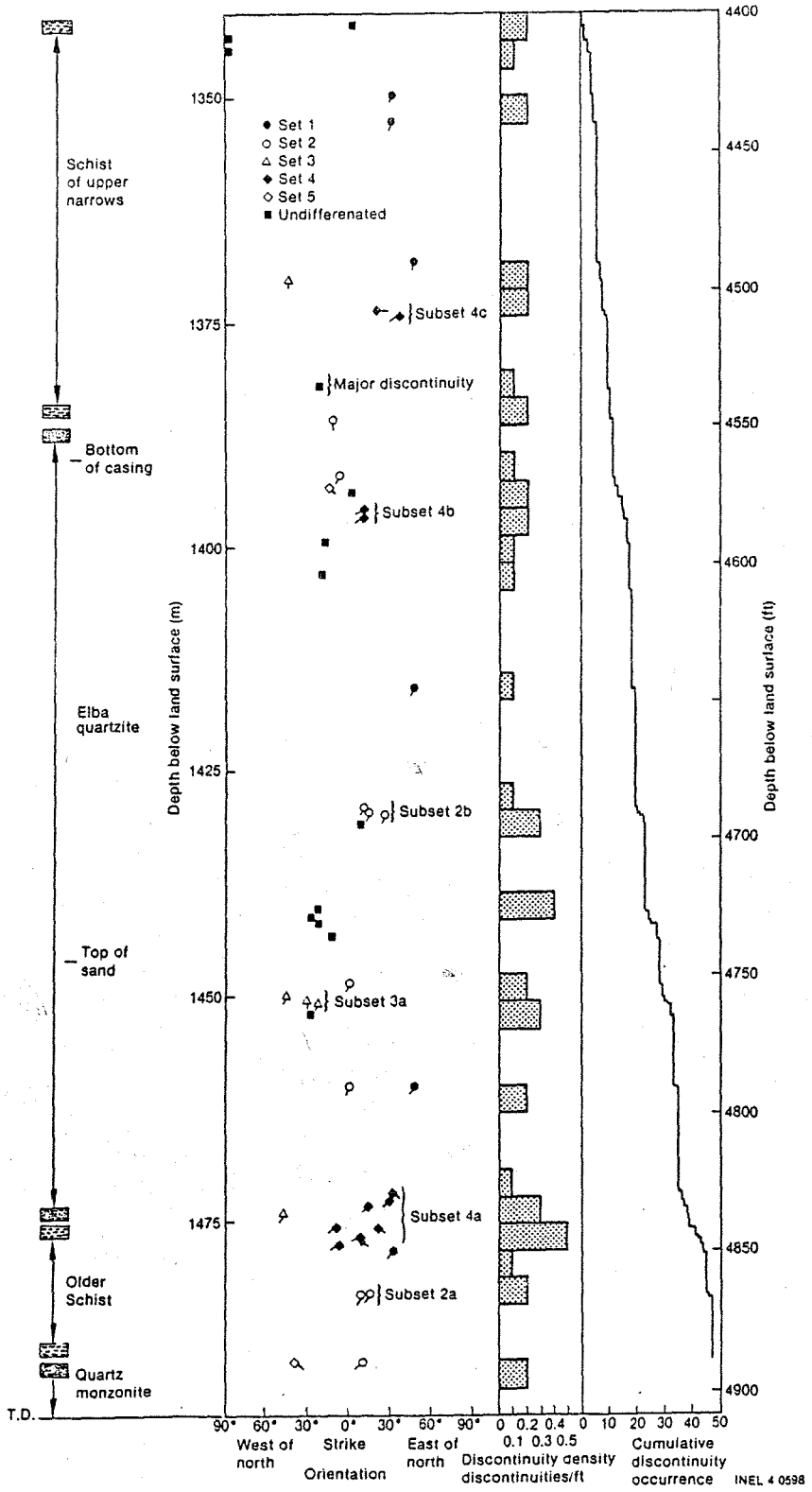

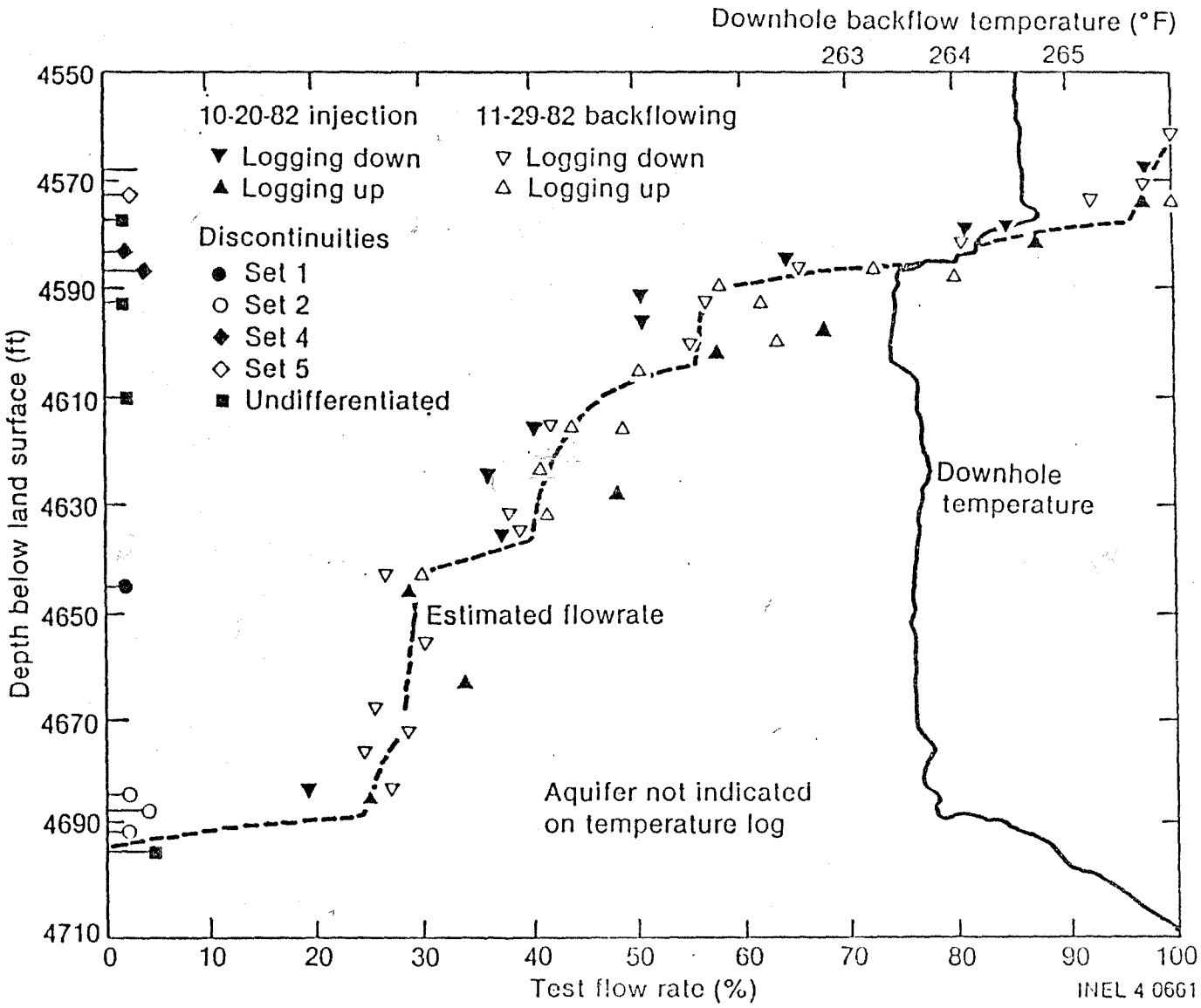

FIGURE 39. Production/receiving zones discharge/uptake as a percentage of flow rate and discontinuity locations for RRGP-5BF. A temperature log during backflow of test 2D is also plotted.

high by 77 feet wide and includes the hydrofracture, the fractures observed in the production interval and the major aquifer observed in leg A of the well. The second model is 500 feet high by 500 feet wide, similarly located, and includes a stochastic fracture system synthesized on the basis of the fracture characterization studies.

The orientation of the two models is parallel to the band shown on the stereonet for fractures with a strike of N9°W. This model plane therefore displays the intersections of the three fracture sets in the band. The other two fracture sets bracket this band and have the same apparent 79°W dip as set 2 which lies in the band.

The effective thickness of the area modeled must be chosen in order to determine the average flow rate across the thickness. This value is then used as the input from the well to the one-foot thick "typical section" modeled. The effective thickness requires an approximation to the fracture distribution in the third dimension. The effect of flow into the thickness dimension cannot be included in this simulation, but tends to be small because of the selected model orientation. Effective thicknesses of 160 and 263 feet were chosen for the small and large models, respectively.

Simulation was conducted with the smaller model in an attempt to scope the range of effective apertures in the fracture system. The actual fracture system and the computer approximations are shown in Figures 40 and 41, respectively. The locations of the various fractures are those given by the acoustic televiewer. Each is assumed to extend to the model boundaries. The apertures of the hydrofracture and the upper aquifer fracture were set at .025 feet since the maximum apparent hydrofracture aperture was given as .05 feet. The apertures of the other fractures were adjusted to match the flow distribution given by the spinner log. The resulting values, moving down from the bottom of the well liner, are .0095, .0095, .018, .018 and .025 feet. The distance to the zero head remote boundary was arbitrarily chosen as 1000 feet. The resulting head at the injection node, corresponding to 150 gpm injection, was .036 feet. This is approximately 3 orders

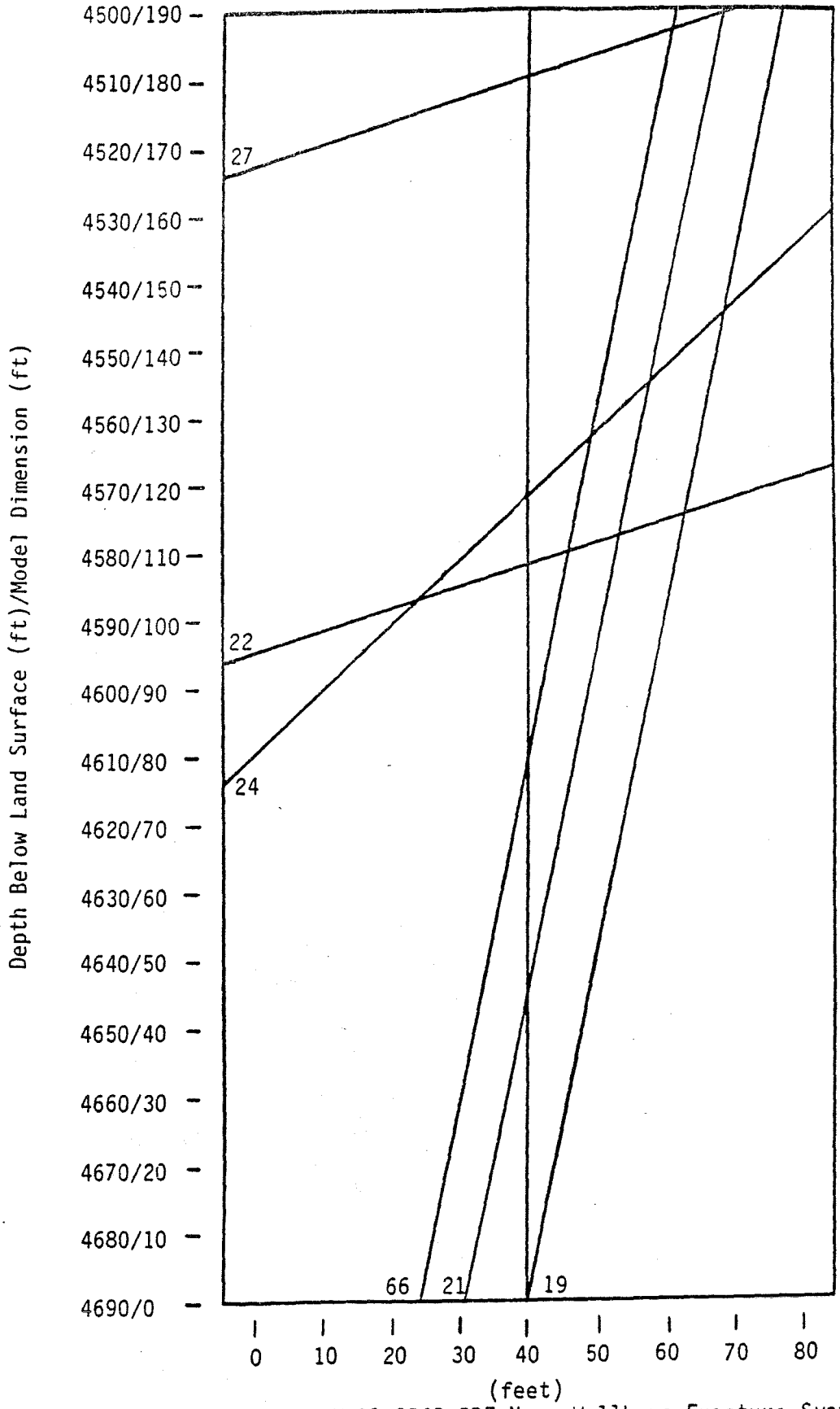

Figure 40. Raft River Well RRGP-5BF Near Wellbore Fracture System

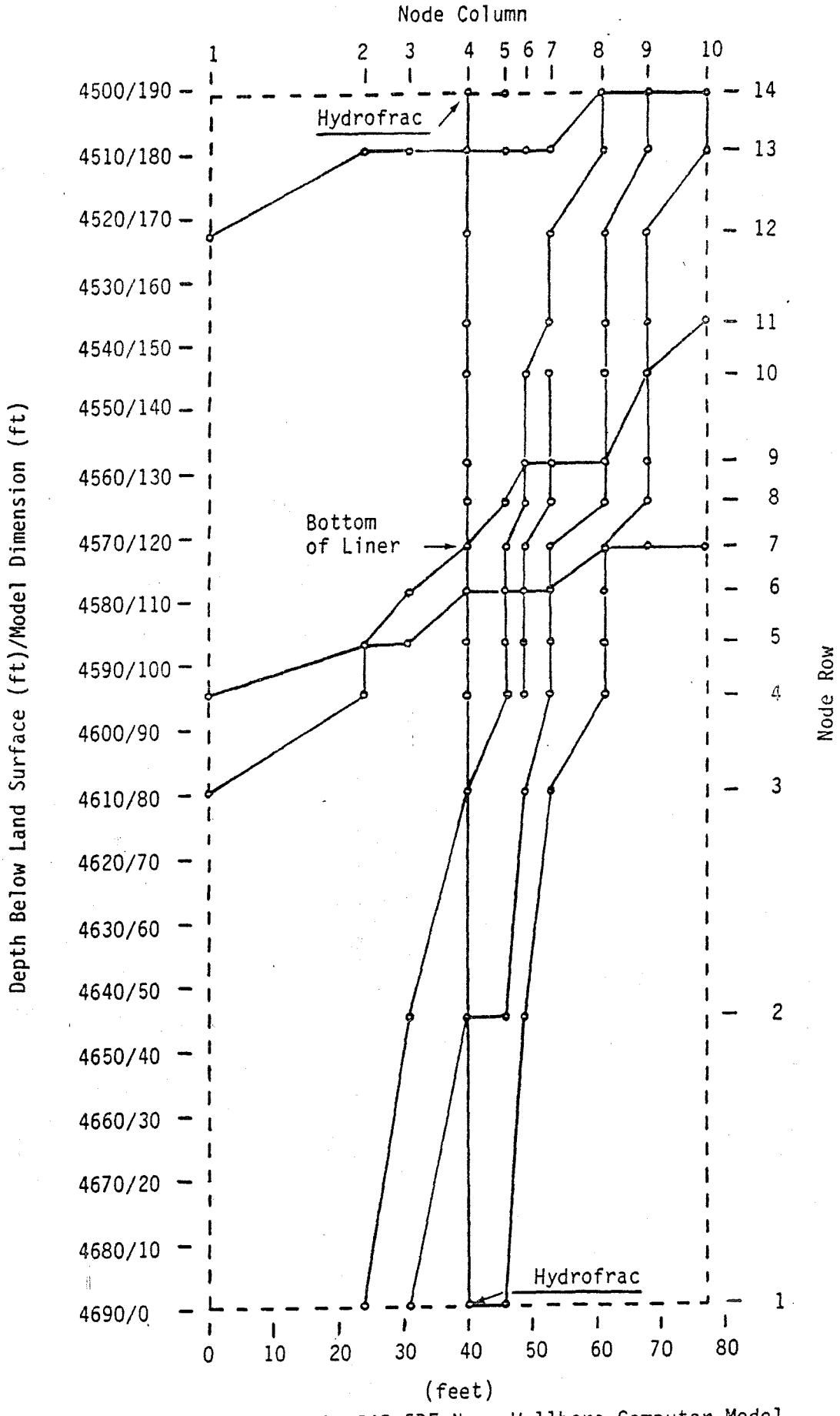

Figure 41. Raft River Well RRGP-5BF Near Wellbore Computer Model

of magnitude lower than the measured value of 49 feet, after allowing for turbulent losses which are not modeled.

The selection of the distance to the remote boundary only affects the computed head by about a factor of three. A second case was therefore run to address the more sensitive aperture parameter. A reduction of all apertures by a factor of 10 yielded a head at the injection mode of 34.6 feet. These apertures are apparently closer to those expected in the real aquifer.

A final simulation performed with this model was an attempt to match the transient pressure response correlated in a series of withdrawal tests at a range of flow rates. A specific storage value of 1.E-7 per foot, which is reasonable in view of data in the literature, was found to give the best match.

The fracture system for the 500 feet by 500 feet model was synthesized using the method given by Andersson (1984). The procedure incorporates the following elements as applied independently to each of the five fracture sets:

1) Fracture traces lie on infinite lines at equally probable locations on a scanline through the center of the model. Each of these lines has a dip equal to the mean of the appropriate set.
2) Length is selected from a log normal distribution with a mean equal to 3.5 times the mean perpendicular spacing as determined from the borehole survey. A range of 3-4 for this factor was given by Gale (1982).
3) The center of the fracture is equally probable over the interval encompassing all fractures of the specified length which intersect the model.
4) Fractures are synthesized until the total number intersecting the scanline corresponds to the mean spacing measured in the RRGP-5 borehole.

Totals of 15 and 5 fractures were synthesized for sets 4 and 5, respectively. A total of 778 fractures were synthesized for sets 1, 2 and 3 combined. Figure 42 shows the synthesized system with only the largest of the fractures from sets 1, 2 and 3 shown. The vertical has been rotated 11°CW to align the steeply dipping fractures from sets 1, 2 and 3 with the model principal axes. Figure 43 shows the computer version of this model with the set 1, 2 and 3 fractures collected laterally into columns.

While successful steady state flow and marker particle dispersion runs were made, the analysis is not completed in FY-84.

4.8 Geophysics

At East Mesa, spontaneous potential (SP) geophysical surveys were conducted in conjunction with injection-backflow testing both during August 1983 and February 1984. Numerical modeling prior to these surveys had indicated that SP effects expected from injection and backflow were small, but perhaps detectable. The survey results showed no clear indication of an SP response from either well 56-30 or well 56-19. The main problem with this type of SP application in this environment appears to be due to the low electrical resistivity of the sedimentary section combined with the depth of injection. The lower the resistivity, the more attenuated is the surface SP response from a source at depth.

Resistivity surveys were not attempted at East Mesa because numerical modeling indicated that the response would be smaller than the detection limit.

In summary, geophysical techniques did not contribute to the experiments at East Mesa. No exotic geophysical techniques were tried due to decisions to spend the limited available funds on geochemical and hydrological experiments.

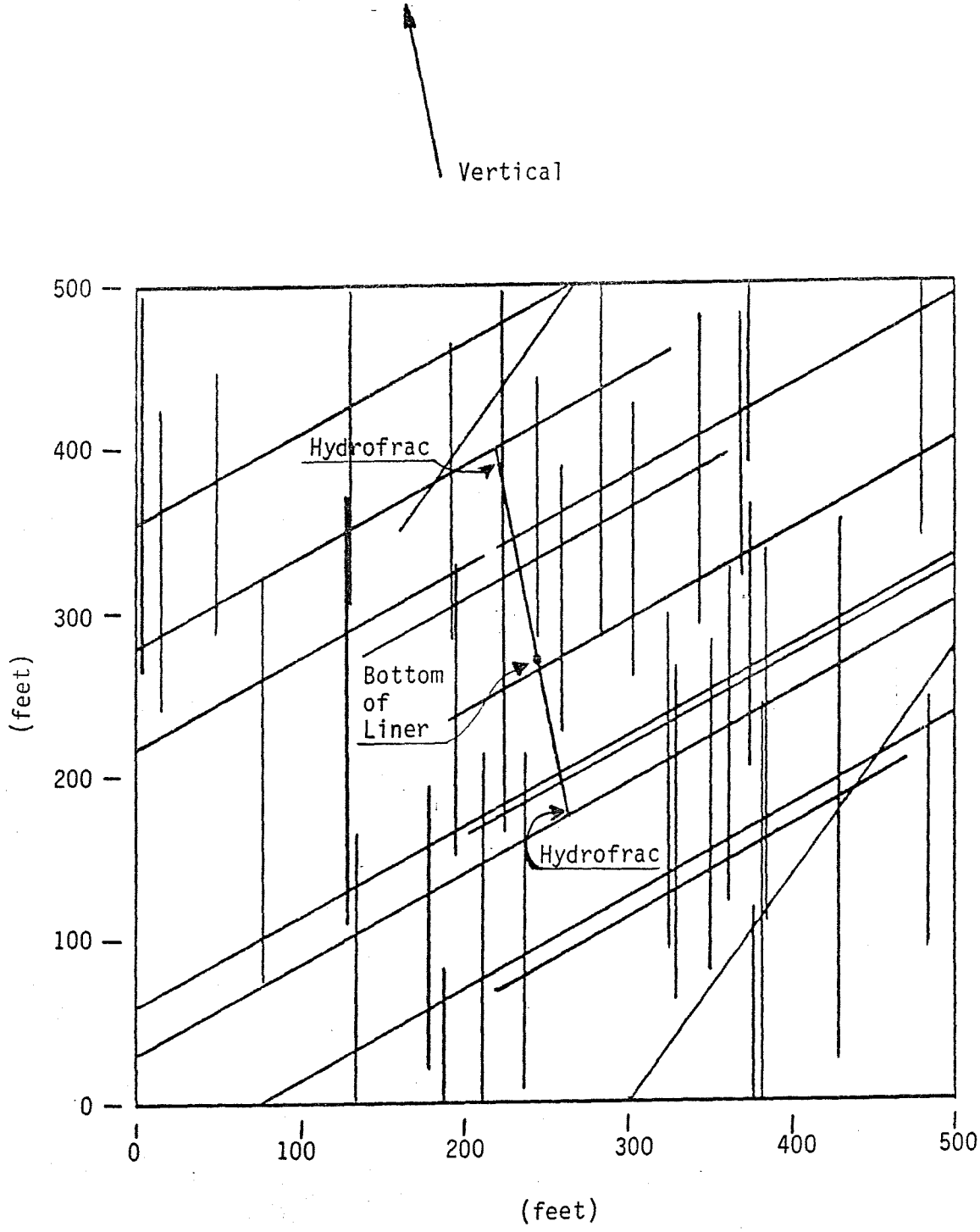

Figure 42. Raft River Well RRGP-5BF Large Reservoir Fracture System

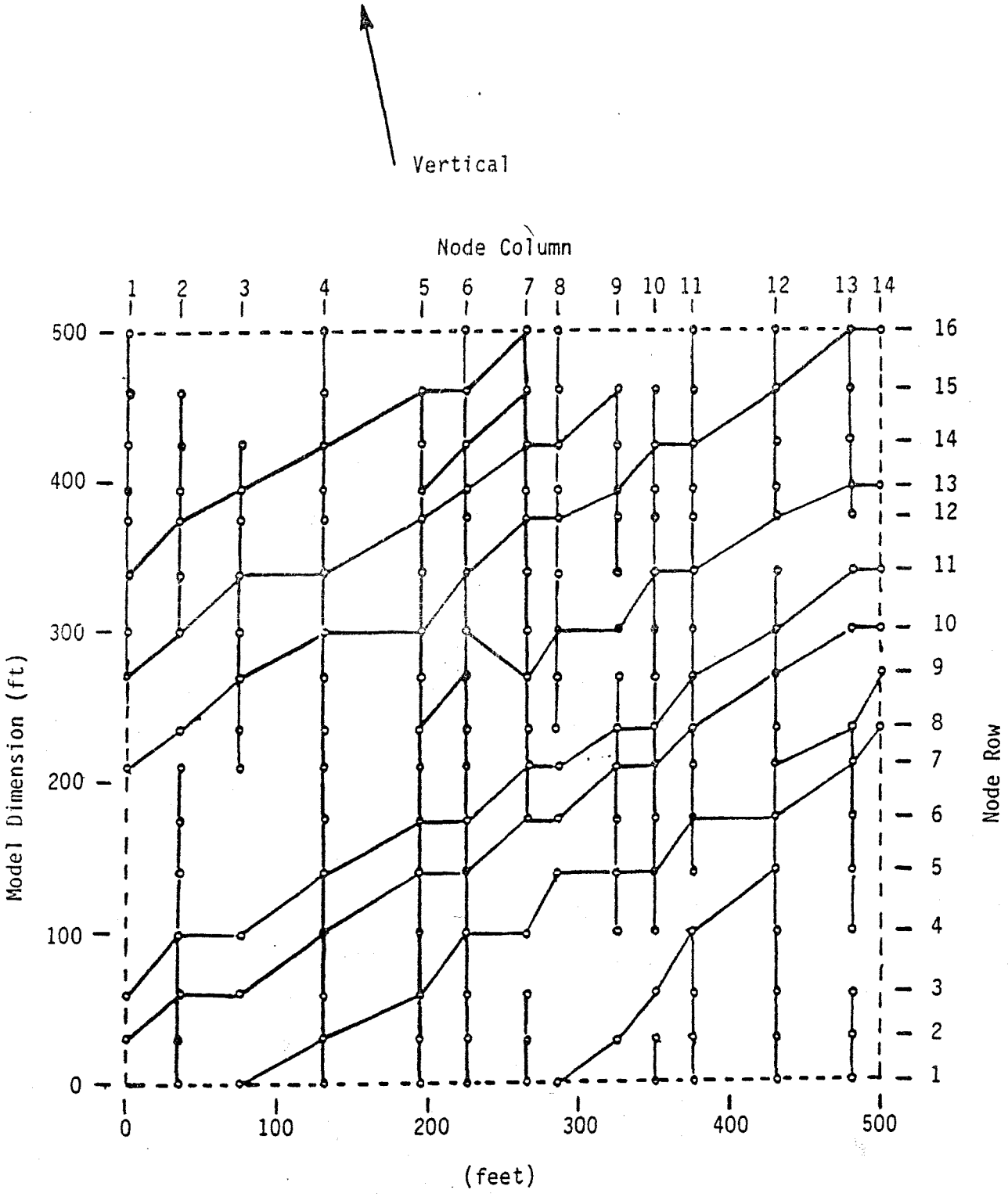

Figure 43. Raft River Well RRGP-5BF Large Reservoir Computer Model

5.0 CONCLUSIONS

1) The injection/backflow technique has been demonstrated as a valuable tool for the following:

   a) Evaluating the conservativeness of tracers in a field application.
   b) Determining the mixing of injected fluids with native fluids in a geothermal reservoir.
   c) Measuring in-situ rock water interactions.
   d) Determining inhibitor effectiveness and assessing the impact of sub-surface precipitation on long term injection and performance.
   e) Measuring the transfer of heat to injected fluids from the reservoir area surrounding an injection well.
   f) Determining the natural convection in a reservoir.
   g) Assessing the shape of the injection fluid plume in a reservoir.
   h) Assessing the type of formation into which the injectate fluid is moving, i.e., fractured or homogeneous flow or a combination of the two.

2) A supporting laboratory program is an integral part of the interpretation of field injection experiments. The five fracture flow models have provided the necessary data to verify that the computer codes being used to analyze the field are properly interpreting the flow characteristics of fractured systems. The models also provide an excellent means to tie theoretical concepts to the interpretation of data.

3) A simulation code with a fluid mixing algorithm is an essential part of analyzing injection/backflow experiments. The simulation code permits the verification of reservoir hydraulic characteristics by simultaneously fitting equations for flow, pressure, heat transfer and fluid mixing to the results of injection backflow tests.

4) The injection/backflow test technique is applicable to a wide variety of applications which extend beyond the geothermal program. Predicting the movement of acquifer contaminants should be a significant application.

6.0 REFERENCES

1. Hydrothermal Injection Research Program Annual Progress Report FY-1983, November 1983, DOE/ID-10117.

2. Michels, D. E., Disposal of Flashed Brine Dosed with $CaCO_3$ Scale Inhibitor, Ninth Workshop on Geothermal Reservoir Engineering, Stanford University, Decmeber 1983.

3. Large, R. M., Hydrothermal Injection Program Phase 1 Test Data Index, Internal EG&G Idaho Report REPB-83-015, July 1983.

4. Friebnrger, R. M., Hydrothermal Injection Program East Mesa 1983-84 Test Data, Internal EG&G Idaho Report SE-PB-84-044, September 1984.

5. Downs, et al., Hydrothermal Injection Program Experiment at the Raft River KGRA Idaho, Eighth Geothermal Reservoir Engineering Conference, Stanford University, December 1982.

6. Downs, et al., Tracer Injection Tests in a Fracture Dominated Geothermal Reservoir, Spring Meeting, American Geophysical Union, 1983.

7. Russel, et al., Response of East Mesa and Raft River Reservoirs to Injection Backflow Testing, Ninth Workshop on Geothermal Reservoir Engineering, Stanford University, December 1983.

8. Skiba, P. A., Unusual Pressure Response of RRGP-5 During Huff-Puff Testing Conducted at the Raft River KGRA in Southern Idaho Rocky Mountain Ground Water Conference, Boise, Idaho, 1983.

9. Capuano, et al., Tracer Recovery and Mixing from Two Geothermal Injection Backflow Studies, Ninth Workshop on Geothermal Reservoir Engineering, Standford University, December 1983.

10. Wright, P. M., et al., Uses of Geochemicstry with Injection Backflow Testing in Geothermal Reservoir Studies, Geothermal Resources Council 1984 Annual Meeting, Reno, Nevada, August 1984.

11. Adams, M. C., Tracer Stability and Chemical Changes in an Injected Geothermal Fluid during East Mesa Injection Testing, Earth Science Laboratory University of Utah Research Institute: In Pres.

12. Adams, M. C., Kronenon, R. L., and Yorgason, K. R., Chemical Analysis of Water Samples Collected During East Mesa Injection/Backflow Testing, Earth Sciences Laboratory University of Utah Research Institute: In Pres.

13. Koslow, K. N., and Hull, L. C., Design of a Model to Study Dispersion in Fracture Networks, Internal EG&G idaho Report EGG-ELS-5718, January 1982.

14. Hull, L. C., and Koslow, K. N., Physical Model of a Fractured Reservoir, Ninth Stanford Reservoir Engineering Conference, Stanford University, December 1983.

15. Koslow, K. N., and Hull, L. C., Comparison of Field and Laboratory Results, International Ground Water Symposium on Groundwater Resource Utilization and Containment Hydrogeology, Montreal, Canada, 1984.

16. Hull, L. C., and Koslow, K. N., Oral Presentation, Penrose Conference, Park City, Utah, September 1984.

17. Kronemon, R. L., Yorgason, K. R. , and Moore, J. N., Preferred Analytical Methods for Water Samples Collected During Injection Testing, Earth Sciences Laboratory University of Utah Research Institute: In Pres.

18. Clemo, T. M., Miller, J. D., Simulation of Flow and Dispersion in the East Mesa Reservoir, Internal EG&G Idaho Report SE-PB-84-056, In Pres.

19. Ogata, Akic and Banks, R. B., A Solution of the Differential Equation of Longitudinal Dispersion in Porous Media, U.S. Geological Survey Professional Paper, 1961, 411-A, PP A1-A7.

20. Hull, L. C., Physical Model Studies of Dispersion in Fracture Systems, Internal EG&G Idaho Report, SE-PB-84-063, 1984.

21. Prickett, T. A., Naymik, T. G., and Lonnquist, C. G., A Random-Walk Solute Transport Model for Selected Groundwater Quality Evaluations, Bulletin 65, Illinois State Water Survey, Champaign, Illinois, 103 p. 1981.

22. Amsden, A.A., Ruppel, H. M., and Hirt, C. W., SALE: A Simplified ALE Computer Program for Fluid Flow at all Speeds, LA-8095, VC-32, 1980, Los Alamos Scientific Laboratory.